Hydrological and hydraulic solutions for the sustainability of habitat life in human altered streams

Thèse N° 9584

Amin NIAYIFAR

2019

EPFL

ÉCOLE POLYTECHNIQUE
FÉDÉRALE DE LAUSANNE

Knowledge is power.

— Abu l-Qasim Firdowsi Tusi

To my family...

Acknowledgements

I have spent around four years to compose this doctoral thesis, but in fact, the number of years required for this accomplishment is much more than this. I am indebted to many who have contributed to both my education and development as a person since my childhood.

In the first place, I would like to express my gratitude to all of my teachers, professors and educational supervisors that I had since my elementary school. All of what I have achieved in this thesis is founded (in many cases directly) on the excellent education I received until the age of 18. I specially thank my parents who were in a way my first teachers (in our village; Davarzan). I did the first and second year of my studies in the elementary school that my father and mother were principles of the school. Then comes the university times, where I completed a bachelor's degree in Mechanical engineering in University of Tehran (UT). During my time in UT, I benefited a lot from the knowledge of its professors and their first-class teaching and supervision. It was in this period that I became interested in perusing PhD, in particular when I started to do research under supervision of Prof. Mohamad Hasan Rahimian.

Later, I moved to Lausanne, Switzerland to conduct my Master and doctoral studies at EPFL. I have to say I am deeply grateful to EPFL for the high level of education and the remarkable quality and quantity of the resources that it provided in a professional and at the same time friendly academic environment. Of course, I would like to single out Prof. Tom Ian Battin and Paolo Perona, who supervised me during my PhD studies. I know Paolo since my first semester at EPFL where I took environmental transport phenomena course. As someone who, at that time, had been restricted solely with the fluid mechanics education, Palo's course helped me to appreciate the synergy research topics, namely, combination of physics and environmental processes. Being excited by this course, I became teacher assistant of the course and afterwards I had the chance to start my PhD. I am sincerely thankful to Paolo for all his supports, both at EPFL and also our meetings at his house in Bern. I owe my great gratitude to Tom for all his support. I appreciate the fact that his office door was always open and he was constantly available for discussions and exchanges about the research. I would like to thank him for his unconditional support in different phases of my PhD. His dedication and passion to research has been always motivating for me. I have learned a lot from him in many aspects. His encouragement has always been helpful to solve challenging problems. I also thank Prof. Alfred Johny Wüest, Prof. Paolo Burlando, Prof. Gregory Characklis and Dr Katharina Edmaier for accepting to examine this work.

During these years, I benefited much from the unique companionship of many friends and colleagues during these years, without whom walking through this road would not have been

Acknowledgements

Abstract

In this thesis, I aim to contribute to the research towards improving the sustainability of habitat life in streams affected by anthropogenic activities. With the growing trend of altering natural water regimes due to hydropower operations, irrigation, and wastewater treatment plants, for instance, it is vital to minimize environmental effects. Here, I aim to address issues regarding human-altered streams that have received less attention in the community. In particular, I intend to provide solutions to improve the water management in the reservoir systems as well as investigating the role of macroroughness elements on the ecosystem functioning.

For the water management part, the aim is to improve the global efficiency of storage systems, with the main focus being on the environmental aspect. Minimum flow releases nowadays are widely used to reduce the environmental effects associated with streams affected by anthropogenic activities. However, these static flow release rules have been found to markedly affect the stream ecosystem, mainly by reducing biodiversity. Aiming to reduce the environmental impacts caused by reservoirs, I propose a Direct Policy Search (DPS) framework based on defining dynamic flow release rules. I employ the mathematical form of the Fermi-Dirac statistical distribution to formulate dynamic non-proportional redistribution rules that partition the flow for energy production and environmental use. The energy production is calculated from technical data and the environmental indicator associated with flow releases by integrating the Weighted Usable Area (WUA) for fishes with Richter's hydrological indicators. State-of-the art multiobjective evolutionary algorithms are used to find optimal flow release policies that have efficient economic and environmental efficiency. The results show that non-proportional flow releases can substantially improve global efficiency, specifically the ecological one, of the hydropower system when compared to minimal flow releases. This is mainly due to better water management of flood events that enables flow releases that mimic natural flow variability.

In the part of my Thesis on streambed macroroughness, I investigate the contribution of macroroughness elements to stream ecosystem functioning, which generally is not considered due to their relatively small scale, using both modeling and fieldwork approaches. Macroroughness elements contribute to stream ecosystem functioning mainly by providing shelter zones for fishes as well as enhancing reach scale gas exchange. I develop an environmental indicator based on the aforementioned benefits of macroroughness elements on stream ecosystem functioning. Environmental indicators help define improved water management strategies by better characterizing the environmental impacts associated with human altered flow regimes. I define a physically based analytical model to estimate the size of wake areas

Résumé

Dans cette thèse, je souhaite contribuer aux recherches visant à améliorer la durabilité de la vie dans l'habitat des cours d'eau qui sont affectés par des activités anthropiques. Avec une tendance croissante à modifier les régimes hydrologiques naturels dus aux opérations hydroélectriques, à l'irrigation et aux usines de traitement des eaux usées, par exemple, il est essentiel de minimiser les effets sur l'environnement. Dans cette optique, mon objectif est d'aborder les problèmes liés aux cours d'eau modifiés par l'homme qui ont reçu moins d'attention dans la communauté. En particulier, je compte proposer des solutions pour améliorer la gestion de l'eau dans les systèmes de réservoirs, et étudier le rôle des éléments de macrorugosité sur le fonctionnement de l'écosystème.

Pour la partie relative à la gestion de l'eau, l'objectif est d'améliorer globalement l'efficacité des systèmes de stockage, en mettant l'accent principalement sur l'aspect environnemental. De nos jours, la libération des débits minimums sont largement utilisés pour réduire les effets environnementaux associés aux cours d'eau qui sont affectés par des activités anthropiques. Cependant, il a été constaté que ces règles de libération des flux statiques affectaient de manière significative l'écosystème des cours d'eau, particulièrement en réduisant la biodiversité. Dans le but de réduire les impacts environnementaux causés par les réservoirs, je propose un cadre de recherche politique directe (DPS) basé sur la définition des règles de la libération des flux dynamiques. J'utilise une forme mathématique de la distribution statistique de Fermi-Dirac pour formuler les règles de redistribution dynamiques non proportionnelles qui divisent le flux pour la production d'énergie et l'utilisation environnementale. La production d'énergie est calculée à partir des données techniques et de l'indicateur environnemental associé aux rejets de flux en intégrant la surface utilisable pondérée (WUA) pour les poissons avec les indicateurs hydrologiques de Richter. Les algorithmes évolutifs multi-objectifs de pointe sont utilisés pour trouver des règles de libération optimales de flux ayant une efficacité économique et environnementale. Les résultats montrent que les rejets non proportionnels du flux peuvent améliorer considérablement le rendement global, principalement le rendement écologique, du système hydroélectrique lorsque celui-ci est comparé aux rejets du flux minimum. Cela est principalement dû à une meilleure gestion de l'eau lors des inondations qui permet les rejets de flux qui imitent la variabilité naturelle des flux.

Dans la partie de ma thèse consacrée à la macrorugosité sur lit de ruisseau, j'étudie la contribution des éléments de macrorugosité au fonctionnement de l'écosystème du flux, qui n'est généralement pas pris en compte en raison de son échelle relativement petite. Ceci en utilisant à la fois des approches de modélisation et le travail sur terrain. Les éléments de

macrorugosité contribuent au fonctionnement de l'écosystème des cours d'eau en fournissant principalement des zones de refuge pour les poissons et en renforçant également les échanges de gaz à grande échelle. Je développe un indicateur environnemental basé sur les avantages susmentionnés des éléments de macrorugosité sur le fonctionnement de l'écosystème des cours d'eau. Les indicateurs environnementaux aident à définir de meilleures stratégies de gestion de l'eau en caractérisant mieux les impacts environnementaux associés aux régimes d'écoulement modifiés par l'homme. Je définis un modèle analytique basé sur la physique pour estimer la taille des zones de sillage en aval des éléments de macrorugosité et j'utilise l'approche de la distribution dérivée pour calculer la distribution statistique des zones de sillage. Pour valider le concept, le modèle est appliqué à quatre exemples de cours d'eau présentant différentes distributions statistiques de la taille du diamètre des éléments de macrorugosité. En outre, l'indicateur environnemental proposé est inclus dans le cadre de DPS afin de résoudre un problème d'optimisation de réservoir multiobjectif. Ensuite, des preuves empiriques sont fournies pour les effets des éléments de macrorugosité sur le fonctionnement de l'écosystème des cours d'eau en effectuant des études sur le terrain. Je combine la télédétection avec un modèle analytique pour estimer les zones de sillage en aval des éléments de macrorugosité de la rivière Aar (Suisse) et je calcule le seuil du débit environnemental de cette rivière restaurée. J'étudie également l'impact des éléments de macrorugosité et des zones de sillage induit sur la turbulence superficielle quasi libre et l'échange de gaz résultant dans un cours d'eau alpin régulé (Trient, Suisse) en utilisant des injections de gaz traceurs en présence et en absence des éléments de macrorugosité expérimentalement manipulés avec différents degrés de submersion. Les résultats montrent que l'ajout des éléments de macrorugosité non immergés au lit du cours d'eau augmente significativement l'échange gazeux à grande échelle, alors que dans mon expérience, l'ajout de sillages à une faible proportion du flux (soit 7%) a entraîné une augmentation des échanges de gaz à un facteur 3. Enfin, les conclusions de cette thèse pourraient aider à réduire les impacts environnementaux dans les cours d'eau altérés par l'homme en proposant des règles de gestion respectueuses de l'eau, une meilleure évaluation du niveau de perturbation de l'environnement et des stratégies visant à améliorer la vie de l'habitat aquatique.

Mots clés : cours d'eau modifiés par l'homme, rejets de flux dynamiques non proportionnels, optimisation multiobjectif, éléments de macrorugosité, zones de sillage, échange de gaz, indicateur environnemental, restauration du cours d'eau

Contents

Contents

List of Figures

List of Tables

1 Introduction

The increasing pace of climate change has caused severe impacts on the environment. This is considered one of the most difficult challenges that has ever threatened the life of humankind. Therefore, it is vital to realistically foresee its magnitude and adopt new policies such as developing greener energy sources aimed to minimize its negative effects. The latter are important, now more than ever, as the disastrous consequences of climate change are appearing. Hence, providing scientifically justified explanations about the consequences of climate change together with finding efficient alternatives to decrease these impacts are vital for convincing the public to take firm and sustainable actions.

Renewable energies are known to be a viable source of energy to mitigate climate change effects. Hydropower is the leading source of renewable energy, which currently accounts for more than 16% of electricity generation worldwide [*IEA*, 2015]. Due to its sustainability in terms of energy production, as well as its capability to balance the energy market with emerging wind and solar power (which have higher uncertainty), hydropower is still very important in supplying energy worldwide. However, hydropower may significantly impact the environment by disturbing natural flow regimes. Nowadays, ecological concerns in the economically developed countries are among the main reasons that the rate of dam removal exceeds the building rate. However, this is not the case in the economically developing countries, as many new dams are being built [*O'Connor et al.*, 2015]. It is estimated that, up to now, only 22% of hydropower potential worldwide has been exploited and therefore hydropower still can play an important role towards supplying green energies. Further exploitation of streams thus must be met with efficient regulation to minimize environmental degradation. A conservative estimate states that 472 million people around the world have been negatively influenced by dams [*Richter et al.*, 2010]. For example, in Isfahan, a historic city in the center of Iran, the tourism industry around the Sio-sepol bridge has been significantly impacted due to the operation of upstream reservoirs which dry out the Zayanderood stream for the most of the year. Operation of reservoirs in Tucurui region of the Amazon has resulted in a 60% loss in fish catches, affecting the lives of 100,000 people [*WCD*, 2000]. Aiming to minimize the negative impacts of dams, especially the ecological aspect, constant minimum flow release rules are widely used. For example, this static rule has been imposed by Swiss

Federal Legislation where all the dams have to release a constant flow rate downstream, namely $Q347$. This discharge corresponds to the flow quantile exceeded on average 95% of the time, which is obtained from the flow duration curve of the natural flow regime. However, this static rule has been found to negatively affect the riverine ecosystem, notably by reducing biodiversity [*Arthington et al.*, 2006].

Environmental restoration of impounded streams necessitates a good understanding of the extent of the level of environmental degradation. The latter is quantified using environmental indicators. However, the use of different indicators to assess the impact of disturbed flow regime on the riverine ecosystem is still crucial [*Gao et al.*, 2009].

Macroroughness contributes to stream ecosystem functioning mainly by providing shelter zones for fishes as well as enhancing the stream gas exchange [*Moghadam and Keshavarzi*, 2007; *Moog and Jirka*, 1999b]. Reduced velocity regions (i.e., wake areas) downstream of macroroughness elements are suitable spots for fishes to rest where they can quickly move to adjacent fast water regions for foraging. Macroroughness also enhances the reach-scale gas exchange by increasing the near free surface turbulence level. Gas exchange through the water surface is critical to stream ecosystem functioning, particularly its metabolism. At the same time, the gas exchange is also a major driver of the evasion of climatically relevant gases from streams. Recently, macroroughness has been found responsible for high gas exchange rates in high-slope streams in the Alps [*Ulseth et al.*, 2019]; hence it can potentially contribute to the CO2 evasion flux from streams — even with global impacts. Gas exchange also controls the concentration of dissolved oxygen (DO) in the streamwater that is an important measure of the overall water quality and the viability of aquatic habitat. DO concentration may decrease and reach a critical level close to hypoxia. This has been reported, for example, from streams receiving effluents from wastewater treatment plants, or from streams with high temperature but low discharge, and finally from streams and rivers receiving low oxygenated bottom waters from a reservoir. Addition of macroroughness on the streambed can substantially increase the level of DO and therefore be an efficient way to ensure the viability of aquatic habitat life in streams with hypoxia problems. Although macroroughness may have substantial ecological significances, their role in the ecosystem functioning is not very well understood, mainly due to their relatively small scale.

In Switzerland, the estimated share of domestic electricity generated by hydropower is around 60% (SFOE, 2013). The currently installed capacity (36,000 GWh per year), produced in over 550 hydropower plants with capacity greater than 300 kW, is expected to increase by at least 2,000 GWh to compensate losses due to nuclear power plant phasing out and to complement the increase in electricity production by other renewable sources (SFOE, 2013). This PhD thesis is part of the HydroEnv project which has the premise that the existing and planned hydropower production increase must be considered together with a rise in possible environmental degradation in riverine ecosystem downstream of dams and intakes.

Motivated by the aforementioned issues, in this PhD thesis I aim to contribute to the research on the following topics, which have received relatively little attention: proposing eco-sustainable flow releases in hydrologically modified streams and providing a better characterization of the role of macroroughness on stream ecosystem functioning. In this regard, this PhD Thesis is

structured as follows. In Chapter 2, I propose a Direct Policy Search (DPS) framework based on defining dynamic flow release rules to improve the global efficiency of storage systems. The water allocation policy is derived based on the mathematical form of the Fermi-Dirac statistical distribution and is optimized using state-of-the art multiobjective evolutionary algorithms for two objectives; namely, energy production and environmental indicator. I also compare the performance of the proposed DPS framework with the commonly used minimal flow release policies. In Chapter 3, I propose an environmental indicator that considers the habitat generated by the wakes downstream of macroroughnesses and can therefore be used to assess the environmental efficiency of flow release rules for impounded streams. I developed a physically based analytical model to estimate the size of wake areas and employ a derived distribution approach to calculate the statistical distribution of wake areas. To validate the concept, I applied the model to four exemplary streams having different statistical diameter size distributions of macroroughnesses. I additionally included the proposed environmental indicator to solve a multi-objective reservoir optimization problem. In Chapter 4, I provide empirical evidence for the effects of macroroughness elements on stream ecosystem functioning. I combined remote sensing with the analytical model (detailed in Chapter 3) to quantify the wake areas downstream from macroroughness elements in the Aare River (Switzerland) and calculate the environmental flow threshold for this restored river. Furthermore, I experimentally investigated the impact of macroroughness and induced wake areas on the gas exchange in a regulated alpine stream (Trient, Switzerland). For this purpose, I measured the gas transfer velocity ($k600$) using tracer gas injections in the presence and absence of manipulated macroroughness elements with different degrees of submergence. Finally, in Chapter 5, I provide a summary of the major findings of my PhD Thesis, and also cast a glance regarding the future development of the work presented.

2 Dynamic water allocation policies improve the global efficiency of storage systems[1]

Abstract

Water impoundment by dams strongly affects the river natural flow regime, its attributes and the related ecosystem biodiversity. Fostering the sustainability of water uses e.g., hydropower systems thus implies searching for innovative operational policies able to generate Dynamic Environmental Flows (DEF) that mimic natural flow variability. The objective of this study is to propose a Direct Policy Search (DPS) framework based on defining dynamic flow release rules to improve the global efficiency of storage systems. The water allocation policies proposed for dammed systems are an extension of previously developed flow redistribution rules for small hydropower plants by Razurel et al. *Razurel et al.* [2016].The mathematical form of the Fermi-Dirac statistical distribution applied to lake equations for the stored water in the dam is used to formulate non-proportional redistribution rules that partition the flow for energy production and environmental use. While energy production is computed from technical data, riverine ecological benefits associated with DEF are computed by integrating the Weighted Usable Area (WUA) for fishes with Richter's hydrological indicators. Then, multiobjective evolutionary algorithms (MOEAs) are applied to build ecological versus economic efficiency plot and locate its (Pareto) frontier. This study benchmarks two MOEAs (NSGA II and Borg MOEA) and compares their efficiency in terms of the quality of Pareto's frontier and computational cost. A detailed analysis of dam characteristics is performed to examine their impact on the global system efficiency and choice of the best redistribution rule. Finally, it is found that non-proportional flow releases can statistically improve the global efficiency, specifically the ecological one, of the hydropower system when compared to constant minimal flows.

2.1 Introduction

The practice of impounding water from mountain streams for anthropogenic uses has been shown to possibly affect - notably to reduce - the biodiversity of riverine ecosystems [*Assani et al.*, 2010; *Kennard et al.*, 2010; *Kern et al.*, 2011; *Konar et al.*, 2013]. The biogeomorphological

---

[1]The contents of this chapter are published in: Niayifar, A. and Perona, P., 2017. Dynamic water allocation policies improve the global efficiency of storage systems. Advances in water resources, 104, pp.55-64.

basis responsible for such an effect is related to the establishment of minimal constant discharges from river intakes and/or reservoirs [*Arthington et al.*, 2006]. In Switzerland, for example, this static rule is regulated by Swiss Federal Legislation and corresponds to the release of a constant (or seasonally constant) flow rate, Q_{347}. This value is close to the flow quantile exceeded on average 95% of the time, which is obtained from the flow duration curve of the natural flow regime [e.g., *Franchini et al.*, 2011]. Many countries have adopted this ecological measure because of its simplicity. An example of the application of the constant minimal flows that modifies a natural flow regime is shown in the hydropower scheme of Figure 2.1, where much of the annual runoff volume is stored in the dam and allocated as flowrate, $Q_{hydro}(t)$, to satisfy energy demand. The flow rate allocated to the environment, $Q_{env}(t)$ based on a minimal flow policy shows almost constant river discharge with the exception of some peaks. The peaks are due to both uncaptured runoff or storage releases to the environment when the maximum capacity of the reservoir is reached during flood events [*Schweizer et al.*, 2007; *Petts*, 2009].

Ultimately, although favorable for certain aquatic species, the application of minimal flow
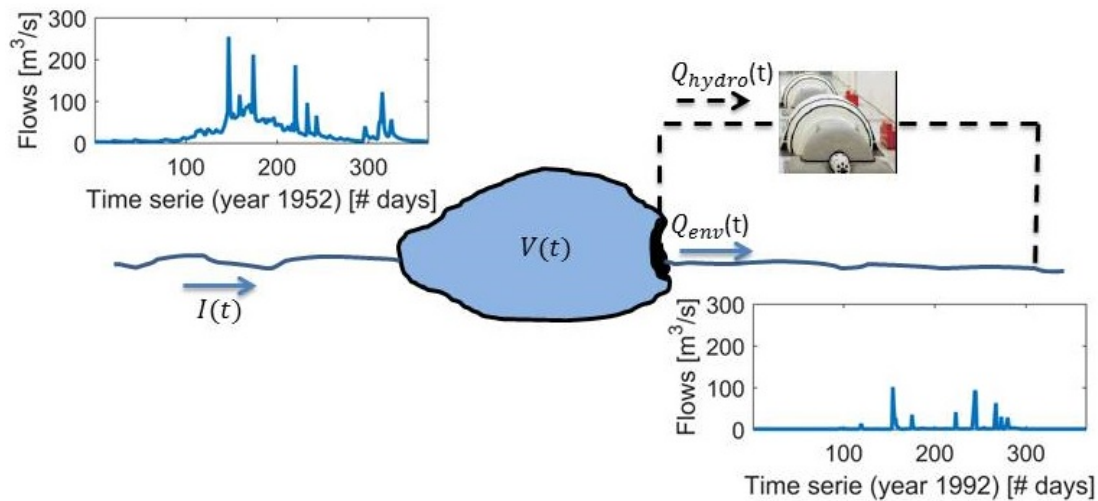
Figure 2.1 – Schematic of the dammed systems. Hydrographs represent the daily flow rate of Maggia river before (1952) and after (1992) installation of the dam.

policies tend to "homogenize" river hydrographs, and produces similar long-term effects even for ecosystems in very different geographic locations [*Arthington et al.*, 2006; *Moyle and Mount*, 2007].

Extensive research has been performed on reservoirs water management and optimization [e.g., *Oliveira and Loucks*, 1997; *Cui and Kuczera*, 2005]. In these works, the best operating rules for storage systems are chosen to optimize one or more objectives. Operating policies usually determine the release rule (e.g., discharge or dam storage) for the reservoir at any time step. In the literature, different methods have been proposed to define efficient operational policies. Dynamic Programming (DP) and its extension, Stochastic Dynamic Programming (SDP), have been widely used in the literature [e.g., *Yeh*, 1985; *Castelletti et al.*, 2008] to define

efficient operational policies in storage systems. These techniques improve the operational efficiency of storage systems, but their application is limited [*Giuliani et al.*, 2015] because of problem dimensionality [*Bellman*, 1966], modeling parameters versus data availability [*Tsitsiklis and Van Roy*, 1996] and representation of multiple objectives [*Powell*, 2007].

Direct policy search (DPS) methods are a viable alternative to overcome the three shortcomings of DP and SDP [e.g., *Dariane and Momtahen*, 2009; *Gorla*, 2014]. DPS methods parametrize the operational policy using a predefined parametric family of functions and optimize it based on the objectives of the studied reservoir [*Giuliani et al.*, 2015]. The choice of defining operational policies is usually performed by defining some empirical and practical approaches. Some recent works [*Salazar et al.*, 2016] have tried to generalize the definition of operational rules using nonlinear approximating networks (e.g., artificial neural networks and radial basis functions). For the optimization approach used in the DPS methods, gradient based and Evolutionary Algorithms (EAs) have been extensively used to find efficient operational rules for reservoir systems. Particularly, EAs have shown better efficiency in handling the performance uncertainties compared to methods based on predicting absolute performance or performance gradient [*Heidrich-Meisner and Igel*, 2008]. Several studies have investigated the performance of methods for optimizing operational rules for reservoir systems [e.g., *Salazar et al.*, 2016].

As discussed before, the goal of defining operational rules for reservoir systems is to optimize their operational efficiency based on the characterization of some objectives. Depending on the function of each reservoir system, several objectives have been considered in the literature, such as electricity production, irrigation, potable water supply, and flood protection. Substantial improvement in the efficiency of reservoir with respect to the considered objectives was achieved [e.g., *Cui and Kuczera*, 2005; *Dariane and Momtahen*, 2009]. The riverine ecosystem is acknowledged to be significantly affected by reservoir operations due to the alteration of the natural flow regime. However, minimizing the related environmental impact has not been considered as a detailed and well-focused objective in the field of defining operational rules for the reservoirs. The primary goal of this study is to develop a new DPS framework by defining a new class of functions (i.e., non-proportional flow release) for reservoir operational rules, whose environmental impact is comprehensively assessed and minimized while maintaining the economical (i.e., energy production) efficiency.

Efforts to summarize existing frameworks and guidelines for determining environmental flows have been recently proposed [*Petts*, 2009; *Poff et al.*, 2010; *Meijer et al.*, 2012]. It is generally accepted that future ecologically sustainable exploitation of water resources in dammed systems requires seeking innovative operational flow release strategies that mimic the natural flow regime. This challenging aspect concerns with the ability to find new dynamic environmental flows that can improve ecological efficiency with respect to constant minimal flow policies [e.g., *Arthington et al.*, 2006; *Bartholow*, 2010a; *Bizzi et al.*, 2012] while maintaining economic benefit. *Perona et al.* [2013] have introduced the idea of engineering Dynamic Environmental Flows (henceforth referred to as DEFs) releases by considering the riparian environment as a non-traditional water use. Increasing hydropower production without straining the environment has then shown to be feasible at least for

water systems without storage such as small hydropower [e.g., *Lazzaro et al.*, 2013; *Gorla and Perona*, 2013; *Ta et al.*, 2016; *Razurel et al.*, 2016]. *Gorla* [2014] and *Razurel et al.* [2016] have generalized the method by introducing the concept of non-proportional redistribution. In this work, we intend to show that the non-proportional redistribution concept is also applicable to traditional dammed systems, and leads to Pareto efficient solution containing non-proportional policies. Compared to the case of small hydropower, dammed systems have storage dynamics that require multiobjective dynamic programming numerical approaches. These can be computationally heavy when thousands of policies have to be simulated. Hence, we use optimization methods (NSGA II and Borg MOEA) to speed up the numerical process and build the efficiency plot. Furthermore, the results of the Borg MOEA and NSGA II are compared in terms of computational cost and fitness of Pareto's frontier to find the efficient optimization method. Eventually, DEFs releases obtained from non-proportional redistribution rules are found to steer future water resources management towards ecosystem functioning and sustainability.

2.2 Methodology

We tackle the problem of finding Pareto-efficient both ecological and economical operational rules for dammed systems by simulating state-dependent non-proportional flow redistribution rules. Ecological benefits for the riverine corridor due to DEFs, are obtained by aggregating the fish habitat suitability indexes (HSI) and Richter's hydrological indicators. We use multiobjective evolutionary algorithms (MOEAs) to build the Pareto's frontier as a computationally efficient alternative to direct simulation of high number of selected strategies. The use of MOEAs guarantees that solutions lying on the frontier satisfy both maximal power production and ecological sustainability. Moreover, this method can be implemented in a graphical user interface form for practical use by stakeholders and water managers. We begin by introducing non-proportional flow redistribution.

2.2.1 Non-proportional flow redistribution

The schematic of a dammed system for hydropower production is shown in Figure 2.1 where the following expression represents the reservoir continuity equation governing stored water volume dynamics at each time step t:

$$\frac{dV(t)}{dt} = I(t) - Q_{env}(t) - Q_{hydro}(t), \tag{2.1}$$

where $V[\mathrm{m}^3]$ is the volume stored in the reservoir, $I[\frac{\mathrm{m}^3}{\mathrm{s}}]$ is the inflow to the reservoir, Q_{env} and Q_{hydro} are the outflows $[\frac{\mathrm{m}^3}{\mathrm{s}}]$ allocated to the river and hydropower plant, respectively. Evaporation and other water losses can easily be introduced as additional terms. For the sake

of convenience in illustrating the method and without loss of generality we assume that such terms can be englobed to generate a net inflow $I(t)$. A time step, Δt, is considered in this study and hence the discretized form of continuity equation is:

$$V(t+1) = V(t) + \Delta t[I(t) - Q_{env}(t) - Q_{hydro}(t)], \tag{2.2}$$

In this work, we consider daily time steps, i.e., Δt=1. The flow redistribution rules proposed in this study for dammed systems are an extension of previously developed water allocation policies for small hydropower plants [*Perona et al.*, 2013; *Gorla and Perona*, 2013; *Razurel et al.*, 2016]. In these prior studies, non-proportional flow releases were found to be more ecologically and economically efficient compared to the other commonly used flow release rules such as constant minimal flows. Considering storage, inflow and hydropower needs, the following non-proportional water allocation to the environment is proposed for dammed systems:

$$Q_{env} = \begin{cases} Q_{mfr} & I < I_{min} \\ f_{fermi}(I)f_s(V)(I - I_min) + Q_{mfr} & I_{min} \leq I \leq I_{max} \\ f_s(V)\alpha \times \max(I) & I > I_{max}, \end{cases} \tag{2.3}$$

where Q_{mfr} is the constant minimal flow release considered compulsory (e.g., as enforced by law), I_{min} and I_{max} define the boundaries of streamflow competition (see equation 2.6), f_{fermi} is the Fermi-Dirac function, f_s is the storage factor and α determines the magnitude of environmental flow. To realize a wide range of possible water allocation policies, we extend the approach of *Razurel et al.* [2016] to systems with storage. That is, we adopt the mathematical form of the Fermi-Dirac statistical distribution to express the fraction of water allocated to the river (f_{fermi}) as a function of inflow. This mathematical distribution is commonly used in quantum statistics to describe a many-particle system in terms of single-particle energy states [*Lifshitz and Landau*, 1984]. The shape of the Fermi-Dirac function depends on only four parameters, which makes it appealing for studying environmental water allocation problems. In order to realize non-proportional environmental flow redistribution rules, we rewrite the Fermi-Dirac function as follows:

$$f_{fermi}(I) = \left[1 - \left(\frac{Y}{\exp[a(X-b)]+c} + M\right)\right](j-i) + i \tag{2.4}$$

where $M = \frac{A}{A-1}$, $A = \frac{\exp(-ab)+c}{\exp[a(1-b)]+c}$ and $Y = (1-M)[\exp(-ab)+c]$. i, j, a, b and c are the parameters that define the shape of the Fermi function. The parameters i and j define the boundaries of the distribution function. When $i < j$, the function monotonously increases and is called the standard Fermi function; when $i > j$, the Fermi function monotonously decreases and is called the inverse Fermi function. The smoothness of the transition between the upper and lower boundaries (i and j) is regulated by parameter a. A small a results in a linear transition between i and j. In contrast, a steeper transition can be realized by increasing

Table 2.1 – The range of Fermi parameters.

Fermi parameter	Range
Beginning of the competition	$0.02 \leq i \leq 0.8$
End of the competition	$0.02 \leq j \leq 0.8$
Curvature	$2 \leq a \leq 8$
Position of the inflection point	$0 \leq b \leq 1$

a. Parameter *b* sets the location of the inflection point where a value of *b* between 0 to 1 can change the location of the inflection point from I_{min} to I_{max}. Finally, the overall shape of the curve is set by parameter *c*. As far as this work is concerned, parameter *c* is set to one. Table (2.1) shows the range in fermi parameters used in this study to realize a wide range of dynamic environmental flows using non-proportional water allocation rules.

Figure 2.2 illustrates an exemplary visualization of Fermi function defined by equation (4) and (5) while fixing i and j and varying 36 combinations of a and b. Substantially different from no-storage systems (e.g., small hydropower), here we need to account for effects due to the storage status, which may affect the allocation decision. These effects are accommodated by introducing a storage factor (f_s). We calculate the Relative Stored Water (RSW) in the dam with respect to the storage boundaries (V_{min} and V_{max}) and then the storage factor is calculated using a logistic function [*Verhulst*, 1845] as:

$$RSW = \frac{V - V_{max}}{V_{max} - V_{min}}, \qquad f_s = \frac{L}{1 + exp(-k(RSW - x_0))}, \qquad (2.5)$$

where *L* is the maximum curve value, k determines the curve's steepness and x_0 is the x-value of the sigmoid curve midpoint. For the purpose of this study, we bound the storage factor between 0 and 1 by defining the logistic parameters as follows: *L*=1, *k*=10 and x_0=0.5. From a practical point of view, the storage factor allows to make enough room in the reservoir in order to recover water from flood events while respecting the minimum storage, V_{min} and maximum storage, V_{max}. This range is regulated by releasing more (less) water to the environment when higher (lower) volume of water is stored in the dam. In this way, environmental flows are dynamic even out of the concomitance of flood events and maximum storage, the latter case happening for minimal-flow managed systems. The use of the storage factor associated with non-proportional allocation rules therefore serves as a flood control, limiting the release of high water pulses in a riverine corridor with low hydrological variability. This efficient water management results in a more ecologically friendly water release and reduces the risks associated with floods as mentioned. Notice that the storage factor acts as a dynamic seasonal minimal flow release where a higher summer threshold for minimal flow is usually imposed to ensure sufficient habitat suitability for different species (i.e., fishes). Considering equation (2.5), the storage factor appears to satisfy this environmental need as higher relative stored water in the dam in summer season results in a higher f_s.

Finally the ranges of competition for equations (2.3) are defined as follows:

$$I_{min} = Q_{mfr}, \qquad\qquad I_{max} = \frac{Q_{env}^{max} - Q_{mfr}}{j f_s} + Q_{mfr}, \qquad\qquad (2.6)$$

where Q_{env}^{max} corresponds to the maximal flow allocated to the environment and is defined as $Q_{env}^{max} = f_s(V)\alpha\max(I)$. Parameters α and f_s determine the magnitude of the maximal environmental flow, and a value of $\alpha = 0.3$ is selected for the purpose of this study. Such maximal environmental flow release allows to save water during floods and limits flood related damages. It should be mentioned that α can be regulated to satisfy the environmental needs of every specific site.
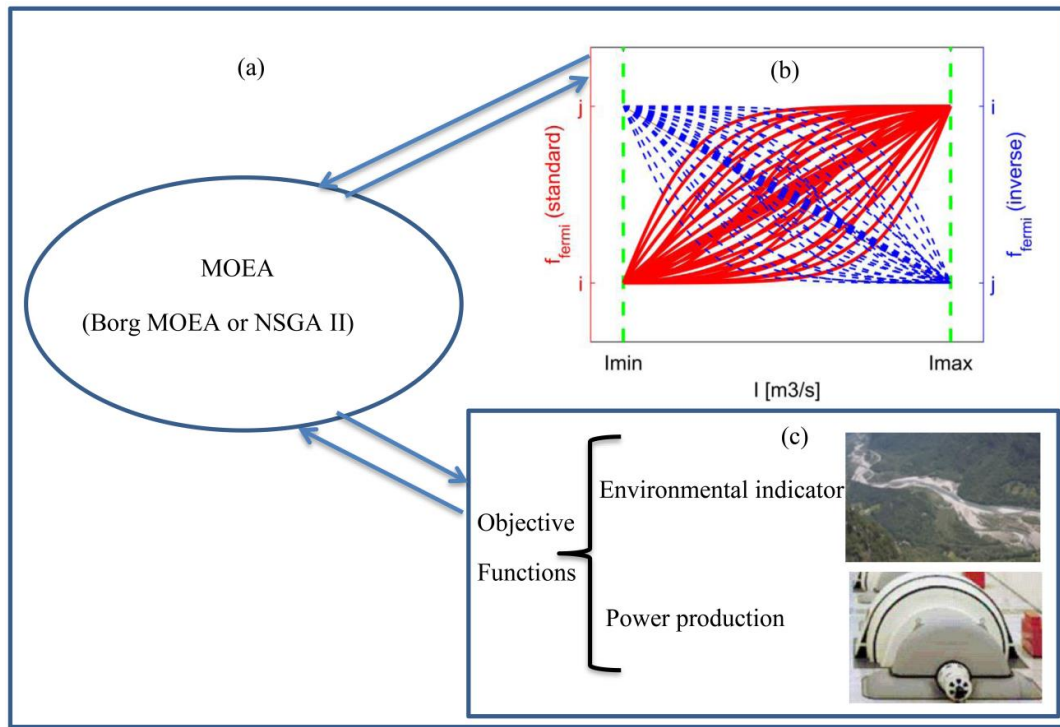
Figure 2.2 – (a) DPS framework (b) 72 Exemplary visualization of fermi function input variables $(i, j, a$ and $b)$ while fixing i and j and varying a and b. Red curves show standard Fermi functions $(i < j)$ and blue curves represent inverse Fermi functions $(i > j)$. (c) Objective functions.

2.2.2 Environmental indicator

The environmental suitability of each water allocation policy that releases Q_{env} to the environment is evaluated by considering both fish habitat suitability and hydrological indicators.
Fish indicators are of practical use because fishes are an important source of food and can assign an economical benefit of a river status to the neighboring human community. Also,

for many fishes habitat requirements are life stage dependent in terms of river morphology and hydrodynamics. Furthermore, because of the migration behavior of many species, fish can provide additional information about the longitudinal and lateral connectivity and the passability of a river [*Schmutz et al.*, 1998]. In the present study, the fish habitat indicator is defined based on the Weighted Usable Area (WUA) curves of the fishes modeled, for example by use of PHABSIM software [*Maddock*, 1999; *Bloesch et al.*, 2005]. The threshold for the environmental flow rate is defined by the point when fish habitat suitability for fishes rapidly becomes unfavorable. Two thresholds for young and adult fishes are defined where the curvature of the WUA curves is maximized (see Section 2.3.1). These thresholds were defined on a basis that above a given flow rate the relative environmental benefits for the fishes does not change significantly [*Gippel and Stewardson*, 1998]. Our methodology to assess the fish habitat suitability is inspired by the tool called the Continuous Under Threshold (CUT) habitat duration curves [*Capra et al.*, 1995] where the maximum number of consecutive days below the threshold for young and adult fishes are considered as the most critical period for fish habitat. We follow the same approach but in addition to only considering consecutive days below a threshold, we also calculate the magnitude of the stress period by summing the difference values of WUA for $Q < Q_{threshold}$ and WUA for $Q_{threshold}$. We call this Continuous Magnitude Under Threshold (CMUT). Then fish habitat indicators (bounded between 0 and 1) for young and adult fishes are defined based on the maximum value of CMUT as:

$$Ind_{f,y} = 1 - \frac{max(CMUT_{d,y}) - max(CMUT_{n,y})}{max(CMUT_{d,y}) + max(CMUT_{n,y})}, \tag{2.7}$$

$$Ind_{f,a} = 1 - \frac{max(CMUT_{d,a}) - max(CMUT_{n,a})}{max(CMUT_{d,a}) + max(CMUT_{n,a})}, \tag{2.8}$$

where d and n indices indicate the river flow rate downstream and upstream of the dam, respectively. Furthermore, y and a represent the young and adult fishes. Finally, the geometric mean is used to integrate young and adult fish indicators into a global fish indicator:

$$Ind_{fish} = \sqrt{Ind_{f,y} Ind_{f,a}}. \tag{2.9}$$

Hydrological regimes play an important role in characterizing riparian ecosystems. Efficient ecosystem management can be realized by good understanding hydrologic alteration due to human activities. In this study, the extent of hydrologic change for every water allocation policy is based on the methodology proposed by *Richter et al.* [1997] called the Indicators of Hydrologic Alteration (IHA). The IHA is based on analyzing flow rate and consists of five groups (Table 2): Magnitude timing (1), Magnitude duration (2), Timing (3), Frequency duration (4), Rates of changes frequency (5). The Rate of non Attainment (RnA) and Coefficient of Variation (CV) for 32 IHA are calculated for post (downstream of water intake) and pre (upstream of water intake) impact flow rates. RnA is defined as the fraction of years in which each indicator falls outside the plus and minus one standard deviation around the mean and CV is the ratio

of standard deviation to mean in each year. These RnAs and CVs characterize hydrological changes by measuring the number of times and quantity the flow regime is below/above a certain threshold (plus/ minus one standard deviation around the mean) [*Gorla and Perona*, 2013]. However, it should be noted that because we are removing water from the river, which is inevitable due to the hydropower consumption and storage, the benefit of the absolute magnitude of flow regime is not captured. Nonetheless, we believe that considering RnAs and CVs can provide a good understanding of the river hydrological changes due to installation of hydropower systems, especially variability of the flow regime. The latter is an important aspect of the flow regime because of the inconsistencies associated with the current imposed flow regulations (i.e., MFR) in many hydropower systems which has caused several environmental shortcomings, such as reduced the ecosystem biodiversity. Furthermore, the mean squared distance between the pre and post impact RnAs and CVs are calculated [*Bizzi et al.*, 2012]. Ultimately, the global hydrological (Ind_{hydro}) indicator is found by aggregating and averaging, as detailed in *Razurel et al.* [2016].

Finally the global environmental indicator is calculated by geometrically averaging the fish habitat and hydrological indicators as follows:

$$Ind_{env} = \sqrt{Ind_{fish}Ind_{hydro}}. \tag{2.10}$$

It should be noted that the choice of defining a single environmental indicator is because it can explicitly show the environmental impact of flow release policies. This way of considering the environmental indicator is more understandable for the community and reservoir operators. Furthermore, all the 66 indicators defined in this study are saved and analyzed for a detailed environmental assessment of flow release policies.

2.2.3   Optimization method

In this study, we use multiobjective evolutionary algorithms (MOEAs) to find the Pareto's frontier of the water allocation problem. That is, we search the optimal Fermi parameters (i, j, a, b) of Pareto optimal water allocation policies, which ensures the most efficient ecological-economical management. Here, we briefly summarize this methodology.

MOEAs are inspired by the mechanism that biological organisms evolve and transfer their characteristics to their offspring. Form a mathematical point of view, MOEAs are stochastic, direct and population based optimization methods aimed at finding the optimal solutions for complex problems without trivial analytical solutions. The term stochastic refers to the use of random operators to search the solution space. It is direct because the fitness of a solution is evaluated by using the value of an objective function and not its derivatives. It is also population based, which means that in every generation a number of potential solutions represent the behavior of the solution space.

MOEAs generate an initial random population and let them evolve to optimal solutions where fitter solutions have a higher chance to survive and reproduce. The evolutionary process is

Table 2.2 – Summary of hydrological parameters used in the indicators of hydrologic alteration and their characteristics.

IHA statistics group	Regime characteristics	Hydrological parameters
Group 1: Magnitude of monthly water conditions	Magnitude timing	Mean value for each calendar month
Group 2: Magnitude and duration of annual extreme water conditions	Magnitude duration	Annual minima 1-day means
		Annual maxima 1-day means
		Annual minima 3-day means
		Annual maxima 3-day means
		Annual minima 7-day means
		Annual maxima 7-day means
		Annual minima 30-day means
		Annual maxima 30-day means
		Annual minima 90-day means
		Annual maxima 90-day means
Group 3: Timing of annual extreme water conditions	Timing	Julian date of each annual 1-day maximum
		Julian date of each annual 1-day minimum
Group 4: Frequency and duration of high/low pulses	Frequency duration	No. of high pulses each year
		No. of low pulses each year
		Mean duration of high pulses within each year
		Mean duration of low pulses within each year
Group 5: Rate/frequency of water condition changes	Rate of changes frequency	Means of all positive differences between consecutive daily values
		Means of all negative differences between consecutive daily values
		No. rises
		No. falls

usually performed by applying two main filtering operators: crossover and mutation. The selection methodology is known as roulette wheel, where the solutions with higher fitness are more likely to be selected and evolved. In this study, we benchmark two state of the art MOEAs (NSGA II and Borg MOEA) to build the Pareto's frontier. NSGA II [*Kalyanmoy et al.*, 2002] is a relatively static MOEA which has been extensively used in the literature. In contrast, Borg MOEA [*Hadka and Reed*, 2013] is a self-adaptive MOEA which has been found by some recent studies to be efficient in finding efficient operational rules for reservoir systems [e.g., *Salazar et al.*, 2016]. An assessment of the quality of the Pareto's frontier, and its associated computational cost, can be made by comparing the results from these two methods. In the following, we briefly review these methods.

NSGA II [*Kalyanmoy et al.*, 2002] is a fast and elitist MOEA which has been extensively used as an efficient tool for solving multiobjective problems. It features a fast nondominated sorting methodology by calculating a domination count and a set of solutions which dominate each solution. For every generation, nondominated solutions are sorted by comparing both current population and previously found best nondominated solutions. This sorting avoids the chance of losing elite solutions which also results in a faster and more efficient convergence. Furthermore, along with the convergence to Pareto's frontier, it is desired to ensure diversity so as to have a wide spread in the optimal set. NSGA II uses a parameter-less mechanism to maintain diversity in the Pareto's frontier. Furthermore, efficient tuning of NSGA II operators significantly affects its successful convergence to the optimal solution [*Salazar et al.*, 2016]. As far as this study is concerned, optimal values for mutation and crossover probability were

found to be 0.1 and 0.9, respectively.

The self-adaptive Borg MOEA [*Hadka and Reed*, 2013] provides robust optimization by proposing several novel features as well as incorporating design components of other MOEAs. Convergence and diversity of Pareto's frontier are ensured using ϵ-dominance archives. ϵ-progress as a computationally efficient measure of search progression and stagnation is also used. In the case of low convergence speed and search stagnation, randomized restarts are triggered. The latter revives the search by diversifying and resizing the population while preserving selection pressure. Furthermore, to enhance the search domain, Borg incorporates multiple recombination operators and automatically adapts their use based on their relative performance. To summarize, the procedure of the DPS proposed in this study is shown in Figure 2.2 where decision variable, objective functions and constraints are defined as follows:

Decision variables: Fermi parameters (i, j, a and b)

Objective functions: Environmental indicator (habitat+hydrology) and power production

Physical constraint: reservoir boundaries (V_{min} and V_{max})

Operational constraint: Q_{max}, I_{max} and the pattern of energy production.

2.3   Results for a synthetic case and discussion

2.3.1   Generation of synthetic data

In this section, our methodology is applied to a synthetic case study. First, we build a synthetic natural flow regime (Figure 2.3a) by rescaling the daily river discharge of the Maggia River located in southeast Switzerland, which is available for the pre-dam period (1929 to 1954). Then, we determine a possible reservoir storage size and hydropower nominal flowrate using the common integral method. The flow duration curve is used to define minimal flow requirement (Q_{mfr}=0.18 $\frac{\text{m}^3}{\text{s}}$ and Q_{2mfr}=0.21 $\frac{\text{m}^3}{\text{s}}$). In this way, the reservoir available storage, V_{max} is set to 41 Mm^3, and a sensitivity analysis for V_{max} will later be performed to evaluate the effect of uncertainties on the choice of reservoir size. For the sake of simplicity to illustrate the basic ideas of our methodology, we consider weekly periodic flowrate demands corresponding to the nominal turbine capacity where turbines operate only in the working days which are assigned to the hydropower as a first priority based on the available storage in the reservoir (Figure 2.3b).

Energy production is computed using the following storage-dependent relationship:

$$P = \rho Q_{hydro} g H(V) \frac{24}{10^6} [Mwh],\tag{2.11}$$

where ρ and g are water density and gravity, respectively. H is the reservoir water level, which is assumed to be a polynomial function of the storage (Figure 2.3c). Furthermore, Figure 2.3d shows the WUA curves considered in this study to calculate fish habitat indicators for both young and adult fishes. The results of our methodology are compared with other simulated policies, which are constant (one and two threshold) minimum flows (Q_{mfr} and Q_{2mfr}), and
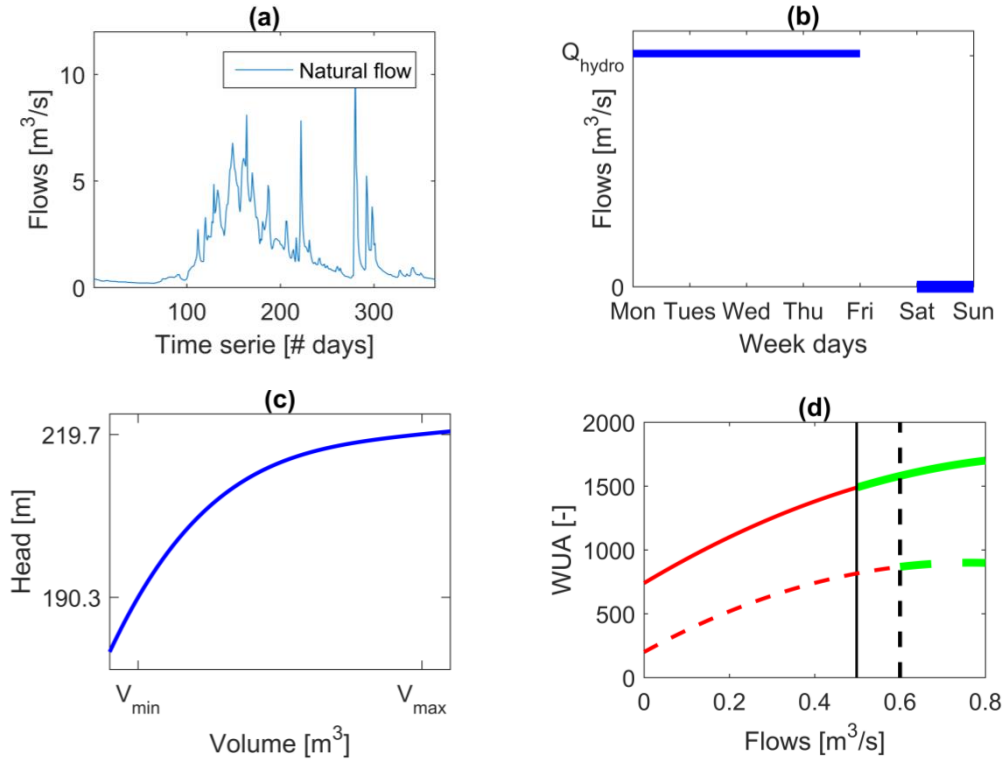
Figure 2.3 – (a) Natural flow regime. (b) Weekly hydropower flowrate demand. (c) Reservoir's head-volume relationship. (d) WUA curves for young (solid line curve) and adult fishes (dashed line curve). Vertical lines denote the assigned thresholds based on the WUA curves. The green and red colors represent the flow rates in which their associated WUA are higher and lower than the threshold, respectively.

proportional releases by assigning fixed percentages (from 1% to 15%) of the inflow.

2.3.2 Pareto frontier and optimal water allocation

Figure 2.4a shows the global efficiency plot resulting from adopting optimal non-proportional redistribution rules based on the Fermi functions and other proportional and MFR policies. Notably, an almost vertical (Pareto optimal) frontier where energy production is maximal can be identified. This is an important result because it shows that DEF releases via non-proportional redistribution rules guarantees better global efficiency of water storage system compared to policies applying constant minimum and proportional flow. The significant improvement in the ecological indicator at almost the same energy production is seen to arise precisely from the reservoir storage dynamic. Furthermore, as discussed in Section 2.2.3, NSGA II performance is dependent on parameters tuning. As shown in Figure 2.4, the Pareto's frontier simulated with Borg MOEA is the same as the one obtained with NSGA II. This indicates that the NSGA II parameters have been efficiently tuned. Also, it should be mentioned that in terms of running time, Borg MOEA used almost half the time as NSGA II to find the Pareto's frontier.

This reveals the fact that using an adaptive optimization approach can substantially speed up the optimization process.
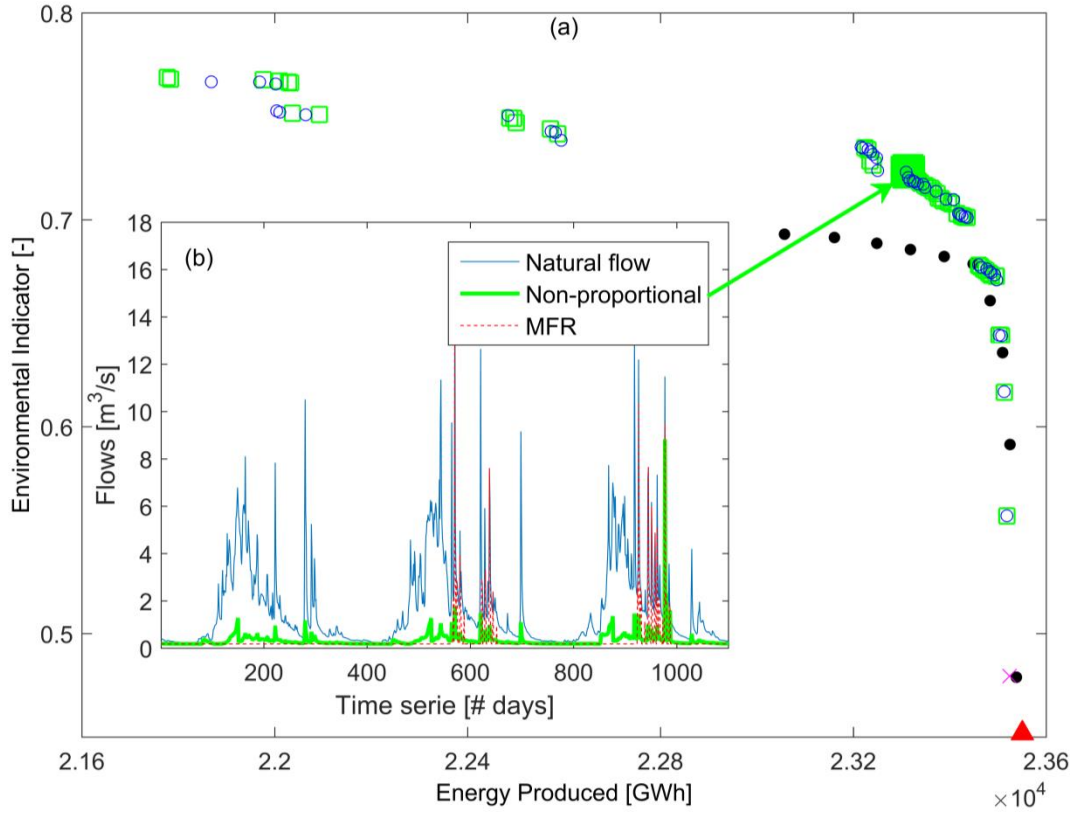
Figure 2.4 – (a) Pareto's frontier and alternative scenarios (minimal flow release and proportional release). Blue circles and green squares represent the scenarios located on the Pareto's frontier obtained with NSGA II and Borg MOEA, respectively. Black, cyan and red dots denote the proportional, seasonal MFR and MFR flow release policies, respectively. The bold green square is selected as an exemplary non-proportional flow release rule from Pareto's frontier and hereafter we perform some detailed analysis which can help for further evaluation and comparison between different flow release rules. The followings characterize the fermi parameters of this non-proportional flow release rule: $i = 0.11$, $j = 0.04$, $a = 7.4$, $b = 0.98$. (b) Hydrographs corresponding to different flow release rules.

Through non-proportional water allocation, the imposed flow releases create enough room in the reservoir to allow to capture and laminate flood events while recovering part of them for energy production. This is clearly seen by comparing the hydrograph resulting from applying the non-proportional flow release policy with that obtained for constant minimal flow (Figure 2.4b). Notably, although the quantities of water allocated in both policies are almost the same, the variability arising from non-proportional redistribution results in a more ecologically sustainable streamflow. From an ecological perspective such variability is indeed important to maintain transversal connectivity between the channel and floodplain, which occurs with a frequency comparable to the natural one.

Figure 2.5 shows the simulated daily volume of stored water in the reservoir resulting from both non-proportional and constant minimal flow requirement water allocation policies. As shown in this figure, an efficient reservoir storage dynamic policy allows for better environmental and economic efficiency. This dynamic behaviour in reservoir storage is mainly due to the use of storage factor in the non-proportional flow release policy, which enables for a more efficient water management. The efficient use of dynamic storage creates flow variability similar to natural flow by making enough room in the reservoir to capture and laminate flood events. The use of the storage factor is an alternative to the traditional way of managing water in dammed systems where a constant minimal flow is always allocated to the environment unless for the time when the maximum storage level in the reservoir is reached. In that case, the overflow must be also released to the river. On the one hand, in extreme conditions such releases may combine with flooding, which may harm urban areas and endanger human lives. Therefore, the storage factor allows to laminate the release of high water pulses during flooding events. As far as our synthetic case is concerned, non-proportional rules decrease the number of days corresponding to flood release due to reservoir overflow by approximately 75% compared to minimal flow policy (Figure 2.4). Furthermore, the ecological impacts of floods are vital for some riparian processes involving vegetation and transport phenomena in general [*Džubáková et al.*, 2015]. The dynamic flow release resulting from non-proportional water allocation policies can meet such environmental needs and enforce the release of higher flow pulses at the time of occurrence.
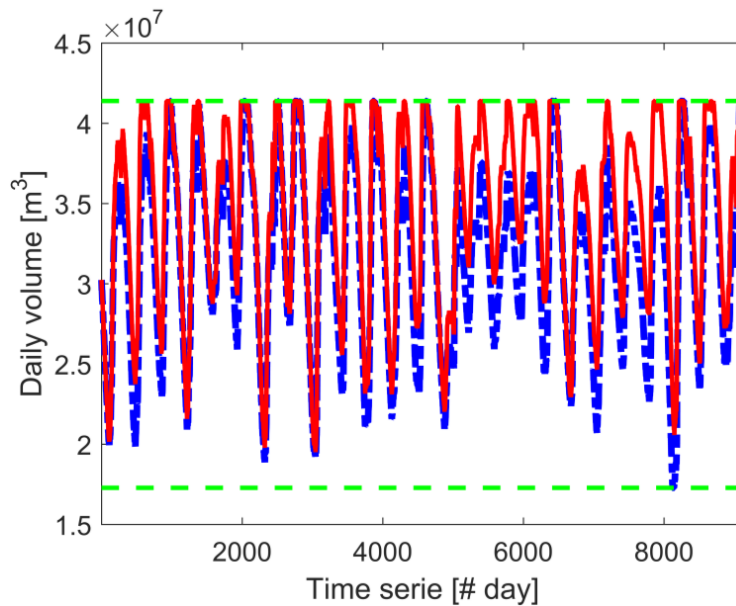
Figure 2.5 – Comparison of the simulated daily volume of stored water in the reservoir. Blue curve denote the non-proportional flow release and red curve represents the constant minimal flow requirement water allocation policy. Green dashed lines show physical boundaries of the reservoir (V_{max} and V_{min}).

Figure 2.6 shows the comparison between the natural regime (green line), constant minimum

flow (red line) and non-proportional flow release (blue line) for three exemplary IHA corresponding to three groups of Richter's hydrological indicators (i.e., 3, 4 and 5 from Table 2.2) representing flow variability. Non-proportional flow redistribution rules impact less on the natural flow regime compared to constant minimal flow water allocation policy. This environmental amelioration is significant when the Julian date (JD) of each annual 1-day maximum is considered (Figure 2.6a). This indicator describes the importance of the timing occurrence of high extreme water conditions within an annual cycle. A comparison of the impact of flow regime and timing provides a mechanism for evaluating if requirements for specific life-cycles are satisfied, the degree of mortality or stress related to extreme water conditions, such floods. As shown in this figure, the minimal flow release rule strongly offsets the annual timing of high events from the natural flow regime. This improvement in environmental efficiency is also seen when indicators of groups 4 and 5 are considered. These indicators describe flow variability based on the flow regime in terms of frequency, duration and rate of change of the flow regime. The time duration that a certain water condition lasts can determine if a particular life-cycle phase can be completed or the extent of a stressful period can accumulate. Furthermore, the rate of change in a water condition can be used as a measure to characterize the rate and frequency of inter-annual environmental change [*Richter et al.*, 1996a]. Figure 6b and Figure 2.6c show two exemplary indicators from groups 4 and 5, which are the number of high pulses each year and number of rises, respectively. These indicators clearly show that the variability arising from a non-proportional water release policy can enable significant environmental improvements. The CVs and RnAs for different flow release rules compared with the natural flow regime confirm these environmental benefits. As an example, Table 2.3 compares the simulated RnAs and CVs corresponding to the number of rising indicators (Figure 2.6c) under different flow regimes.
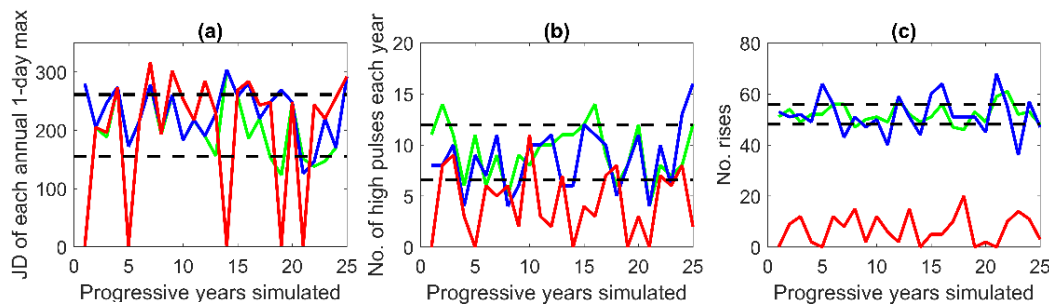
Figure 2.6 – Comparison of three selected IHA corresponding to three groups between the natural regime (green line), constant minimum flow (red line) and non-proportional flow release (blue line). Dashed lines define ± SD around the mean of the natural regime IHA.

2.3.3 Influence of reservoir storage and river hydrology

We now investigate the impact of storage size on dam ecological-economical efficiency under the assumption that our design for reservoir size in the synthetic case was conservative. We

Table 2.3 – Comparison of the simulated RnAs and CVs belonging to the number of rises indicator between the natural regime, constant minimum flow and non-proportional flow release.

	Natural flow regime	Non-proportional	Minimal flow requirement
RnA	0.4	0.6	1
CV	0.07	0.12	0.84

perform a sensitivity analysis where we vary the maximum storage size of the dam in the range $0.9V_{max} \div 1.4V_{max}$. Figure 2.7 shows that increasing the storage size allows for better environmental and economical (Pareto) efficiencies up to a certain storage size (i.e., in this case $\approx 1.3V_{max}$), as expected. This value corresponds to the reservoir volume that allows to capture and best allocates all the incoming water under the assigned hydrologic/climatic and energy production conditions. Furthermore, it should be mentioned that the energy production, corresponding to the vertical part of Pareto's frontier, slightly increases (1.8%) when the reservoir size changes from V_{max} to 1.3 V_{max}.
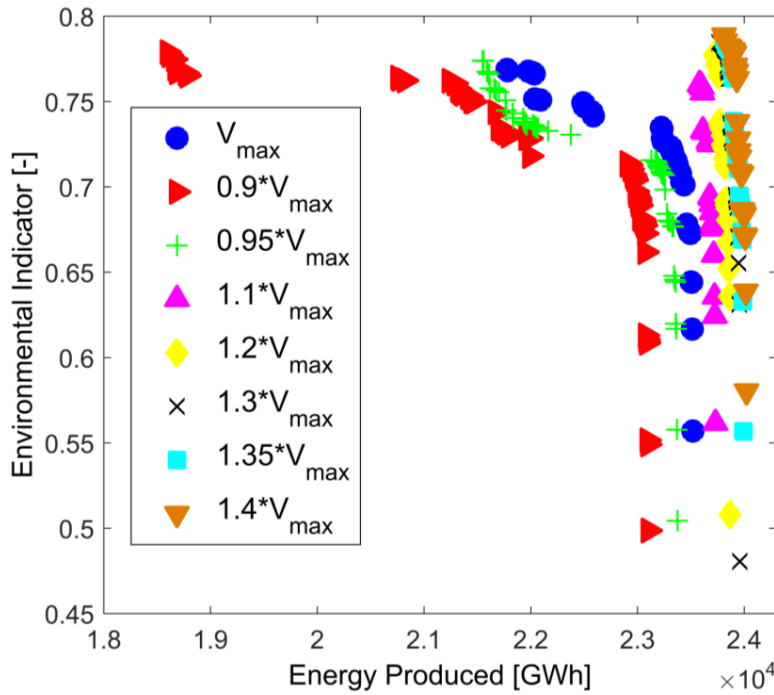
Figure 2.7 – Maximum reservoir storage size sensitivity analysis.

Another important variable that may influence the Pareto's frontier shape is the variability of the natural flow regime. To this purpose, we generate 100 random hydrological regimes by shuffling the 25 years of inflow data annually and investigating the change in the efficient frontier. While performing this shuffling process, the linear statistics of the inflow signals remains the same, thus preserving the catchment dynamics. Figure 2.8a shows the simulated

Pareto's frontiers resulting from all 100 hydrological regimes. In the lower-right side of the figure, the flow release policies are similar to constant minimal flow policies where less diversity is observed in the Pareto's frontier shape. Hence, when less water is allocated to the environment, the ecological-economic efficiency is less dependent on that particular hydrological regime. However, the Pareto's frontier shape is more sensitive to hydrological regimes when more water is released to the environment. This can be seen in the top-left side of the figure where the Pareto's frontier shapes are more dispersed. Furthermore, from these Pareto's frontiers, non-dominated scenarios (red squares in the figure) can be selected from the most efficient both economical and environmentally friendly flow release policies under different hydrological regimes as described. Therefore, we can investigate the performance of these specific efficient scenarios when they are operated with the same 100 random hydrological regimes. Flow release rules that are less dependent on hydrological regimes are more appealing because they can still perform efficiently under hydrological changes. In that respect, we consider only those scenarios that are expected to be less dependent on the flow regime (nondominated scenarios which have energy production more than $2.3*10^4$ GWh in Figure 2.8a). As it can be seen in Figure 2.8b, these selected flow release rules still show efficient environmental and economic performances when they operate under different hydrological regimes. In particular these non-proportional flow release rules guaranty better global efficiency under different hydrological regimes compared to minimal flow release policies.
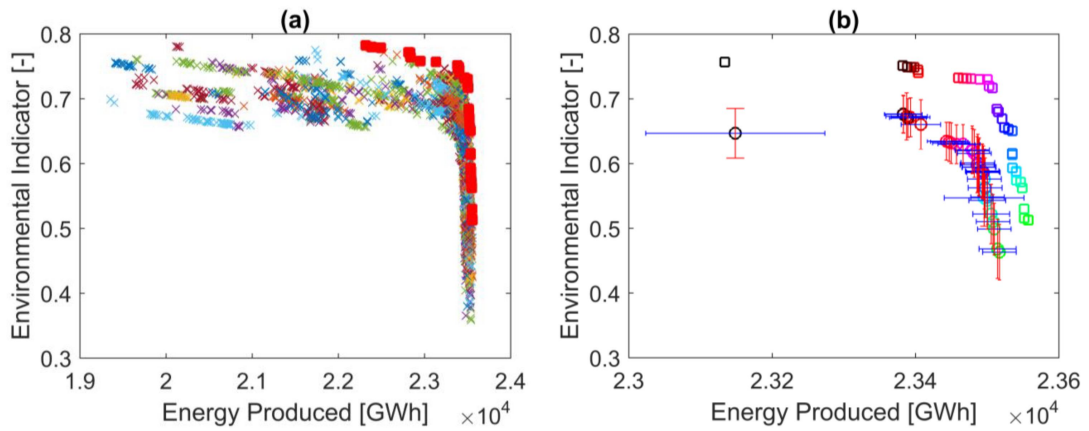
Figure 2.8 – The impact of hydrological changes on the shape of Pareto's frontier: (a) comparison of the simulated Pareto's frontiers resulting from 100 random hydrological regimes. Every color represents a Pareto's frontier and red squares denote to nondominated scenarios among all the Pareto's frontiers. (b) Evaluation of the selected flow release rules (squares) performances under random hydrological regime changes. Symbols with the same color represent the calculated energy production and environmental indicator with the same flow release rule. Circles denote the mean environmental and economical efficiencies simulated with 100 hydrological regimes; horizontal and vertical error bars represent ± SD around the mean of the simulated power productions and environmental indicators, respectively.

The results shown here are promising, although we stress that implementing non-proportional

redistribution rules in existing power plants should be carefully evaluated. For example, for power plants that are already capable of storing all incoming flows and laminate all flooding, it may not be possible to improve the environmental indicator at equal energy production. In particular, this should be done in relation to specific river hydrologic regime, size of the actual dam and the flexibility of intakes that impound the surrounding water courses. This requires additional and more thorough numerical analyses, as well as an evaluation of the environmental benefits, by means of case by case specific indicators.

2.4   Conclusion

We make use of two MOEAs (NSGA II and Borg MOEA) and compare their relative performance in our DPS framework to build Pareto's frontier. The results suggest that non-proportional flow releases provide a broader spectrum of globally-efficient performances of the whole system (i.e., hydropower plus environment) compared to constant minimum flow release operational policies. More explicitly, a vertical Pareto's frontier in the global efficiency plot means that substantial improvement in the environmental indicator can be achieved without inducing a significant loss in energy production. This result can be realized by engineering new (i.e., non-proportional) dynamic environmental flow release policies. Such an improvement is found to be mainly due to a better use of reservoir storage dynamics, which enables to capture and laminate flood events while recovering part of them for energy production. Although not for all, these changes could bring substantial improvement to hydropower systems with specific basin soil and hydrological characteristics. Regarding reservoir size, it was shown that Pareto solutions maintain a vertical frontier over a reasonable storage size range, which offers some design flexibility. The Pareto's frontier shape under different hydrological regimes was also assessed, indicating that non-proportional flow releases remain efficient also under uncertainties of the hydrological statistics.

3 Modeling macroroughness contribution to fish habitat-suitability curves[1]

Abstract

Improved water management strategies necessitate a solid understanding of environmental impacts associated with various flow release policies. Habitat suitability models use hydrodynamic simulations to generate Weighted Usable Area (WUA) curves, which are useful in characterizing the ecological suitability of flow release rules. However, these models are not conveniently run to resolve the hydrodynamics at the smaller scales associated with macroroughness elements (e.g., individual stones), which produce wakes that contribute significantly to habitat suitability by serving as shelter zones where fishes can rest and feed. In this study, we propose a robust environmental indicator that considers the habitat generated by the wakes downstream of stones and can thus be used to assess the environmental efficiency of flow release rules for impounded streams. We develop an analytical solution to approximate the wake areas behind macroroughness elements, and the statistical distribution of wake areas is then found using the derived distribution approach. To illustrate the concept, we apply our theory to four exemplary river streams with dispersed stones having different statistical diameter size distributions, some of which allow for an analytical expression of the WUA. We additionally investigate the impact of spatiotemporal changes in stone size distributions on the usable area and the consequent threshold flows. Finally, we include the proposed environmental indicator to solve a multiobjective reservoir optimization problem. This exemplifies its practical use and allows stakeholders to find the most favorable operational rules depending on the macroroughness characteristics of the impounded stream.

3.1 Introduction

Changing the natural flow regime causes an environmental degradation in alpine streams. Such changes occur due to climate change and other anthropic pressures (e.g., hydropower, irrigation, urban and industrial uses, etc.) on alpine streams [*Poff et al.*, 1997; *Birsan et al.*,

---

[1]The contents of this chapter are published in: Niayifar, A., Oldroyd, H.J., Lane, S.N. and Perona, P., 2018. Modeling Macroroughness Contribution to Fish Habitat Suitability Curves. Water Resources Research, 54(11), pp.9306-9320.

2005; *Arthington et al.*, 2006; *Assani et al.*, 2010]. Quantifying the environmental impacts of altering the natural flow regime on the riverine ecosystem still remains difficult and hence, controversial. Environmental indicators are typically used to assess the extent of disturbances in a riverine ecosystem, and indicators based on the habitat availability have been widely used in the literature [e.g., *Bloesch et al.*, 2005; *Razurel et al.*, 2016]. Habitat availability is often assessed for different species by using modeling software such as CASiMir and PHABSIM [*Schneider*, 2001; *Milhous et al.*, 1989; *Maddock*, 1999]. These software packages model Weighted Usable Area (WUA) curves for the fishes to define a fixed threshold for minimal flow releases, or the rules imposed, usually by government entities, to continually release at least a minimum discharge to the environment. Determination of this minimum is typically based on the break point of the WUA curve, or the point below which the habitat suitability for the fishes decreases significantly. There are different approaches proposed to define break points [e.g., *Stalnaker and Arnette*, 1976; *Annear and Conder*, 1984; *Gippel and Stewardson*, 1998], and a common technique used in habitat suitability modeling is to consider the break point to be the discharge for which the WUA curve is maximized. The fish habitat indicator is then calculated by counting the maximum number of consecutive days characterized by flows below this critical threshold [e.g., *Capra et al.*, 1995; *Razurel et al.*, 2016].

The WUA curve and the associated threshold are calculated based on the streamflow characteristics such as the flow velocity. The threshold is very sensitive to the low velocity regions, i.e., quiet zones at the bank, in wakes behind macroroughness elements (i.e., big stones), etc. [*Carolli et al.*, 2017]. Figure 3.1a shows an exemplary change in the flow pattern due to the presence of a macroroughness element, marked by a significant decrease in flow velocity in the wake region. These low velocity or stationary regions act as refuge zones, as fishes minimize energy expenditure by resting in such regions where they can also quickly move to nearby faster waters to feed [*Hayes and Jowett*, 1994]. Some recent studies have investigated the role of swimming energetics in fish habitat suitability [e.g., *Tritico and Cotel*, 2010; *Taguchi and Liao*, 2011; *Lacey et al.*, 2012; *Enders and Boisclair*, 2016]. For example, *Enders et al.* [2005] proposed a relationship to calculate the swimming cost for juvenile Atlantic salmon (salmo salar) based on the local hydrodynamic conditions and the fish body mass. Position choice and swimming costs of salmo salar in turbulent flow was also studied by *Wilkes et al.* [2017] who found that fishes most often select the cells adjacent to obstacles (i.e., in wakes). Additionally, these low shear stress zones significantly affect the diversity of periphyton and invertebrates in a stream [*Biggs et al.*, 1997]. Furthermore, the enhancement of the local turbulence intensity near the edges of the wakes results in an increased oxygenation rate [*Moog and Jirka*, 1999b]. In general, all of these factors make wake regions suitable fish habitats.

Numerical software packages can model the usable area curves corresponding to the riverine ecosystem on large scales, but their low spatial resolution is not able to capture the smaller scale features such as the wakes downstream of macroroughnesses. Substantial advancements in computer science and technology have made it possible to develop high resolution 2D models [e.g., *Ernst et al.*, 2010; *Pasternack et al.*, 2008]. These models can have up to meter

resolution and therefore, in the future, might also be able to efficiently resolve the wakes associated with very large boulders over long river reaches. However, for a full river-scale simulation, the typical mesh resolution scale used in 2D numerical simulations is larger than the macroroughness size for practical reasons [*Lane et al.*, 2006] and also to reduce computational costs in 3D models. Consequently, the presence of macroroughness elements is filtered (or cannot be properly resolved), and their effects on the simulated WUA curves are omitted. Habitat suitability models, at best, can consider a criterion of presence/absence of stones at the meso-scale as an input to determine the suitability of a mesohabitat [*Parasiewicz*, 2007; *Vezza et al.*, 2014]. However, these approaches are rather qualitative and do not directly calculate the wake areas associated with stones of various size distributions.

<div align="center">(a)   (b)</div>
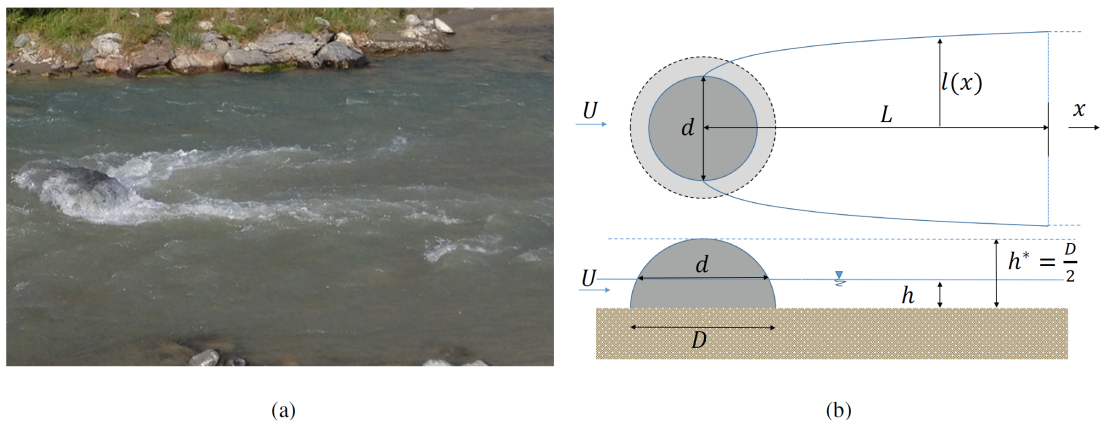
Figure 3.1 – (a) A visual example of the macroroughness effects on local river flow (b) schematic of the wake and related variables.

There have been extensive numerical and experimental studies investigating the effects of obstacles on the free stream flow [e.g., *Tennekes and Lumley*, 1972; *Coutanceau and Bouard*, 1977; *Roulund et al.*, 2005]. Complex flow patterns generated by a single macroroughness element and the associated ecological impacts have been further investigated by using computational fluid dynamic (CFD) models [*Shen and Diplas*, 2008]. *Negretti et al.* [2006] developed an analytical solution for the characteristic spatial scales of a turbulent wake in shallow flows. They started from the depth-averaged mass conservation equation and Reynolds-averaged equations for shallows flows and found an approximated solution by introducing scaling arguments and using the dominant balance approach, which considers leading order terms. Their solution consists of two analytical expressions to characterize the longitudinal and transversal length scales of shallow flow wakes.

Flow around rocks and the consequent ecological ramifications have also been studied in laboratory experiments and field studies. For example, *Moghadam and Keshavarzi* [2007] measured the flow structure behind a quarter-sphere fish habitat, mimicking a stone, in a laboratory flume. They characterized the low velocity wake region downstream of the 'stone'

that is favorable for fishes for various flow depths. In addition to ecologically favorable wake velocities, lab experiments have shown that macroroughness elements play a role in enhancing the oxygenation rates in streams [e.g., *Kucukali and Cokgor*, 2008], which promotes overall ecological health and helps to sustain habitat for aquatic life [*Kramer*, 1987]. These enhanced oxygenation rates have been found to sharply decrease as the macroroughnesses start to become submerged due to the decrease of the free surface turbulence level. Furthermore, field studies by *Buffington et al.* [2004] in mountain catchments indicate that hydraulic roughnesses are important fish spawning habitats.

In this paper, we aim to develop an analytical approach to model the total wake area for alpine water courses characterized by the presence of sparsely distributed macroroughness elements, i.e., stones, whose spatial characteristics could be obtained via remote sensing techniques (e.g., drones and image processing). To investigate the model's capabilities and exemplify its practical use, the model is applied to four examples of stones with sparse but different statistical distributions of diameter sizes. We use these to calculate the respective usable area curves as a function of discharge, which can be used to define environmental flow thresholds for alpine streams. We further investigate the impact of stone size distributions on the threshold flow and apply the results in a multiobjective optimization problem to find the most efficient operational release rules for a hydropower system. This paper is structured as follows: The analytical model is described in Section 3.2, followed by results presented in Section 3.3. Finally, a discussion of the model results and conclusions are provided in Section 3.4 and 3.5, respectively.

3.2 The model

3.2.1 Usable Area behind a single stone

We consider a straight river reach of width, w, slope, s, and bed roughness given by an average Manning coefficient, n, which includes the resistance to the bulk flow introduced by the presence of macro-scale roughness elements. We assume local, uniform flow conditions for the flowrate, Q, which can however, slowly change in time, and stones are considered to be hemispherically-shaped with maximum diameter, D. The range of hydrodynamical conditions suitable for fish habitat can vary by species. However, favorable habitat conditions generally tend toward lower velocities and so we additionally assume that the low velocity wake region is usable habitat area [e.g., *Buffington et al.*, 2004; *Kucukali and Cokgor*, 2008], as detailed in Section 3.1.

From the Manning-Strickler relationship, we obtain the river depth, h

$$h = \left(\frac{Qn}{ws^{1/2}} \right)^{3/5},$$

(3.1)

which also determines whether a stone is partially-submerged ($h < \frac{D}{2}$) or fully-submerged ($h \geq \frac{D}{2}$), as shown in Figure 3.1b. Note that $h^* = \frac{D}{2}$ denotes the water depth where the

stone becomes submerged. In this case, we assume the wake is no longer relevant for defining "suitable" conditions. This assumption is validated by study by *Moghadam and Keshavarzi* [2007], which shows a significant reduction in the wake size when the 'stone' becomes submerged. In addition, a submerged stone does not perturb the free surface to enhance oxygen entrainment and therefore cannot benefit the stream by increasing the oxygenation rate [*Kucukali and Cokgor*, 2008].

From equation (3.1), the submerged condition can be specified in terms of the flowrate, Q_D, submerging stones of size, D, i.e.,

$$Q_D = \frac{D^{5/3} s^{1/2} w}{2^{5/3} n}.$$ (3.2)

For the partially-submerged condition with a given flowrate, Q, the water surface intersects the stone of size D at the elevation, h, where the local, free surface stone diameter, d, is

$$d = \frac{2h}{Tan[ArcSin[\frac{2h}{D}]]} = D\sqrt{1 - \frac{4\left(\frac{nQ}{\sqrt{s}w}\right)^{6/5}}{D^2}},$$ (3.3)

which is a function of both D and Q (see also Figure 3.1b).

Under the assumption that the stone's wake is determined by its diameter at the water surface (for given submergence conditions), we use the analytical model of *Negretti et al.* [2006] to estimate the longitudinal and transversal expanse of the wake in the far wake region. It should be mentioned that the analytically derived wake size for a cylinder, as used by *Negretti et al.* [2006], provides a slightly conservative estimate of the wake region for a hemisphere which has a larger diameter at lower depths. For shallow water flow, *Negretti et al.* [2006] derived the longitudinal interaction length, L, from first principles, which reads

$$L = \frac{8h}{f_d},$$ (3.4)

where f_d is the river bed friction factor, which is related to the Manning coefficient by

$$f_d = \frac{8n^2 g}{h^{1/3}},$$ (3.5)

where g is gravitational acceleration. They additionally derived the transversal width of the wake as

$$l = d\sqrt{\frac{1 - e^{-\frac{x}{L}}}{8S}},$$ (3.6)

where e is the exponential function, x is the distance downstream from the stone center and S is the stability number, which is defined as [*Negretti et al.*, 2006]

$$S = \frac{f_d}{4} \frac{d}{h}. \tag{3.7}$$

Note that L equation (3.4) depends on the hydrodynamic conditions, whereas equation (3.6) also depends on the stone size and varies as a function of L (see also Figure 3.1b). Hence, for a given stone size and set of hydrodynamic conditions, we can develop an expression for the area of the wake behind a stone. Since $L >> D/2$, the wake area is much larger than half of the horizontal cross-sectional area of the stone. In addition, we assume that the far-wake solution by *Negretti et al.* [2006] also provides a reasonable estimate of the near-wake areal expanse. Therefore, we obtain the wake area, A_w, by integrating the analytical expression for l, the transversal length scale equation (3.6), from the stone center to the longitudinal interaction length, L,

$$A_w = 2 \int_0^L l(x) dx = 2L \left(d \frac{h}{2f_d} \right)^{1/2} B, \tag{3.8}$$

where B is a constant given by equation (3.10). Finally, combining equation (3.8) with equations (3.1), (3.4) and (3.5), one finds

$$A_w = \sqrt{ \frac{D \sqrt{1 - \frac{4\left(\frac{nQ}{\sqrt{s}w} \right)^{6/5}}{D^2}} \left(\frac{nQ}{\sqrt{s}w} \right)^{12/5}}{4g^3 n^6} } B, \tag{3.9}$$

where

$$B = -2C + ln \left(\frac{1+C}{1-C} \right), \tag{3.10}$$

and

$$C = (1 - \frac{1}{e})^{1/2}. \tag{3.11}$$

Hence, for a given stone size, D, the wake area given by equation (3.9) is the available habitat, or usable area, behind a single stone as a function of the flowrate, Q, stream width, w, slope, s and manning coefficient, n. Figure 3.2 shows the usable area as a function of specific flow rate, $Q^* = \frac{Q}{\sqrt{s}w}$, for different stone diameters and manning coefficients. This area increases non-monotonically for increasing flowrate, Q; that is, it increases up to a maximum, A_w^{max}, and then decreases to zero in correspondence with the flowrate, Q_D, for which the stone becomes submerged, i.e., equation (3.2).
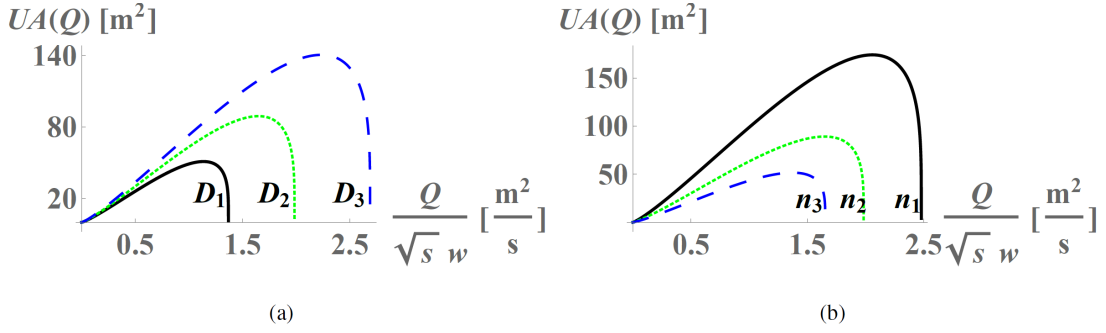
Figure 3.2 – Exemplary visualization of the wake area with different parameters: (a) different stone diameters (n=0.05 [$\frac{s}{m^{1/3}}$]); $D_1 < D_2 < D_3$ (b) different Manning coefficients (D=0.5 [m]); $n_1 < n_2 < n_3$.

Thus, the wake size is flow-limited for flowrates approaching zero, and becomes obstacle-size-limited for flowrates approaching Q_D. Alpine streams may not dry up completely, and the flow-limited condition may not be reached. We will, however, include the possibility that the water course dries up for the sake of generality. To upscale this result for UA, we additionally calculate the total wake area for stones randomly and sparsely distributed in a river reach, and investigate how it changes for varying flow conditions.

3.2.2 Total usable area behind randomly-distributed, sparse stones

As in Figure 3.1, stones can be assumed to be sparse and distributed randomly in the river reach. If no two wakes interact, i.e., that each wake is dependent only on D and the *bulk* hydrodynamic conditions, then the relative distance between any two stones is larger than L, the interaction length (equation (3.4)), for any flowrate, $0 < Q < Q_{D_{max}}$, where $Q_{D_{max}}$ is the flowrate for which the largest stone in the size distribution becomes submerged. Stones are detectable from aerial view, and assuming they are approximately semi-spherical, the characteristic size density distribution, $p_s(D)$, can be determined (e.g., by surveying with a drone and implementing image processing; see Section 4.2). Note that for a given, specific flowrate, Q^*, equation (3.9) also provides the change in total wake area for variable stone size (Figure 3.3). Supposing stones are distributed sparsely and with a size density distribution, $p_s(D)$, defined in the range ($D_1 \leq D \leq D_2$) such that $\int_{D_1}^{D_2} p_s(D)dD = 1$, where D is the dummy variable of integration, the density distribution of the wakes for a given flow rate can be obtained by using the derived distribution approach. First, we invert the wake-stone size relationship equation (3.9) to obtain

$$D(A_w) = \frac{2\sqrt{\frac{\left(\frac{nQ}{\sqrt{s}w}\right)^{6/5}(B^4 Q^6 + 4A_w^4 g^6 n^6 s^3 w^6)}{B^4 Q}}}{Q^{5/2}}, \tag{3.12}$$
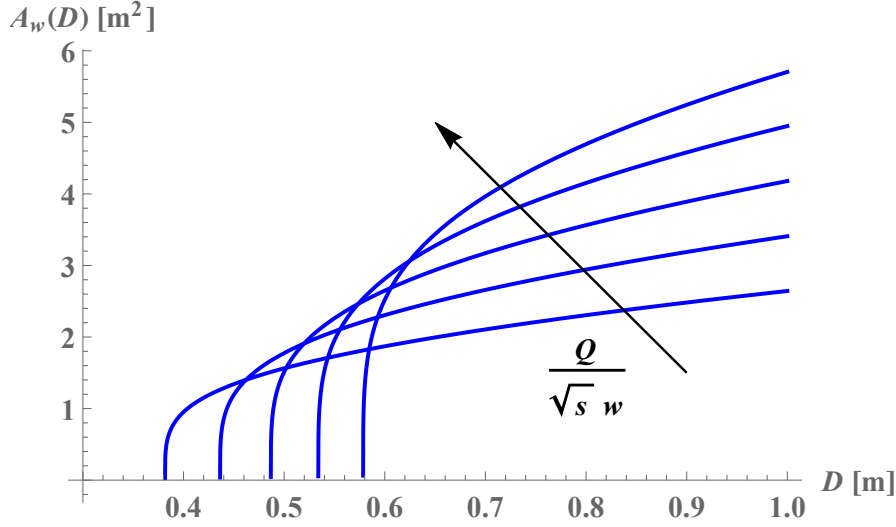
Figure 3.3 – Wake area as a function of stone size using different parameters ($n=0.05$ [$\frac{\text{s}}{\text{m}^{1/3}}$]). Notice that all stones with a size smaller than D_m are submerged and do not contribute.

through which the conditional density function of the wakes given Q, $p_w(A_w|Q)$ is

$$p_w(A_w|Q) = p_s(D(A_w))\|\frac{dD}{dA_w}\|, \tag{3.13}$$

where

$$\frac{dD}{dA_w} = \frac{16A_w^3 g^6 n^6 s^3 \left(\frac{nQ}{\sqrt{s}w}\right)^{6/5} w^6}{Q^{7/2}B^2\sqrt{\frac{\left(\frac{nQ}{\sqrt{s}w}\right)^{6/5}(4A_w^4 g^6 n^6 s^3 w^6 + B^4 Q^6)}{Q}}}. \tag{3.14}$$

This conditional density distribution function is defined within the range ($A_{w1}(Q) \leq A_w \leq A_{w2}(Q)$), where the limits, $A_{w1}(Q)$ and $A_{w2}(Q)$ are given respectively by

$$A_{w1}(Q) = \begin{cases} A_w(D_1) & Q \leq Q_{D_1} \\ 0 & Q > Q_{D_1}, \end{cases} \tag{3.15}$$

and

$$A_{w2}(Q) = \begin{cases} A_w(D_2) & Q \leq Q_{D_2} \\ 0 & Q > Q_{D_2}. \end{cases} \tag{3.16}$$

It should be noted that in equations (3.15) and (3.16), Q is included as a varying parameter, which enhances the boundaries for A_w.

Therefore, the normalized usable area, $UA_n(Q)$, provided by the stones for a given flowrate is the weighted sum of the individual wake areas,

$$UA_n(Q) = \int_{A_{w1}(Q)}^{A_{w2}(Q)} \omega_w p_w(\omega_w, Q) d\omega_w, \tag{3.17}$$

where ω_w is the dummy variable of integration. The fraction of submersed stones for a given flowrate that do not contribute is simply an atom of finite probability at zero for $p_w(A_w)$,

$$p_w^{at}(0) = \int_{D_1}^{D_m} p_s(\delta) d\delta, \tag{3.18}$$

where δ is the dummy variable of integration and D_m is the diameter in which all the stones get submerged. Equation (3.17) can be plotted for varying flowrate conditions to build up the normalized usable area as a function of the flowrate and $D_1 \leq D \leq D_m$ as the range of stones already submerged. Hence, by using known (or surveyed) frequency distributions for each stone size, the normalized usable area, UA_n from equation (3.17), returns the sum of the real usable area associated with each stone size for a given flowrate.

3.2.3 Threshold flow

Once the usable area curve is found, it can be used to help define the environmental threshold for managing stream discharge. We define this threshold as the flowrate for which the usable area is maximal, which implies that the derivative of the usable area curve becomes zero. Flowrates lower than this threshold (Q_t) are critical for the riverine ecosystem as the ecological benefits associated with the wake area generated by macroroughness elements rapidly decreases. The following is the mathematical definition of the environmental threshold:

$$\left. \frac{dUA}{dQ} \right|_{Q_t} = 0. \tag{3.19}$$

3.3 Results

3.3.1 The impact of stone-size distributions on the usable area curve

3.3.1.1 Stone-size distributions

We investigate the model's behavior by showing some examples using different stone size distributions. The range of stone sizes, number of stones and stream parameters used in the test cases are given in Table 3.1. For these examples, we maintain the assumptions that the spatial distributions are sparse and stones are hemispherically shaped, as discussed above.

Table 3.1 – Stone and stream parameters used in examples cases

Range of stones diameter	Number of stones	Manning's coefficient	Width	Slope
$0.1 < D < 0.7$[m]	$N = 50$	$n = 0.05[\frac{\text{s}}{\text{m}^{1/3}}]$	$w = 5$[m]	$s = 0.01$

Example 1: Stones with a constant diameter size distribution: This example utilizes a Dirac delta function (Figure 3.4a) to prescribe the size distribution of stones with diameters, $D = D^*$, that is

$$p_s(D) = \delta(D - D^*),\qquad(3.20)$$

where

$$\int_0^\infty p_s(D)dD = 1.\qquad(3.21)$$

As the Dirac delta distribution is discontinuous, the distribution of the wakes will also be a Dirac delta function around the wake area, A_w^*, as given by equation (3.9) for $D = D^*$,

$$p_w(A_w|Q) = \delta(A_w - A_w^*),\qquad(3.22)$$

whose integral over the wake sizes gives the cumulative distribution,

$$P_w(A_w|Q) = \int_0^\infty \delta(\omega_w - \omega_w^*)d\omega_w = \Theta\left(\sqrt{\frac{D^* Q^2 \sqrt{1 - \frac{4\left(\frac{nQ}{\sqrt{s}w}\right)^{6/5}}{D^{*2}}\left(\frac{nQ}{\sqrt{s}w}\right)^{2/5}}}{g^3 n^4 s w^2}}\right),\qquad(3.23)$$

where ω_w is the dummy variable of integration and $\Theta(\cdot)$ is the Heaviside function. Note that the Heaviside function depends on the flowrate, Q, because the location of the Dirac delta distribution for A_w is a function of Q. For this case, the usable area becomes

$$UA(Q) = N\sqrt{\frac{D^*\sqrt{1 - \frac{4\left(\frac{nQ}{\sqrt{s}w}\right)^{6/5}}{D^{*2}}\left(\frac{nQ}{\sqrt{s}w}\right)^{12/5}}}{4g^3 n^6}}\Theta\left(\sqrt{\frac{D^* Q^2 \sqrt{1 - \frac{4\left(\frac{nQ}{\sqrt{s}w}\right)^{6/5}}{D^{*2}}\left(\frac{nQ}{\sqrt{s}w}\right)^{2/5}}}{g^3 n^4 s w^2}}\right),\qquad(3.24)$$

which simplifies to

$$UA(Q) = N\sqrt{\frac{D^*\sqrt{1 - \frac{4\left(\frac{nQ}{\sqrt{s}w}\right)^{6/5}}{D^{*2}}\left(\frac{nQ}{\sqrt{s}w}\right)^{12/5}}}{4g^3 n^6}},\qquad(3.25)$$

because $\Theta(x) = 1$ for $x \geq 0$. Here, the Heaviside function specifies that all stones contribute to the total wake area for the range of flowrates up to Q_D, which submerges all stones.

(a)

(b)
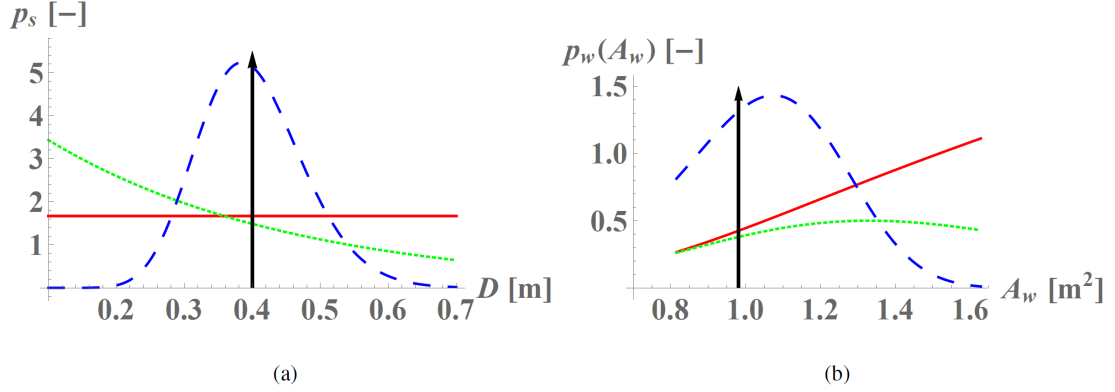
Figure 3.4 – Statistical distribution of: (a) stones diameters $0.1 < D < 0.7$ [m] (number of stones; N=50); (b) wake area for an assigned flowrate. The thick black arrow denotes the delta distribution, the red curve shows the uniform distribution and the green dotted and blue dashed curves represent the truncated exponential and truncated gamma distributions, respectively. The pdfs of the wake area correspond to the flow rate $Q = 0.5[\frac{m^3}{s}]$.

Example 2: Stones with a uniform distribution of diameters: This distribution corresponds to imposing a rectangular function (Figure 3.4a) to represent stone size over a range of diameters ($D_1 \leq D \leq D_2$), or

$$p_s(D) = \begin{cases} \frac{1}{D_2-D_1} & D_1 \leq D \leq D_2 \\ 0 & \text{otherwise.} \end{cases} \tag{3.26}$$

The resulting conditional distribution of the wakes given Q is

$$p_w(A_w|Q) = \begin{cases} \frac{1}{D_2-D_1} \dfrac{16 A_w^3 g^6 n^6 s^3 \left(\frac{nQ}{\sqrt{s}w}\right)^{6/5} w^6}{Q^{7/2} B^2 \sqrt{\frac{\left(\frac{nQ}{\sqrt{s}w}\right)^{6/5}(4A_w^4 g^6 n^6 s^3 w^6 + Q^6 B^4)}{Q}}} & A_{w1}(Q) \leq A_w \leq A_{w2}(Q) \\ 0 & \text{otherwise,} \end{cases} \tag{3.27}$$

where $A_{w1}(Q)$ and $A_{w2}(Q)$ are given by equations (3.15) and (3.16), respectively.

The total wake area can be obtained by computing the integral equation 3.17 for various flowrates. This integral cannot be solved analytically and must be computed numerically. Obviously, in the limit where $D_1 \rightarrow D_2$, the area of the wake coincides with that for which all of the stones have equal diameter (i.e., the first example case).

Example 3: Stones with a truncated exponential distribution of diameters: In this case, we implement an exponential function (Figure 3.4a) to represent the stone size distribution as

33

follows

$$p_s(D) = \frac{1}{\mu_D} e^{-\frac{1}{\mu_D} D}, \tag{3.28}$$

where μ_D is the mean diameter of the distribution. To satisfy $\int_{D_1}^{D_2} p_s(\delta) d\delta = 1$, the exponential distribution is truncated between D_1 and D_2 as

$$p_{s,\text{truncated}}(D) = \frac{p_s(D)}{P_s(D_2) - P_s(D_1)}, \tag{3.29}$$

where $P_s(D)$ is the cumulative distribution function of the exponential distribution. Since the concept of the derivation of the wake areas has been shown in the previous examples, and also because the equations for the wakes area corresponding to the truncated exponential distribution are prohibitively long, we do not print them herein. However, they can be obtained from the data repository address [2].

Example 4: Stones with a truncated gamma distribution of diameters: This example investigates the use of a gamma function (Figure 3.4a) to represent the size distribution of stones in terms of their diameters:

$$p_s(D) = \frac{\beta^\alpha D^{\alpha-1} e^{-\beta D}}{\Gamma(\alpha)}, \tag{3.30}$$

where α and β are the shape parameter and rate parameter, respectively, and $\Gamma(\alpha)$ is a complete gamma function. Similar to the exponential distribution, the gamma distribution is also truncated between D_1 and D_2 using the same procedure described above. Again, the equations for the wakes area corresponding to the truncated gamma distribution are prohibitively long, and can be accessed from the data repository address.

3.3.1.2   Wake area distributions

Figure 3.4b shows the conditional distributions of the wake areas given the flow rate, Q, for the various stone size distributions presented as examples and shown in Figure 3.4a. As mentioned in Section 3.2, knowing the statistical distribution of stone diameters allows for the pdf of the wake areas to be found by using the derived distribution approach equation (3.13). Notice from equation (3.13) that as the flowrate initially increases, the pdf $p_w(A_w, Q)$ has an area of 1 because all stones contribute to the total wake area, i.e. none of them are submerged. Once the flowrate reaches the minimum Q_D for the smallest stone diameter, $p_w(A_w, Q)$ starts decreasing with flowrate and has an area less than 1 because submerged stones no longer contribute to the total wake area. This generates an atom of finite probability that submerged

---

[2]https://drive.google.com/open?id=18CXUbFQI6hsPohqF6yCVHgzPZIKle253

stones do not contribute to the wakes anymore. The area becomes zero when all stones are submerged where an atom of finite probability is equal to 1.

Using equation (3.3), in case of $Q = 0.5\,[\frac{\mathrm{m}^3}{\mathrm{s}}]$, the diameter for which stones start to contribute to the wake area is $D \geq 0.33$ [m]. Except in the case of delta distribution, the size distributions used as examples included stone diameters between 0.1 to 0.7 [m]. Hence, there is a fraction of stones that are submerged and therefore not ecologically relevant in these examples. In Figure 3.4b, the fraction of submerged stones for uniform, truncated exponential and truncated gamma distributions is $p_w^{at}(0) = 0.39, 0.59$ and 0.19, respectively. It is worth mentioning that this result is consistent with equations (3.13) and (3.14). Since the truncated exponential distribution has a higher frequency of stones with relatively small diameters, a higher fraction of stones becomes submerged as the discharge increases. Conversely, based on equation (3.14), $\frac{dD}{dA_w}$ monotonically increases with A_w. Therefore, a size distribution of stones with a higher frequency of large diameters results in a higher frequency of large wake areas, as shown in Figure 3.4b. In other words, larger stones generate a more substantial contribution to the total wake areas in streams than smaller stones, as expected.

3.3.1.3 Total usable area

Figure 3.5 shows the total usable area resulting from the wakes that form downstream of the stones as a function of stream discharge for the example cases of stone size distributions. The highest usable area for most flowrates, especially for high flow rates, corresponds to the case with the uniform distribution of stones diameters. This is due to the fact that the uniform distribution has the highest frequency of large stones and hence, the most significant contribution to shelter zones generated by macroroughness elements. In addition, to validate the solution described in this study (Section 3.2), the total usable area for the uniform distribution of stones diameters was also calculated numerically (i.e., red crosses in Figure 3.5). The numerical calculations were done by considering a discretized size distribution of macroroughnesses, $p_s(D)$, and building the UA curve by use of equations (3.9), (3.13) and (3.17). As shown in this figure, the proposed solution and numerically calculated total usable areas completely overlap. However, the developed solution in this study requires substantially less computational resources and therefore is more preferable.

The usable area curves shown in Figure 3.5 can be used to determine the environmental thresholds for the stream from equation (3.19). Among the four examples for stone size distributions that we consider here, the uniform distribution and truncated gamma distribution have the highest and lowest environmental thresholds, respectively. In addition to defining the environmental threshold, these curves can be used to evaluate the extent of environmental suitability for flow release policies in hydropower facilities based on the Continuous Magnitude Under Threshold (CMUT) method described in *Niayifar and Perona* [2017]. The CMUT method calculates the magnitude of the stress period (e.g., for fishes), considering consecutive days below Q_t, by summing the difference between values of UA for the $Q < Q_t$ threshold and UA for Q_t. Then the ecological indicator is calculated as the fraction of the maximum

magnitude of the stress period between regulated and non-regulated flow ((see equation (8) in *Niayifar and Perona* [2017]).
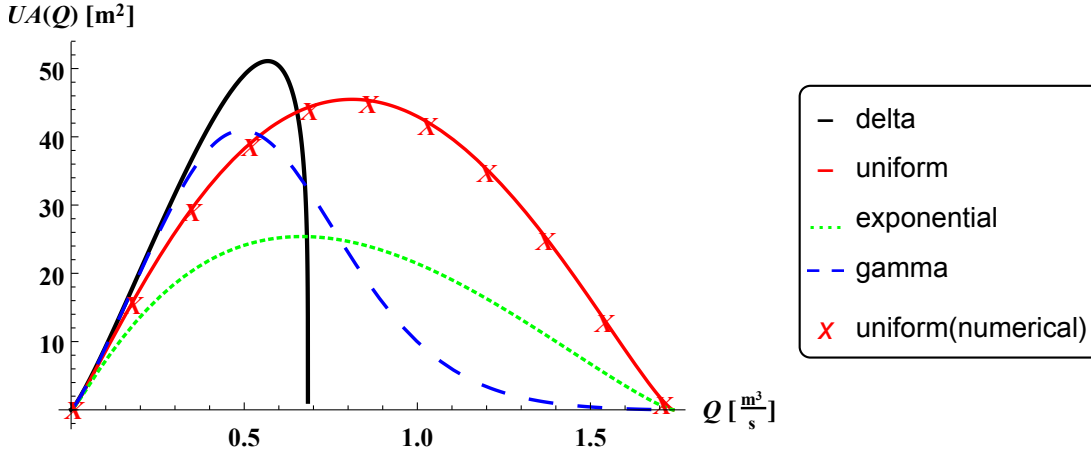
Figure 3.5 – Total usable area as a function of flowrate for the different distributions of stone sizes.

3.3.2 The impact of stone diameters on threshold flow caused by sediment sorting

3.3.2.1 Delta distribution

In equation (3.19), the environmental threshold is defined as the flowrate for which the derivative of the usable area curve becomes zero. For the delta distribution of stone diameters, this environmental threshold can be found analytically to be:

$$Q_t = \frac{s^{\frac{1}{2}} w D^{\frac{1}{3}}}{n}. \tag{3.31}$$

Equation (3.31) suggests that the environmental threshold for the delta distribution scales linearly with the stream width, w. This is consistent with the fact that two identical streams which differ only by having unequal widths are expected to have environmental flowrates that are linearly proportional to their respective widths. This result also shows that a steeper slope or larger stone diameters imply a higher environmental threshold. Additionally, if the river bed has higher roughness, n, the environmental threshold decreases. From a practical point of view, equation (3.31), considering uni-diameter stones, can provide a very simple and robust estimation of the environmental threshold for riverine ecosystems. This simple equation only requires four parameters (i.e., s, w, D and n) to determine the environmental threshold in a stream, which can be easily found by performing simple field surveys.

3.3.2.2 Gamma distribution

In alpine streams, the stones size distribution may change temporally and spatially. The latter can happen due to changes in the stream morphology caused by climate change [e.g., *Marchese et al.*, 2017; *Mao et al.*, 2017] or anthropic pressure [e.g., *Heinemarm*, 1981; *Fan and Morris*, 1992; *Yang et al.*, 2006]. For example, the macroroughness element sizes in alpine streams gradually decrease from upstream to downstream due to the available mechanical energy in a stream and the associated sediment transport. To investigate this situation and its impact on the threshold flow, three gamma distributions with different mean stone diameter values (i.e., 0.4, 0.5 and 0.6 m) are considered (Figure 3.6a). The distributions with the highest and lowest means could mimic a spatial or temporal change in the stones size distribution. Figure 3.6b shows the total usable areas calculated for these different stone size distributions as a function of flowrate. From this figure, it is clear that the distributions with the smaller mean diameters result in a significant and nonlinear, decrease in the usable area generated by stones. This occurs mainly because of the loss of large stones, which generate larger contributions to the total wake area. This nonlinear relationship can strongly affect the riverine ecosystem, for example, by reducing the regions which are ecologically suitable for the fish. Furthermore, not only does this shift in size distribution generate a substantial loss in the usable area, the environmental threshold also decreases since the peak of the usable area moves toward lower discharges.

(a) (b)
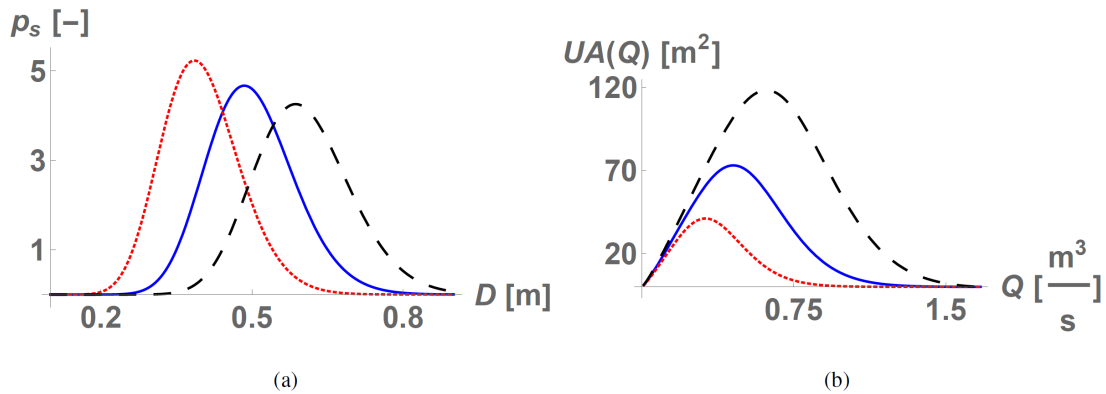
Figure 3.6 – The impact of sediment size distribution on the usable area curve: (a) stone diameter distributions; (b) usable area for different distributions of stone sizes. Dotted red, blue and dashed black curves denote the gamma distribution with the mean of 0.4, 0.5 and 0.6 [m], respectively.

3.3.3 Application to reservoir optimal flow release policies

In this section, we investigate an application of the modeled usable area generated by wakes downstream of stones and its use as ecological indicator in a multiobjective reservoir optimization case study. The new indicator is used in the Direct Policy Search (DPS) model, which was recently proposed by *Niayifar and Perona* [2017] to optimize the global efficiency of reservoirs.

The DPS model uses a dynamic flow release approach to partition the flow for environmental use and energy production. The energy production is computed from the technical data (e.g., turbine characteristics and reservoir head), and the environmental efficiency associated with the flow release policies is calculated by geometrically averaging the indicators of hydrologic alteration [*Richter et al.*, 1996a] with the WUA for fishes [e.g., *Niayifar and Perona*, 2017; *Razurel et al.*, 2018]. Additionally, we apply the Borg MOEA [*Hadka and Reed*, 2013], an efficient multiobjective evolutionary algorithm, to find the optimal flow release policies (i.e., Pareto's frontier). In the case of the multiobjective reservoir optimization, Pareto's frontier consists of a set of non-dominated optimal solutions if no objective (e.g., environmental indicator) can be improved without worsening at least one other objective (e.g., energy produced). Non-dominated policies denote the solutions in which there is no other solution that has better quality with respect to all objectives. The reader is referred to *Niayifar and Perona* [2017] for details about the numerical implementation of the flow redistribution policies.

The analytical model proposed in this study to calculate the usable area curve can be used to characterize the available ecological habitat generated by flow release policies in relation to the stone size distribution within the impounded river reach. To test this concept, the usable area curves in Figure 3.5 are used to calculate the fish indicator based on CMUT method and to develop the efficiency plot for the case study described in *Niayifar and Perona* [2017]. Figure 3.7 shows the Pareto's frontiers calculated for different size distributions of stone diameters (see Section 3.3) in the streamflow. As expected, the Pareto's frontiers corresponding to the cases with the uniform and truncated exponential distribution of stone diameters are inferior to cases with the delta and truncated gamma distributions because the latter two example cases have lower environmental thresholds. In other words, since the uniform and truncated exponential distribution have higher frequencies of larger stones, they will have higher environmental thresholds meaning that less water from the river reach can be withdrawn for energy production. This can be seen in the Pareto's frontier by comparing equal environmental indicators for the various diameter size distributions (see Figure 3.7). The flow release policies near the top-right of the Pareto's frontier are more ecologically and economically advantageous because they provide higher energy production without a large reduction in environmental efficiency. Therefore, the cases with delta and truncated gamma distributions have the potential to provide better global efficiencies.

3.4   Discussion

3.4.1   General utility of the model

Changes in natural flow regimes resulting from the ever-increasing exploitation of freshwater streams for anthropic activities (e.g., hydropower, irrigation, urban and industrial use, etc.) have created a critical need to develop strategies to preserve or restore riverine ecosystems. Furthermore, this need will likely be exacerbated by factors associated with climate change. The methodology developed in this work helps to characterize the environmental impacts associated with changing a stream's natural flow regime, and is of vital importance for promoting
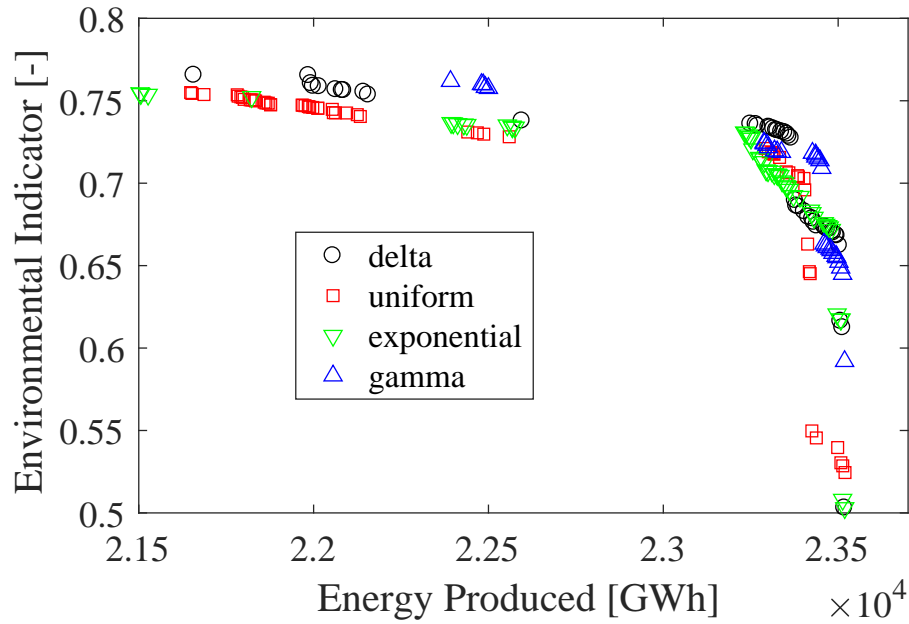
Figure 3.7 – Pareto's frontiers simulated for different distributions of stone diameters

more ecologically sustainable riverine ecosystem management policies.

Compared to the standard methods of calculating the WUA (e.g., from habitat modeling software packages like CASiMir and PHABSIM), the methodology proposed in this study provides a simpler technique to directly take the presence of macroroughness elements and their effects on the stream hydrodynamics into account. Owing to coarse resolution, typical habitat modeling software packages cannot capture the role that stones play in generating shelter zones for fishes or the related ecological threshold that are key to defining environmental flow release constraints (e.g., the minimum flow requirements). Our physically-based, analytical model allows for calculating the usable area from quantities that can be obtained by aerial surveys (e.g., the distribution of stone diameters, channel width, slope and Manning's coefficient of the stream). This usable area can then be used to refine WUA curves calculated from standard techniques.

To exemplify and validate the importance of the concept above, we considered four distributions of stone diameter sizes in a stream, and calculated and compared their associated usable area curves. We found that the total wake area is highly sensitive to the stone diameter distributions and proved that different stone size distributions within the river reach will affect optimal water exploitation rules under various release scenarios. In the case of considering stones with the same diameter (i.e., the delta distribution), an analytical equation which only requires four parameters (i.e., s, w, D and n) was derived to estimate the environmental threshold for the stream discharge (equation 3.31). We also investigated the effect of potential temporal and spatial changes in stone size distributions in alpine streams and found that the loss of large stones significantly decreases the usable area in the stream.

The potential for our modeling tool to define sustainable environmental flow policies is

thus very broad. Consider the case of hydropower, which accounts for more than 16% of the electricity generation worldwide, making freshwater the most widely-used resource for renewable energy [*IEA*, 2015]. Given its substantial footprint in the renewable energy market, hydropower operation policies must implement procedures to minimize the environmental degradation in riverine stretches downstream of dams and intakes. Hence, this study complements several recent studies that have addressed the issue above by solving multiobjective optimization problems to find the best operating policies for hydropower units [e.g., *Gorla and Perona*, 2013; *Salazar et al.*, 2016; *Niayifar and Perona*, 2017]. In general, these operation policies, which set water release rules, seek to optimize the operational efficiency of hydropower facilities with respect to multiple objectives (e.g., power production and environmental sustainability). As a demonstration, we applied the new indicator and the usable areas calculated from our analytical solutions, to a multiobjective reservoir optimization problem and investigated shape changes of the Pareto's frontier for the different distributions of stone diameters (Figure 3.4). Pareto's frontier shape was found to be sensitive to stone size distributions, and of the four cases that we studied, the streams with the delta and truncated gamma distributions showed better global efficiencies compared to uniform and truncated exponential distributions.

These results suggest that the optimal minimum flow may not just change in space (i.e. the same minimum flow may be better or worse as macro roughness elements change in size from upstream to downstream), but also in time as a stream's geomorphology shifts. This is likely to be crucial from a practical point of view, especially for hydroelectric power operators and decision makers building hydropower units. For example, the methodology proposed here can be useful to better select the location of hydropower systems where maximal power production is achievable, while also considering the ecological needs.

3.4.2 Model application overview

Figure 8 shows the field survey and calculations required to characterize the ecological benefits associated with the macroroughnesses. The statistical size distribution of macroroughnesses can be obtained by taking aerial photographs with drones during the period of low stream discharge (e.g., October in the northern hemisphere). Figure 3.8 shows an exemplary photograph of stones distributed in a stream. Notice that this size distribution corresponds to the free surface stones diameter, d, and has to be converted to size of stones diameter at the stream bed, D, using equation (3.3). Stream width, w, can be found from the aerial images. Slope, s, is found by calculating the relative change in elevation with respect to the distance along the stream. Sodium chloride slug releases or other stream gauging techniques can be used to determine the stream discharge, Q, and velocity, V. Thus, the water depth can be calculated from the continuity equation for the incompressible flow ($h = \frac{Q}{Vw}$). Finally, the Manning coefficient, n, can be found using equation (3.1). Furthermore, the calculations required to calculate the usable area and the consequent environmental flow threshold have been summarized in the flow chart (Figure (3.8)).

The usable area calculated by equation (3.17) considers the contribution of the wakes generated by the presence of macroroughnesses, e.g. stones. While the suitable condition can vary

depending on species and hydraulic conditions in the wake, we herein consider the total wake areas as the suitable habitat conditions where lower velocities have been found to be generally more favorable for species [e.g., *Buffington et al.*, 2004; *Kucukali and Cokgor*, 2008]. However in the case of low flows, some areas external to the wakes (e.g., pools) may become important. Since the aerial survey will be performed in low flow periods, the base flow usable area due, for instance, to the presence of pools can be corrected by detecting the suitable areas external to the wakes from the drone images and obtain how it changes with flow by means of standard numerical simulations. It should be noted that these areas quickly will disappear as the flow rate increases. Another potential issue with this method arises when the wakes interact with each other (i.e., violating the sparse distribution assumption). In many cases for which stones are located very close to each other, they can be merged into a single stone for the sake of the habitat analyses. In a more sophisticated approach, the overlapping wake areas can be detected by geometrically sketching the boundaries of the wakes to correct the total usable area by obtaining the arrangements (i.e., positions) of stones via drone photographs. While the importance of the suitable habitat area external to the wakes during low flows and also that of the interacting wakes is case specific, we believe that they are generally negligible, and ignoring them does not cause a significant error compared to the total wake area.

The aim of this study is to present a generalized statistical approach that can be applied to efficiently investigate the eco-hydraulic benefits provided by macroroughness elements, as opposed to presenting a detailed analysis for any particular stream. When it is needed, our model can easily be adapted for more case-specific studies in future works. Such studies may consider using 2D numerical modeling in combination with the framework we present herein to obtain estimates of the wake-size distributions as well as the possible suitable area external to the wakes in periods of low flows for a particular stream.

3.5 Conclusions

In this study, we employed the analytical model by [*Negretti et al.*, 2006] to estimate the characteristic length scales of the wakes downstream of macroroughness elements in open channel flows, and extended it to calculate the total wake area associated with various stone size distributions that generate usable habitat for fishes. The distributions of wake areas for different case studies were found by using the derived distribution approach. Subsequently, each usable area curve was built by calculating the total wake area a function of the stream discharge, and the environmental threshold was defined as the discharge for which the derivative of usable area curve becomes zero.

The methodology proposed here can be an efficient tool to calculate the environmental impacts of flow release policies. Different from common approaches to define environmental flow threshold which are solely based on hydrology (i.e., the hydrograph), our results suggests some important general principles regarding the fact that the characteristics of the stream bed, in this case, stones acting as macroroughness elements, will largely affect the optimal

minimum flow release by lowering constraints to dynamic environmental flow policies. Compared to other habitat modeling approaches, which require substantial field work and do not account for the wakes downstream of macroroughness elements, the new model can be a viable alternative. Therefore, it can reduce subjectivity in interpreting streamflow requirements and developing hydropower operation policies by considering more fully the macroscale physical dynamics in streams with respect to the ecological needs for the riverine ecosystem.
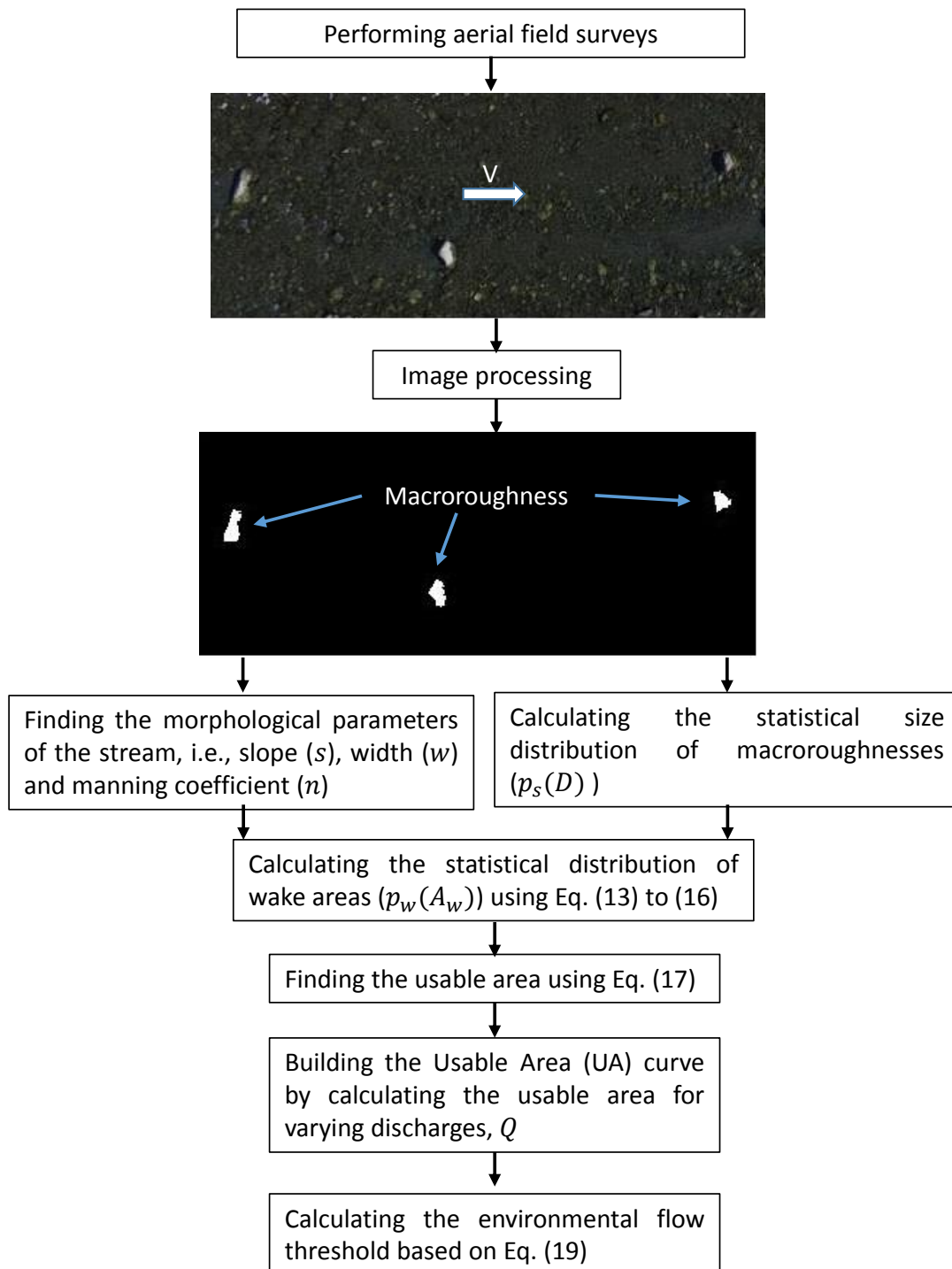
Figure 3.8 – Overview of the model application methodology.

4 Bed macroroughness contributes significantly to gas exchange in stream ecosystems

Abstract

The air-water gas exchange drives the evasion of climatically sensitive gases (e.g., carbon dioxide, methane) from streams and rivers to the atmosphere. At the same time, gas exchange can contribute to the sustainability of aquatic life in streams through oxygenation. Experimental work has shown that macroroughness elements in engineered flumes can enhance gas exchange by breaking the water surface and thereby increasing the air-water boundary turbulence. However, empirical evidence for the effects of macroroughness elements, including large rocks or boulders, on the gas exchange in natural streams is missing. In this study, we combined remote sensing with a novel analytical model to quantify the wake areas downstream from macroroughness elements in the Aare River (Switzerland). This allowed us to establish the environmental flow thresholds for a restored river. Next, we explored the impact of macroroughness and related wake areas on the gas exchange in a regulated alpine stream (Trient, Switzerland). To do so, we experimentally manipulated macroroughness and quantified gas transfer velocity ($k600$) from tracer gas injections into the stream in the presence and absence of artificial macroroughness elements, and with different degrees of submergence. Our results showed that the addition of non-submerged macroroughness elements to the streambed significantly increased k600, whereas fully submerged macroroughness elements did not. Our findings highlight the role of macroroughness for the gas exchange in streams, particularly at low flows when oxygenation is most likely to be an issue, and so provide guidance for environmental restoration of streams affected by anthropogenic activities.

4.1   Introduction

Macroroughness is well known to impact the hydraulics and hydrodynamics of streams. For example, there are several studies [e.g., *Nitsche et al.*, 2011] underlining the importance of the resistance imposed on the streamflow by macroroughness, which in turn can affect bedload transport. Several studies have highlighted the ecological significance of macroroughness as linked, for instance, to oxygenation and refuge zones for fishes [e.g., *Kucukali and Cokgor*, 2008; *Moghadam and Keshavarzi*, 2007].

Chapter 4. Bed macroroughness contributes significantly to gas exchange in stream ecosystems

Gas exchange through the water surface is key to ecosystem metabolism and hence to carbon and nutrient cycling. At the same time, it drives the evasion of climate-relevant gases from streams and controls in part the concentration of dissolved oxygen (DO) in the streamwater. This is critical given that DO concentration is a proxy for the overall water quality and the viability of the aquatic habitat. The air-water gas flux depends on the turbulence level, especially in the top 10 percent of the water column near the free surface [e.g., *Moog and Jirka*, 1999b]. Partially submerged macroroughness elements, such as large rocks and boulders, may enhance the near-surface turbulence level in streams and rivers by inducing wake areas. The latter are regions formed due to the no-slip condition imposed by macroroughness on the streamflow where velocity decreases and turbulence increases. These highly turbulent regions enhance the mixing and therefore the air-water gas exchange.

Several laboratory studies have investigated the impact of macroroughness elements on gas exchange [e.g., *Chen and Jirka*, 1995; *Chanson*, 1997; *Kucukali and Cokgor*, 2008; *Moog and Jirka*, 1999b]. For instance, *Moog and Jirka* [1999b] used flumes to study the relationship between macroroughness and gas exchange. They found that ignoring the presence of macroroughness and solely considering smooth bed turbulence would lead to substantial error in predicting gas exchange. For this reason, they distinguished between bed friction and form drag resulting from macroroughness the two separate forces resisting flow and suggested interpolating a near-surface dissipation rate based on these two terms to calculate the gas exchange rate. The boulder-flow interactions associated with self-aeration were investigated by *Kucukali and Cokgor* [2008]. Their flume experiments were performed with different boulder arrangements and submergence ratios under a range of turbulent flow Reynolds numbers. These authors proposed an equation for the maximum local aeration efficiency as a function of the blockage ratio for a flow range where macroroughness elements are not fully submerged. Furthermore, their data showed that the gas exchange velocity significantly decreases when macroroughness elements are fully submerged.

Ulseth et al. [2019] estimated the gas exchange in steep mountain streams using gas tracer techniques. Aiming to consider streams varying in geomorphology and hydraulics, they combined their data with other previously published data and found that high-slope streams have substantially higher gas exchange compared to low-slope streams. They showed that the gas exchanged scaled differently with the energy dissipation rate in low-slope streams as compared with high-slope streams; in low-slope streams, $k600$ attenuates with energy dissipation, whereas it accelerates with energy dissipation in high-slope streams. As high-slope streams in mountainous terrain have elevated bed macroroughness [*Knighton*, 2014; *Moghadam and Keshavarzi*, 2007; *Schneider et al.*, 2015], *Ulseth et al.* [2019] argued that elevated roughness in high-slope streams is the main driver for gas exchange in these ecosystems. This argument was in an agreement with their observations of a positive relationship between reach-scale roughness and $k600$. Although several laboratory studies have shown the impact of macroroughness on gas exchange, we are currently lacking evidence for this relationship at the reach scale in natural streams.

Alterations of natural flow regimes owing to climate change or regional human activities can degrade the natural stream environment. Good understanding of this environmental

degradation is important to mitigate cascading effects on stream ecosystem functioning and integrity. Today, the various indicators available to assess the environmental impacts of altered flow regimes on stream ecosystems are still debated [*Gao et al.*, 2009]. For instance, indicators based on suitable habitat conditions have been widely used [e.g., *Bloesch et al.*, 2005; *Niayifar and Perona*, 2017; *Razurel et al.*, 2018]. Recently, *Niayifar et al.* [2018] proposed an environmental indicator based on the ecological contribution of macroroughness and related wake areas. One rationale to this approach is that fish can reduce energy expenditure in these low-velocity refuge zones and can easily move to adjacent patches for foraging [*Hayes and Jowett*, 1994; *Moghadam and Keshavarzi*, 2007]. Despite their ecological significance, most habitat suitability models do not properly capture small-scale features such as the wake areas downstream of macroroughness elements due to computational constrains. In this regard, *Niayifar et al.* [2018] developed an environmental indicator by calculating analytically the size of the wake area downstream of a macroroughness element and using statistical analysis to estimate the cumulative wake area at the reach scale.

In this study, we experimentally explore the effect of macroroughness on $k600$ at the scale of an entire reach in a regulated alpine stream (the Trient River) devoid of natural macroroughness. We designed the distribution of the macroroughness elements in the experimental reach following the macroroughness distribution in a restored alpine stream (Aare River). We modeled the wake areas and environmental flow threshold as induced by the macroroughness in the Aare River using the recent approach by *Niayifar et al.* [2018]. We conducted multiple argon injections and quantified k600 with and without macroroughness elements. We considered the size of wake areas as a proxy for the free surface turbulence (i.e., a major driver of gas exchange) and explored its relationship with reach-scale $k600$ values. Our results provided first experimental insights on the relationship between macroroughness and gas exchange at a scale relevant to stream ecosystem restoration.

4.2 Material and Methods

4.2.1 Site description

4.2.1.1 Aare River

We studied the macroroughness size distribution of a blank type of stream reach by performing unmanned airborne surveys of a straight 400 [m] reach from the Aare stream in Innertkirchen (625 [m] a.s.l.) in the center of Switzerland (Figure 4.1). Knowing the size distribution of macroroughness allows estimation of their ecological significance, e.g., enhancing the oxygenation and generating shelter zones for fishes, and subsequently calculation of the environmental flow thresholds. This reach had an average width of 16 [m] which has been engineered by placing macroroughness elements for ecological improvements allows for better realization of the contribution of macroroughness to the stream ecosystem. The discharge of the study reach is regulated by the upstream reservoirs that release constant minimal

flows, but vary seasonally due to glacier and snowmelt. It has low discharge in winter and the discharge increases in summer due to glacier and snowmelt. Therefore, for more precise characterization of macroroughness diameters, the survey was performed during the low flow (i.e., February) where the discharge was 305.27 [l/s].
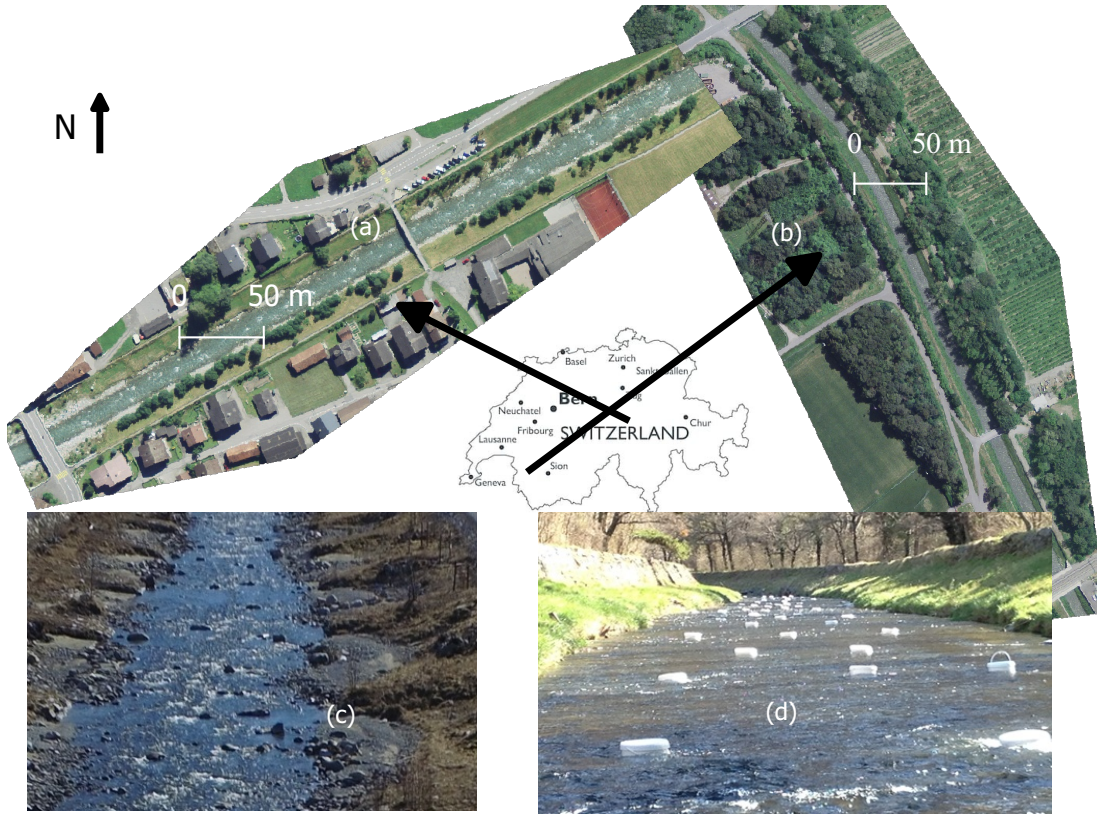
Figure 4.1 – Case studies; (a) Aare; (b) Trient; (c) macroroughness in the Aare stream; (d) buckets as simulator of macroroughness elements in the Trient stream.

4.2.1.2 Trient River

To study the relationship between the turbulence and air -water entrainment, the impact of experimentally-manipulated macroroughness on stream gas exchange was studied at the Trient stream in Vernayaz (452 [m] a.s.l.) in the south of Switzerland (Figure 4.1a). We performed multiple simultaneous gas exchange measurements and aerial flights in a 450 [m] reach of the river. The reach is 9 [m] wide and discharge is regulated by an upstream reservoir that releases constant minimal flows. However, the discharge increases during the snow melt season. This high-order stream (i.e., 4th order) was selected because it has the shape of a channel flow with a very simple bed morphology that allows for studying exclusively the impact of macroroughness on gas exchange. Within our study reach, the streambed consists

of coarser gavels and finer cobbles (5 to 15 cm) with no bedforms or macroroughness. To introduce macroroughness, we placed 70 buckets (30 [cm] diameter and 17.5 [cm], equivalent to boulders in sedimentological terms) onto the streambed (Figure 1b). Buckets were placed (repetitive rows of 3 and 2 buckets) far enough from each other to avoid wake interaction as to maximize the wake areas and therefore the gas exchange. Each time we performed the experiment, we first placed the buckets onto the streambed to measure *macroroughness* gas exchange; next we removed the buckets and measured *no- macroroughness* gas exchange. This happened within the same day and we took care that no change in discharge occurred during that time.

4.2.2 Physical attributes

4.2.2.1 Travel time, velocity and discharge

Stream discharge was estimated from slug additions of dissolved sodium chloride (NaCl) at the sites used for Ar gas injection so that the background electrical conductivity in the streamwater increased by 50 %. Simultaneously, we measured the electrical conductivity, $C_{mes}(t)$ [μScm^{-1}], at the last station using WTW conductivity loggers every Δt=1 [s] until conductivity returned to the background condition. We calculated stream discharge, Q, by numerical integration of the measured conductivity as following:

$$Q = \frac{C_{add}}{\sum_{n}^{t=1}(C_{mes}(t)\Delta t)}, \tag{4.1}$$

where C_{add} is the electrical conductivity of the added NaCl that we calculated empirically in the laboratory by establishing a relationship between the sodium chloride in solution and conductivity. $n\Delta t$ denotes the travel time [s] which was the amount time between the injection of sodium chloride and when the conductivity reached maximum at the last station. Stream velocity, v, was calculated by dividing the length of study stream [m] by the travel time [s].

4.2.2.2 Slope

We measured stream channel slope, s [-], using differential global positioning systems (DGPS, Trimble R10 GNSS receiver) by calculating the relative change in the elevation [m] with respect to the distance [m] along the stream.

4.2.2.3 Calculating the wake areas

To estimate the wake areas downstream of macroroughness elements at the reach scale and the consequent environmental flow threshold, we used the model recently developed by

Niayifar et al. [2018]. We briefly describe the model here. Figure 4.2 shows the schematic of the wake and related length scales and variables. By integrating the transversal length scale [*Negretti et al.*, 2006] $l(x)$ [m], from the macroroughness location up to the longitudinal length scale, L [m], for a given discharge, Q, we calculated the wake area as following:

$$A_w = \sqrt{\frac{D\sqrt{1 - \frac{4\left(\frac{nQ}{\sqrt{s}w}\right)^{6/5}}{D^2}\left(\frac{nQ}{\sqrt{s}w}\right)^{12/5}}}{4g^3n^6}}B, \tag{4.2}$$

where D [m] is the stone diameter, $n[\frac{s}{m^{\frac{1}{3}}}]$ the manning coefficient, $g[\frac{m}{s^2}]$ the gravitational acceleration and B is:

$$B = -2C + ln\left(\frac{1+C}{1-C}\right), \tag{4.3}$$

where

$$C = (1 - \frac{1}{e})^{1/2}. \tag{4.4}$$
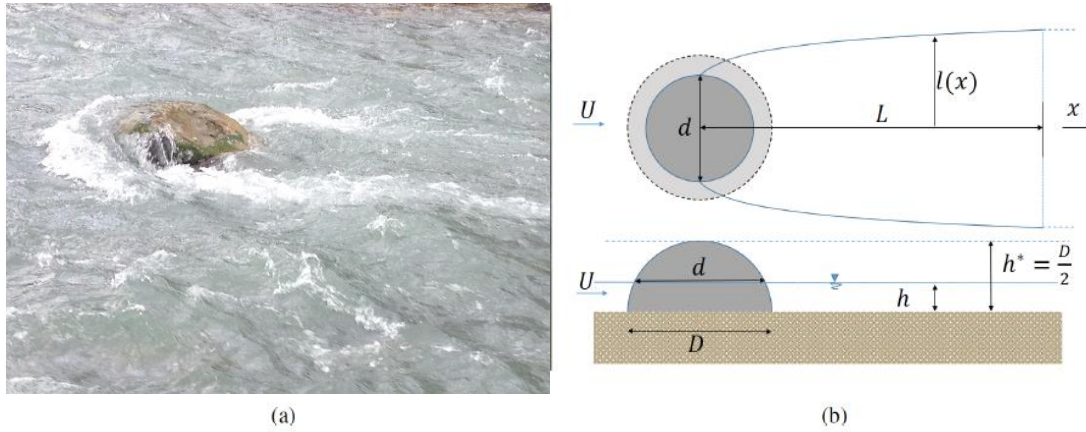
Figure 4.2 – (a) Exemplary macroroughness effect in the stream flow (b) schematic of the wake downstream of a macroroughness and related length scales and variables.

Knowing the size density distribution of macroroughnesses, $p_s(D)$, within the range $D_1 \leq D \leq D_2$, the conditional density function of the wakes given Q, $p_w(A_w|Q)$ can be found using the derived distribution approach as:

$$p_w(A_w|Q) = p_s(D(A_w))\|\frac{dD}{dA_w}\|, \tag{4.5}$$

within the range $A_{w1}(Q) \leq A_w \leq A_{w2}(Q)$, where the limits are:

$$A_{w1}(Q) = \begin{cases} A_w(D_1) & Q \leq Q_{D_1} \\ 0 & Q > Q_{D_1}, \end{cases} \tag{4.6}$$

and

$$A_{w2}(Q) = \begin{cases} A_w(D_2) & Q \le Q_{D_2} \\ 0 & Q > Q_{D_2}, \end{cases}$$

(4.7)

where Q_D is the discharge when a macroroughness of size, D, gets submerged:

$$Q_D = \frac{D^{5/3} s^{1/2} w}{2^{5/3} n}.$$

(4.8)

Therefore, the normalized wake areas, i.e., normalized usable area, $UA_n(Q)$, created by macroroughnesses at the reach scale can be found as:

$$UA_n(Q) = \int_{A_{w1}(Q)}^{A_{w2}(Q)} \omega_w p_w(\omega_w, Q) d\omega_w,$$

(4.9)

where w_w is the dummy variable of integration. They proposed to build up the usable area curve by plotting Equation 4.9 for varying discharges. Finally, they defined the environmental flow threshold as the discharge for which the derivative of the usable area becomes zero.

4.2.3 Macroroughness

We characterized the size distribution of macroroughness using remote sensing. We took low altitude aerial photographs (80% overlap) with a DJI Phantom 4 Pro drone equipped with a 12.4 megapixel camera, flown at two elevations. We performed the aerial flights at baseflow to increase the precision of the estimation of the macroroughnesses diameter. To eliminate the effects of distortion on acquired data, imagery was acquired to 3 river widths either side of the river. Ground control points were installed in the floodplains. As we were not interested in calculating topographic change, but simply macroroughness and stream bed dimensions, and given the zone of interest was in the middle of the derived orthoimagery, we can assume that the effects of systematic distortion will be negligible. We processed the images with Pix4D software (Pix4D SA, Switzerland) and yielded a sub-centimeter spatial resolution. Owing to the color contrast between the macroroughness elements and the streamwater, image segmentation techniques were deployed to detect the boundary of macroroughness and calculate their size after accounting for the water depth corrections. It should be noted that the macroroughness size seen from the images corresponds to the free surface diameter, d, and has to be converted to the size of macroroughnesses diameter at the streambed, D. Considering Figure 4.2, with some mathematical manipulations, D can be found as:

$$D = \frac{h}{tan(\Theta)} + h(cos(\frac{\pi}{2} - \frac{\Theta}{2})),$$

(4.10)

where

$$\Theta = arctan(\frac{2h}{d}).$$ (4.11)

Since the aerial surveys were done at baseflow, Θ would be close to zero ($d >> h$) and therefore the first term in the right-hand side of equation (4.10) will dominate compared to the second term. Also, it should be noted that d is equal to the first term in this equation, which implies $d \approx D$. Hence, as we know the first term in the equation from the aerial survey, the only source of error in calculating D would be the second term, and because this term is non-dominant in terms of its relative magnitude, the resulting error is assumed to be negligible.

4.2.4 Calculating gas exchange from argon tracer additions

We measured k600 by adding argon (Ar) as a tracer gas to the stream. *Hall Jr and Madinger* [2018] recently found Ar to be promising as a tracer gas because of its low background concentration in streamwater and its conservative character. Furthermore, the Schmidt number and solubility of Ar are similar to oxygen (O_2), which is often used to estimate stream metabolism, making Ar an appealing tracer gas for calculating the O_2 exchange in streams. Gas tracer techniques estimate the gas exchange coefficient by releasing a gas into a reach and measuring the downstream loss of the gas. To ensure full lateral mixing, we injected Ar via a string of 10 microdiffusers across the stream channel (Figure 4.3). To measure the *background* stream water characteristics before injecting Ar, we measured conductivity, temperature, air pressure and we took replicate water samples for gas analysis at multiple downstream points (i.e., stations) from the injection point. For gas releases, we continuously injected Ar into the streamwater until steady state conditions were reached (~4 times the travel time [*Workshop*, 1990]); the latter were estimated based on the travel time of a sodium chloride slug addition to reach peak concentration in the streamwater [*Ulseth et al.*, 2019]. At steady state conditions, we measured the plateau streamwater characteristics with the same procedure as described for background measurements. We also collected streamwater samples upstream of the injection site at background and plateau to monitor any potential temporal variation in Ar concentration.

We measured Ar concentrations as $Ar:N_2$ using a membrane inlet mass spectrometer (MIMS) (*Kana et al.* [1994]) as detailed in *Hall Jr and Madinger* [2018]. We measured Ar:N2 because the accuracy of the MIMS for measuring ratios is substantially higher than absolute gas concentrations. Furthermore, for this reason, we did not enrich the Ar concentration more than 5% from background, as to ensure that we did not also affect the N2 concentration (and therefore the Ar:N2). $Ar:N_2$ was corrected for ambient ratios and normalized to the $AR:N_2$ of the first station (i.e., nearest station downstream the gas injection point). To estimate the decay rate of Argon at streamwater temperature, K_A [m^{-1}], we modeled the exponential decline of corrected and normalized $AR:N_2$, A_x, as follows:

$$A_x = A_0 e^{-K_A x},$$ (4.12)

where $A_0 = A_x$ (at $x = 0$) and x [m] is the distance along the stream with the first station being considered as the origin. We calculated K_A by fitting equation (4.12) to the background corrected ArN_2 data using Matlab software. Then, we calculated the gas exchange velocity, $k_A[\mathrm{md}^{-1}]$, from KA by:

$$k_A = K_A v \bar{z} 86400, \tag{4.13}$$

where $v[\mathrm{ms}^{-1}]$ is the average stream velocity, $\bar{z}$[m] is the average stream depth and 86400 is for the conversion of second to day. We standardized k_A to the Schmidt number of 600, $k600[\mathrm{md}^{-1}]$, [*Jähne et al.*, 1987; *Wanninkhof*, 1992] to compare gas exchange velocities across dates. We estimated stream discharge, $Q[\mathrm{m}^3\mathrm{s}^{-1}]$, and v using a sodium chloride slug addition (see section 4.2.2.1). Average stream width, w [m], was calculated using aerial pictures (see Section 4.2.3) and finally $\bar{z}$ was estimated from the mass conservation equation (i.e., $\bar{z} = \frac{Q}{wv}$).
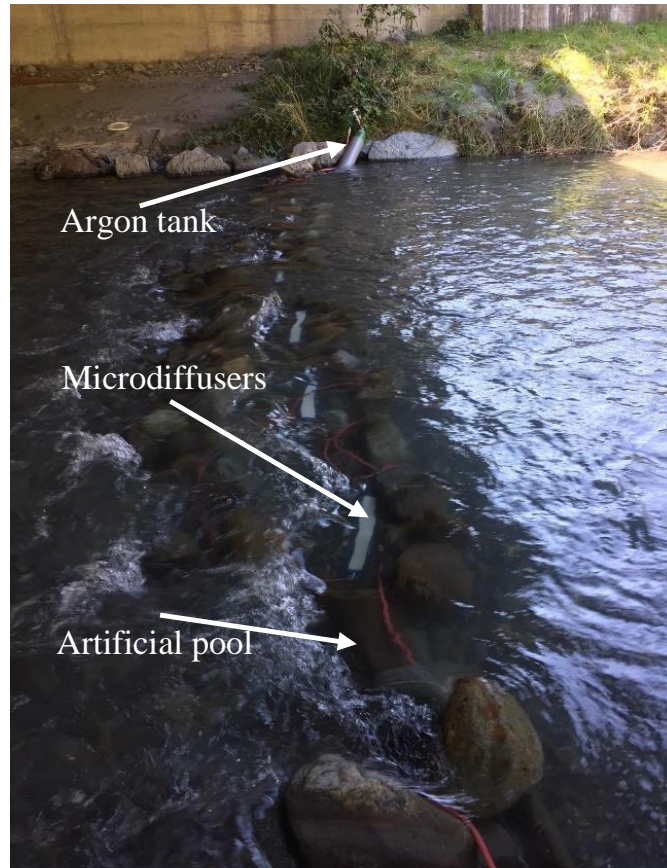
Figure 4.3 – Injection site.

4.3   Results and discussion

The average size (D_{mean}) of the macroroughness elements placed in the Aare River was 0.64 m (standard deviation, 0.19 m) following a Gaussian diameter size distribution (Figure 4). Based on this statistical size distribution of macroroughness, we calculated the reach-scale
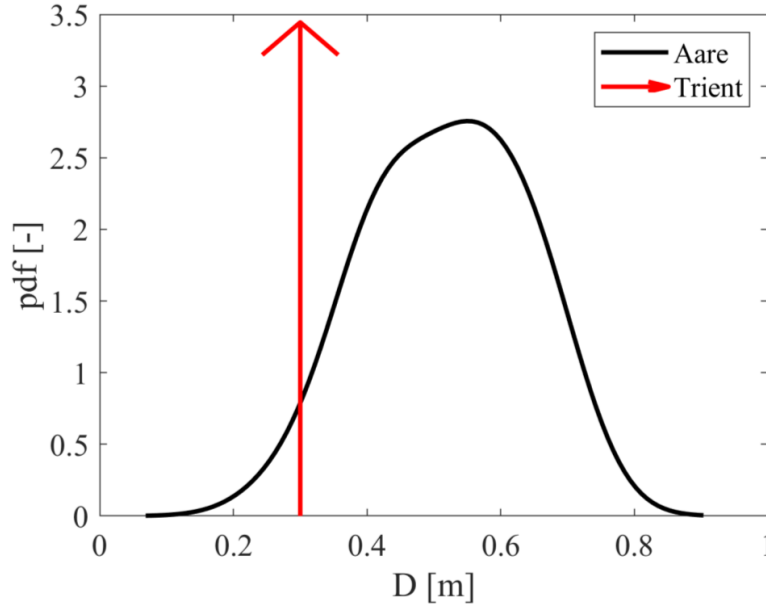
Figure 4.4 – Size distribution of macroroughness.

cumulative wake area as a function of the stream discharge (Figure 4.5). As the discharge increased, wake areas expanded due to the enhanced blockage effect imposed by the macroroughnesses to the streamflow to a certain discharge. At this discharge, the wake area contracted because the free surface macroroughness diameters decreased up to the discharge where macroroughness elements became fully submerged and no longer contribute to the wake area. The balance of the wake area expansion and contraction determines the overall trend of the cumulative wake area with respect to stream discharge. In our study reach in the Aare River, the cumulative wake area increased with the discharge up to where $Q = 2.5 [\mathrm{m}^3/\mathrm{s}]$ and then started to contract. It should be noted that $Q = 2.5 [\mathrm{m}^3/\mathrm{s}]$ corresponds the stream depth of $h = 0.28 [\mathrm{m}]$ which is approximately equal to the average height of the macroroughnesses (i.e., $\frac{D_{mean}}{2}$). This discharge can be considered as the environmental flow threshold because the ecological benefits of the macroroughness (i.e., wake areas) decreased with higher flow rates. Therefore, this can provide guidance to minimize environmental effects due to anthropogenic activities, such as reservoir operations. To investigate the relationship between the wake areas induced by macroroughnesses on the stream gas exchange, we performed multiple measurements in the presence and absence macroroughnesses in Trient stream (Figure 4.6). In comparison, when we applied the wake model to our artificial 'buckets' macroroughness, we found that the cumulative wake area (Figure 4.5) moronically increased to the point where macroroughness
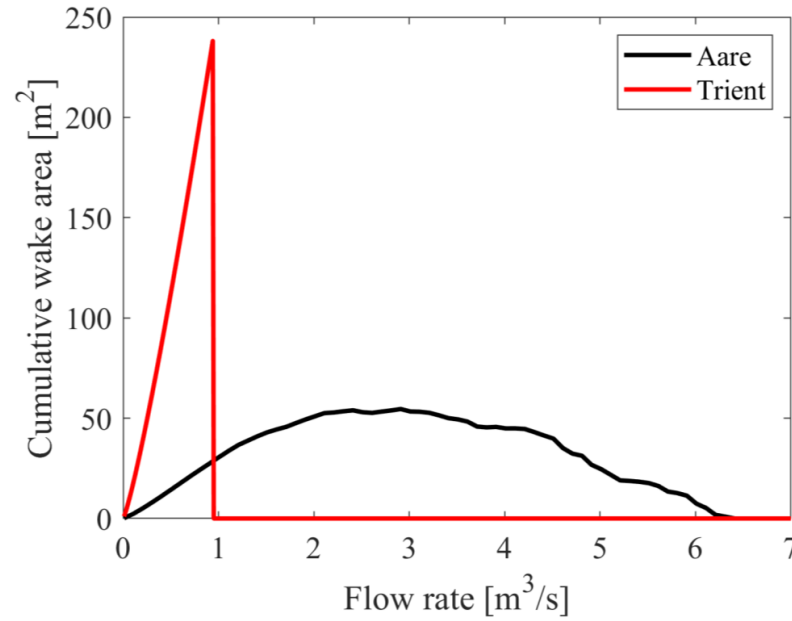
Figure 4.5 – Usable area.

elements became submerged (i.e., $Q \approx 1 [\frac{\text{m}^3}{3}]$). Above this discharge, macroroughness no longer contributed to the wake areas.

We found that non-submerged macroroughnesses (Q=0.83 and 0.88 $[\frac{\text{m}^3}{3}]$)) substantially enhanced the gas exchange (Figure 4.6). The $k600$ increased by 3-fold with the artificially macroroughness using the buckets. At higher discharge, however, $k600$ did not differ between fully submerged macroroughness and no macroroughness at all. Therefore, wake areas induced from non-submerged macroroughness lead to air entrainment into the water. This air-water entrainment in streams is driven by the turbulence level at the free surface. The latter is generally originated from the bed friction and the depth-scale form drag. Energy dissipation resulting from bed friction is the near the free surface energy dissipation rate based on turbulence originating from the channel bed of the stream [*Moog and Jirka*, 1999b]. If the turbulence originating from bed friction does not affect the air-water interface, then this turbulence will not enhance the gas-exchange. Energy dissipation from the depth-scale form-drag acts across the depth of flow (e.g., the wake generated by the non-submerged macroroughness). In this regard, high gas exchange velocities measured in steep mountain streams correlated with the level of macroroughness ([*Ulseth et al.*, 2019]) and where low submergence ratio (i.e., streams with a high ratio of roughness to water depth) resulting in high free surface turbulent levels. These high free-surface turbulent levels likely drove the extremely high k600 in these mountain streams. This was also evident in our results where only non-submerged macroroughness increased the gas exchange.

It is known from oceanography and physical limnology [*Moog and Jirka*, 1999b; *Wüest et al.*, 1992] that gas exchange is either bubble mediated (k600>35 [m/d]) or driven by the diffusive flux ($k600 < 35[\frac{\text{m}}{\text{d}}]$). Recently, such a shift in regimes was also reported from streams [*Ulseth*
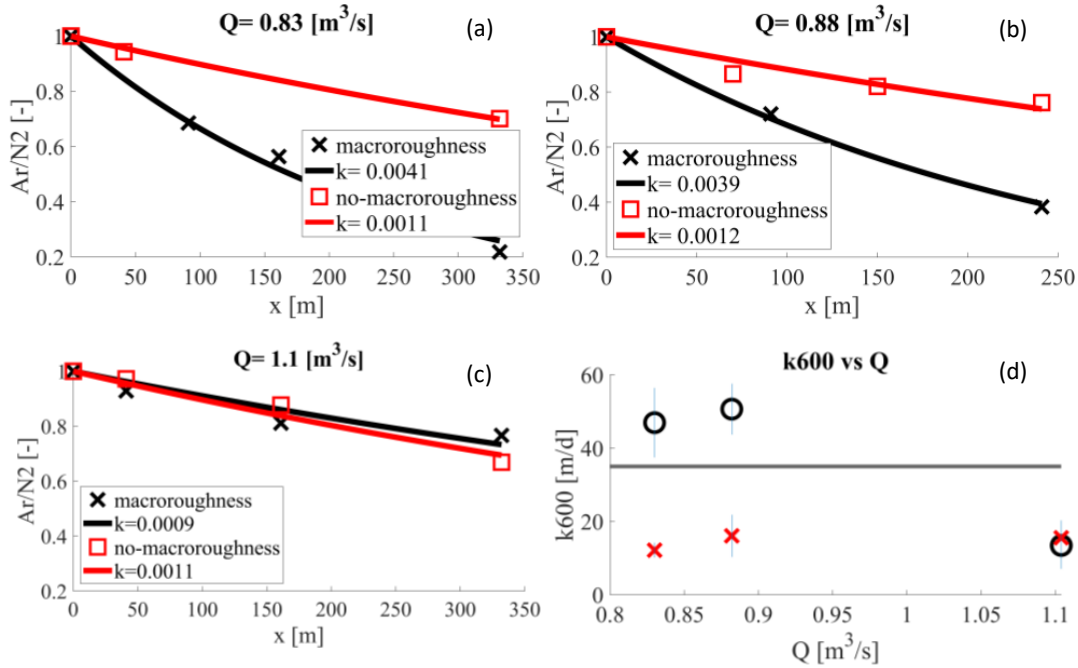
Figure 4.6 – Gas exchange in the presence and absence of macroroughness where in (a) and (b) macroroughness elements are not submerged and in (c) macroroughness elements are fully submerged. (d) $k600$ of all cases as a function of the stream discharge. Vertical lines denote the 95% confidence bounds.

et al., 2019]. Our results also support this notion. In fact, in the absence of macroroughness we did not observe 'white waters' with bubble formation and we obtained $k600$ values lower than 35 $[\frac{m}{d}]$. Bubble formation in streams enhances the gas exchange by creating additional turbulence due to the interactions between entrained bubbles and by significantly increasing the surface area of the air-water interface [*Chanson and Toombes*, 2003]. When we installed artificial macroroughness elements, $k600$ was greater than 35 $[\frac{m}{d}]$. This higher gas exchange velocity, could be, in part, bubble mediated because of the added turbulence in the free surface. This was also evident from the aerial images where partially submerged macroroughnesses created zones of white water.

To calculate the impact from macroroughness on the stream gas exchange, we calculated the difference in $k600$ with and without macroroughness. This impact decreased with increasing submergence ratio (Figure 4.7), that is, the fraction of the water depth to the macroroughness (i.e., bucket) height. Furthermore, owing to high turbulence in the wake areas and their consequent enhanced gas exchange, the wake area can be considered as the proxy of the regions with high rates of mixing and are therefore the likely main drivers of the reach scale gas exchange. Submerged macroroughness did not affect the gas exchange (Figure 4.7) since the energy dissipation rate from the depth-scale form-drag was likely to be negligible due to the high relative submergence. However, non-submerged macroroughness, by inducing wake areas at the air-water interface, significantly increased reach-scale gas exchange. These

findings are in agreement with the lab experiment results of *Kucukali and Cokgor* [2008] where the local aeration efficiency increased with increasing discharge and eventually declined to zero in case of full submergence. It is worth mentioning that the cumulative wake area induced by non-submerged macroroughness elements was less than 7% of the total stream area (i.e., length × width). In our case where only a small part of the streambed was covered by the wakes, gas exchange increased 3-fold. This is in line with the findings by *Ulseth et al.* [2019], on high-slope streams with significant contributions of 'white waters' and gas exchange velocities higher by one order of magnitude than for low-slope streams.
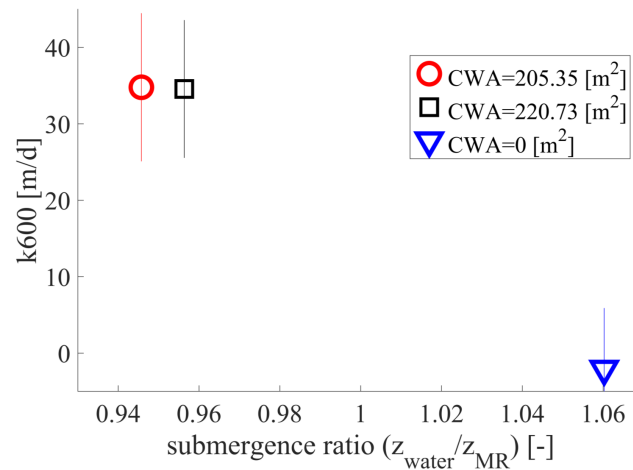
Figure 4.7 – Macroroughnesses impact on the gas exchange.

4.4 Conclusion

In this study, we provide the first experimental evidence of the role of macroroughness elements and associated wakes for the gas exchange in streams at the reach scale. Our findings show that the experimental addition of macroroughness to the streambed increased the gas exchange beyond the $k600$ threshold of 35 m/d where a regime shift from diffuse flux to a bubble mediated flux is expected. Our study paves the way towards a better design of restoration strategies aiming at enhancing water quality and habitat life in regulated streams. It may provide new guidance for hydropower operators charged with reducing downstream ecosystem impacts by defining environmental flow thresholds based on the ecological needs of particular streams. The fact that adding macroroughness and thereby inducing wakes to a small proportion of the stream (i.e., 7%) remarkably increases gas exchange shows the potential of artificial macroroughness elements for combating hypoxia in streams where minimum flows may now be sufficient to secure the required environmental improvement.

5 Conclusions and suggested future works

The development of water infrastructure provides services that are key to human wellbeing. Water engineering supports renewable energy, irrigation, urban development, and industry. But the growing trend in using water infrastructure significantly alters the natural flows of affected streams. As streamflow changes, environmental impacts will follow. Therefore, the use of water resources, such as from impounded streams, should be done in an environmental friendly manner to minimize impacts. Therefore, in my PhD thesis, I aimed to develop hydrological and hydraulic solutions for habitat sustainability in human-altered streams.

To reduce cascading effects downstream from dams, minimum flow releases are widely used. However, these static flow release rules cause new problems, such as the loss and homogenization of biodiversity. To address this issue and also to improve the environmental efficiency of flow releases, I developed a Direct Policy Search (DPS) framework for reservoir systems based on defining dynamic flow release rules (i.e., non-proportional flow releases) that finds optimal flow release policies towards efficient economic and environmental efficiency. My results showed that non-proportional flow releases provide better performances of the reservoir system compared to constant minimum flow release operational policies. We detected a vertical Pareto's frontier in the global efficiency plot that means substantial improvement in the environmental indicator is possible without compromising a significant loss in energy production with efficient water management policies. Dynamic environmental flow release policies allowed for a better use of reservoir storage dynamics, which enabled to capture and laminate flood events while recovering part of them for energy production. We assessed the Pareto's frontier shape under different hydrological regimes, showing that non-proportional flow releases remain efficient under uncertainties of hydrological changes.

The contributions of macroroughness to stream ecosystem functioning have not been well studied due to their relatively small scale. I developed an environmental indicator, which is based on the estimation of wake areas induced by macroroughness elements. The proposed environmental indicator was included in the DPS framework to find optimal flow releases for a reservoir. Different from common approaches to define an environmental flow threshold that are only based on hydrology, my findings showed that streambed roughnesses will largely affect the minimum threshold flow.

Aiming to provide empirical evidence for the effects of macroroughness elements on stream ecosystem functioning, I performed field studies in two streams. In a restored stream (Aare, Switzerland), I used drone-borne remote sensing to find the statistical distribution of macroroughness elements. Next I used it to calculate the induced wake areas and the consequent environmental flow threshold for this stream. I also studied the relationship between the near free surface turbulence generated by the macroroughness-induced wake areas and the stream gas exchange in a regulated stream (Trient, Switzerland). Here I used tracer gas injections in the presence and absence of experimentally manipulated macroroughness elements with different degrees of submergence, representing different turbulence levels. While the gas exchange was not affected by submerged macroroughness elements, non-submerged macroroughness elements significantly increased the reach scale gas exchange. In particular, the addition of wakes to a small proportion of the stream (i.e., 7%) led to a 3-fold gas exchange increase.

As the development of water infrastructure is growing because of human population growth but also because of climate change, the findings of my PhD thesis will help promote more environmentally sustainable river management policies by better characterizing affected streams, as well as proposing more environmentally friendly flow release rules.

The work presented in my PhD thesis certainly leaves much room for future research and development. The key point is that future research topics should be done in a more and rational manner to address challenging and meaningful problems that affect our society. The potential issues of what could/should be done in continuation of this thesis are discussed in the following:

• Regarding water management policies in reservoir systems, I developed a new dynamic flow release policy and tested it in a synthetic case study. A good continuation of this work would be to apply this flow release rule to an existing reservoir case study. Reservoir operators are sometimes hesitant to share data. However, I do believe that through good communication, especially in explaining the importance of environmental sustainability, relevant data can be made available to researchers. I also believe that it is the fundamental right of the society to know the usage of natural resources. Therefore, from the legislative point of view, hydrological data and others related to water resources should be disclosed to the public.

• In the DPS framework, I included 34 different indicators and then integrated them into single one, namely, the "environmental indicator". The goal was to develop an indicator as general as possible which can then be applied to specific cases. Therefore, a thorough sensitivity analysis of 34 indicators and the way they are integrated can shed more light on the efficiency of the environmental indicator to represent more precisely the level of ecological disturbance. Also, it may be worth to investigate whether a single environmental indicator is more meaningful than using all indicators, and solve an optimization problem with several objectives (in my case 34 objectives).

• In the streambed macroroughness section of my PhD thesis, we investigated the impact of submerged and non-submerged macroroughness elements on reach-scale gas exchange. However, since the stream did not have significant flowrate variability because of the operation of an upstream reservoir, we could not investigate the relationship between different submergence levels (i.e., turbulence magnitude) and stream gas exchange. Therefore, performing further

experiments in streams with more discharge variability can help to establish an empirical equation, linking gas exchange and turbulence.

• The other potential research topic regarding gas exchange is to study its relationship with white water areas of streams. White waters are known to be regions of high gas exchange rates. With the recent advancements in remote sensing, it is now possible to obtain high precision images from the stream via drones. These images can be analyzed via image processing to detect white water areas. Since measuring gas exchange using gas tracer additions is still crucial, developing models to predict the gas exchange based on the white water areas would substantially simplify the process.

A Improving the ecohydrological and economic efficiency of Small Hydropower Plants with water diversion[1]

Abstract

Water exploitation for energy production from Small Hydropower Plant (SHP) is increasing despite human pressure on freshwater already being very intense in several countries. Preserving natural rivers thus requires deeper understanding of the global (i.e., ecological and economic) efficiency of flow-diversion practice. In this work, we show that the global efficiency of SHP river intakes can be improved by non-proportional flow-redistribution policies. This innovative dynamic water allocation defines the fraction of water released to the river as a nonlinear function of river runoff. Three swiss SHP case studies are considered to systematically test the global performance of such policies, under both present and future hydroclimatic regimes. The environmental efficiency is plotted versus the economic efficiency showing that efficient solutions align along a (Pareto) frontier, which is entirely formed by non-proportional policies. On the contrary, other commonly used distribution policies generally lie below the Pareto frontier. This confirms the existence of better policies based on non-proportional redistribution, which should be considered in relation to implementation and operational costs. Our results recommend abandoning static (e.g., constant-minimal-flow) policies in favour of non-proportional dynamic ones towards a more sustainable use of the water resource, also considering changing hydroclimatic scenarios.

A.1   Introduction

Small Hydropower Plants (SHP) are a class of low-capacity (typically lower than 10 MW) energy production power plants often based on either flow diversion from water intakes or run-of-the-river water use concepts. Whenever there is water diversion from the river,

---

[1]The contents of this chapter are published in: Razurel, P., Gorla, L., Tron, S., Niayifar, A., Crouzy, B. and Perona, P., 2018. Improving the ecohydrological and economic efficiency of Small Hydropower Plants with water diversion. Advances in Water Resources, 113, pp.249-259. I contributed to development of the model, performing the simulation and data interpretation.

and depending on the operational policy, a residual flow is generally released downstream the intake. In part driven by the fear of a Fukushima scenario and in view of limiting carbon emissions from fossil fuel power generation, energy production is turning to renewable sources. Among others, SHP installations are growing although the installed global (i.e., all power plant types) hydropower potential in some countries already exceeds 70% of the feasible potential (e.g., USA and Switzerland, see Figure A.1). Some other country, e.g the United Kingdoms, currently uses less than 60% of its potential. Indeed, due to both economic reasons and limitations of technology, sites with lower hydraulic heads or power outputs were not considered as suitable for energy production in the past. This offers some interesting development opportunities for the future provided that environmentally friendly solutions are adopted for further exploitation of freshwater resources. In this work we show how the global (i.e. economic and environmental) performance of flow-diversion practice for feeding SHPs can be improved by engineering a new class of dynamic residual flow policies, and will show this on three real SHP case studies.
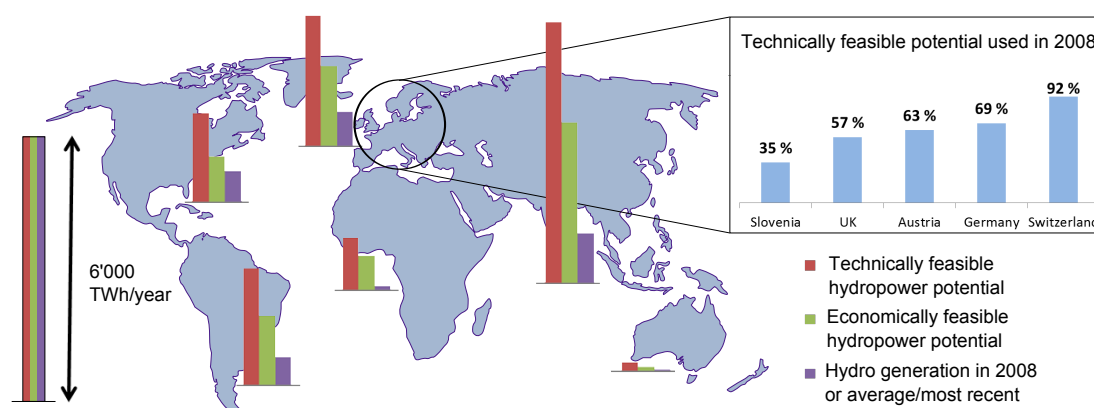
Figure A.1 – Worldwide consumption of hydropower energy potentials. A detailed view of selected European countries is also provided. Up-to-date (2016) installed vs potential SHP power capacities for Africa (580 vs 12198 MW), Americas (7864 vs 44161 MW), Asia (7231 vs 120588 MW), Europe (18685 vs 32943 MW), Oceania (447 vs 1206 MW) are available in detail from *UNIDO* [2016].

We focus on SHPs without significant storage capacity, which withdraw water from an intake installed at a specific river transect, and return it downstream below the power house (Figure A.2). Among SHPs, the latter is the scheme with the highest environmental impact in terms of affected riverine corridor length. In the majority of the cases, SHPs also apply residual flow policies set to constant minimal amounts (minimum flow release, henceforth referred to as MFR). Politically simple to define, MFR policies have no specific ecological basis, and their extensive use systematically affected first the morphology and then the ecosystem of river corridors [*Poff et al.*, 2007; *Moyle and Mount*, 2007]. As today's society acknowledges the value of ecosystem services under resource exploitation [*Arthington et al.*, 2006], the classic MFR policy is not sustainable anymore [*Poff et al.*, 2010]. Hence, dynamic environmental flow releases mimicking the natural flow regime variability have recently been suggested

as preferable (e.g. *Basso and Botter* [2012]; *Perona et al.* [2013]) in order to cope with the ecosystem resilience to perturbations and reduce the risk of critical transitions to different statistical equilibrium states [*Scheffer*, 2009; *Scheffer et al.*, 2012]. Such dynamic redistribution practices (called "proportional" from now on) consist of the release of a certain percentage of the total flow to the environment (e.g., 20%, 30%) while exploiting the remaining fraction up to the plant nominal capacity. Although innovative and beneficial for the environment compared to minimal-flow, proportional policies suffer from the fact that the percentage of redistribution is, by definition, independent of the incoming flow carried by the river.
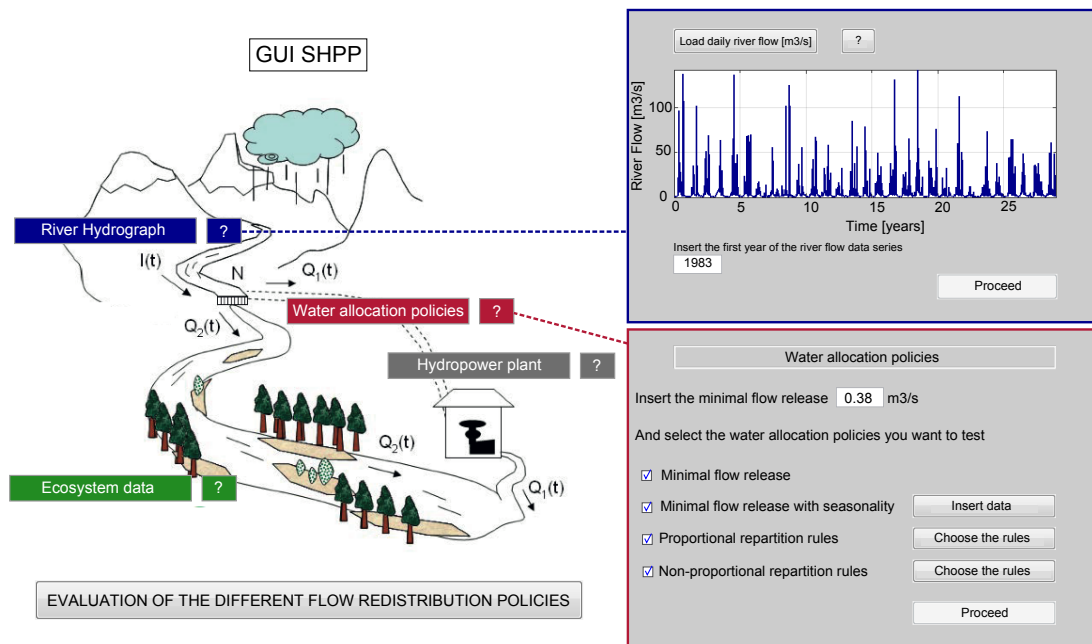
Figure A.2 – SHP schematics and the corresponding river reach affected by reduced water variability. The two panels on the right show the Graphical User Interface (GUI) developed to perform the numerical simulations. In the top panel the user enters the natural hydrograph used as an input for the model. On the bottom panel, the different water allocation policies simulated by the model can be selected.

In order to find more efficient redistribution rules, non-proportional policies have been proposed [*Perona et al.*, 2013; *Gorla and Perona*, 2013] and their global efficiency preliminary investigated by *Gorla* [2014] and *Razurel et al.* [2016]. In contrast to proportional policies, the fraction of water released to the environment is defined by a non-linear function which depends on the value of the incoming flow . The conceptual basis of non-proportional redistribution is the paradigm of sustainable development, which recognizes the right of applying limited human pressure to the environment [*Arthington et al.*, 2006]. Hence, the more flexible the redistribution rule is, the more efficient the use of water by the riverine ecosystem will be. In this paper we extend the work of *Razurel et al.* [2016] by first improving the description of the ecohydrological indicators; second, we numerically simulate hundreds of thousands of non-proportional policies and show that Pareto efficient redistribution rules

(i.e., the Pareto frontier) are indeed made by non-proportional policies; third, we perform a sensitivity analysis on the weight used to compute the ecohydrological indicator. We show the results for three Swiss case studies also under the effect of changing hydroclimatic scenarios. Potentially, these policies may be successfully applied to any river intake structures, which are primarily used to intercept and divert water from the main stream to serve, as either a storage reservoir or directly for a human use.

A.2   Methodology and data description

A.2.1   Non-proportional water allocation policies

The problem of defining the optimal water allocation for dammed systems [*Castelletti et al.*, 2007; *Soncini-Sessa et al.*, 1999; *Niayifar and Perona*, 2017] clearly simplifies for water intakes with negligible storage capacity. With reference to Figure A.2, let us assume that the fraction $Q_1(t)$ of the total incoming flow $I(t)$ at the intake is delivered to the power house. By virtue of the conservation law, the difference

$$Q_2(t) = I(t) - Q_1(t) \tag{A.1}$$

will be allocated to the riparian ecosystem. The environmental utility for using that water has been shown to be indirectly evaluated by the human use benefit function [*Perona et al.*, 2013]. The optimal water allocation can be identified by evaluating which redistribution rule maximizes the global (i.e., economic and environmental) benefits obtained by assigning $Q_1(t)$ to the power house and $Q_2(t)$ to the environment over a reference time frame [*Gorla and Perona*, 2013].

With the purpose of systematically exploring a large number of water allocation policies representing both proportional and non-proportional redistribution rules, *Razurel et al.* [2016] introduced a class of nonlinear functions [*Gorla*, 2014] by modifying the Fermi-Dirac distribution well known in quantum physics [*Lifshitz and Landau*, 1984]. Other ways could have been used to define the non-proportional allocation function but this one has been chosen because it comprises many reasonable redistributions in a simple mathematical function, which is also parsimonious in the number of involved parameters. Thus, the fraction of water that is released to the environment is defined by the following equation:

$$f(x) = \left[1 - M - \frac{Y}{\exp[a(x-b)] + c} \right] (j - i) + i \tag{A.2}$$

with $M = \frac{A}{A-1}$, $Y = (1-M)[\exp(-ab) + c]$ and $A = \frac{\exp(-ab)+c}{\exp[a(1-b)]+c}$. This function allows the generation of water allocation policies by varying only few parameters (i, j, a, b), as hereafter described. The parameters i and j are used to set the bound of the Fermi function. The parameter i ranges within [0;1] and represents the fraction of water left in the river at the

beginning of the competition ($I = I_{min}$). The parameter j ranges also within [0;1] and correspond to the fraction of the incoming flow rate left in the river at the end of the competition ($I = I_{max}$). Non-proportional allocation starts for an incoming flow rate $I_{min} = Q_{mfr} + Q_{mec}$, where Q_{mfr} represents the minimal flow release and Q_{mec} is the minimum flow required to activate the turbines; below I_{min}, all the water goes to the environment. Initially, a fraction i of the dimensionless flow $x = \frac{I - I_{min}}{I_{max} - I_{min}}$ above 0 (for $I = I_{min}$) is allocated to the environment as

$$Q_2 = f(x) \cdot (I - I_{min}) + Q_{mfr}, \tag{A.3}$$

the minimal flow requirement being thus always guaranteed. The competition ends at an incoming flow rate $I_{max} = \frac{Q_N - Q_{mec}}{1 - j} + Q_{mfr} + Q_{mec}$, when the nominal power of the turbine is reached at $Q_1 = Q_N$. Therefore, for $I_{min} < Q < I_{max}$ the water is dynamically allocated between the environment and the hydropower plant, depending on the value of the incoming flow I. At the end of the competition, $j < 1$ is the fraction of x left to the environment (see also *Razurel et al.* [2016] for details). Beyond I_{max}, river discharge exceeding Q_N is allocated to the environment spilling.

When $i = j$ the model generates proportional repartition rules. In this particular case, the quantity of water Q_2 allocated to the river is a fixed percentage (e.g., 10%, 20%) of the water inflow I in addition to the minimal flow requirement. The parameter a allows a variation of the smoothness of the transition between the environmental water allocation i relative to low flows and j relative to high flows (see Figure A.3). In the limit of a very large a, one obtains a steep-like transition. Conversely, a small a yields a linear interpolation between i and j. By varying the parameter b, one introduces a change of concavity and controls the position of the inflection point. If the change of concavity is outside the interval [I_{min}, I_{max}], one obtains either a convex or a concave function. Finally, the parameter c gives the overall shape of the curve. Gray curves in Figure A.3 show a representative sample of feasible non-proportional water repartition rules given by Equation A.2. These were obtained from 36 combinations of a and b, while fixing i and j. Pink curves correspond to the same 36 combinations of a and b, but are obtained by inverting i and j.

A.2.2 Ecohydrological indicators

River rehabilitation often relies on restoring a more natural flow regime [*Petts*, 2009; *Bartholow*, 2010b], which suggests that optimal flow releases should be dynamic and show a variability similar to that of the natural flow regime [*Poff et al.*, 1997]. We propose to evaluate the environmental performance of the dynamic releases by building a dimensionless synthetic ecohydrological indicator. In particular, this joins the assessment provided by the Indicators of Hydrologic Alteration proposed by Richter et al. [*Richter et al.*, 1996b] with an evaluation of the habitat availability for fish (Figure A.4). Other indicators like the hydro-morphological index of diversity (HMID) developed by *Gostner et al.* [2013a] exist, and have already been applied to real case studies [*Gostner et al.*, 2013b]. Their choice is a valid alternative, which

Appendix A. Improving the ecohydrological and economic efficiency of Small Hydropower Plants with water diversion
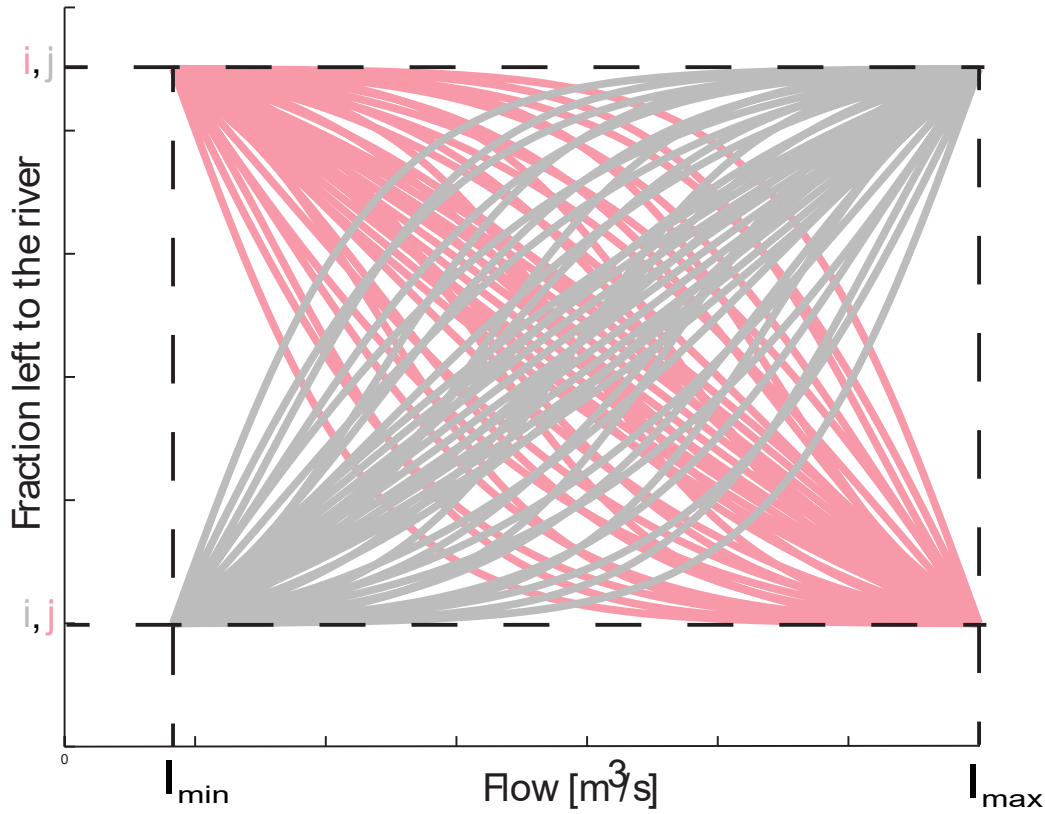
Figure A.3 – Example of non-proportional repartition rules obtained with the modified Fermi function (Eq. A.2). The gray curves show an example of 36 non-proportional functions obtained for different combination of the parameters a and b while i and j are fixed ($i < j$).The pink curves correspond to the same combinations of a and b but parameters i and j are inverted ($i > j$).

depend, however, on river morphological complexity and general data availability.

The 32 Indicators of Hydrologic Alteration (IHA) proposed by Richter et al. (1996) are an effective attempt to quantify the variability of the natural flow dynamics and deviations from it for altered flow regimes. Coherently with this idea we use the IHAs to minimize the "hydrologic distance" (in terms of *Rate of non Attainment (RnA)* and *Coefficient of Variation (CV)*) between natural conditions and the flow regime resulting from every regulation policy, as detailed in *Gorla and Perona* [2013]. We recall here that the *RnA* is defined as the fraction of simulated years in which each IHA falls outside a range defined from the natural flow regime (for each IHA).

From $RnA(k)$ and $CV(k)$ we compute the indicators $Hyd1_{sim}$ and $Hyd2_{sim}$ by first intra- and subsequently inter-groups of arithmetic means of the IHA (see *Gorla and Perona* [2013] and *Razurel et al.* [2016] for details),

$$Hyd1_{sim} = 1 - E\left[(RnA_{sim}(k) - RnA_{nat}(k))^2\right], \tag{A.4}$$
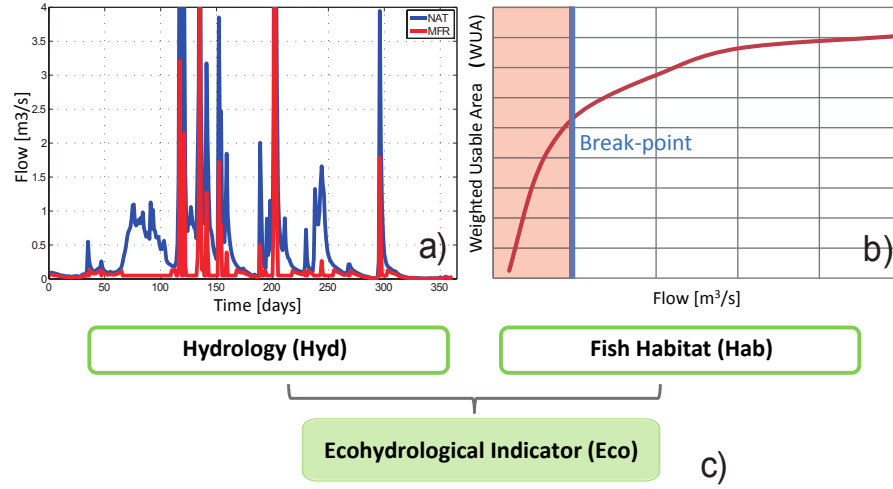
Figure A.4 – a) Hydrologic differences between the natural flow and environmental releases generated by a classic minimal flow requirement approach (data from the Buseno case study). b) Sketch of the common shape of a Weighted Usable Area (WUA) curve, computed on the basis of surveying and PHABSIM simulations. The break-point generally corresponds to a remarkable change in the slope of the curve. c) Generation of the dimensionless and synthetic ecohydrological indicator Eco from hydrologic (Hyd) and fish-habitat (Hab) information.

$$Hyd2_{sim} = 1 - E\left[(CV_{sim}(k) - CV_{nat}(k))^2\right], \tag{A.5}$$

where k refers to each of the 32 IHA.

In addition to hydrologic alteration, habitat availability also plays an important role in species protection. This can be assessed by modelling habitat preference curves generally obtained from river surveys and hydraulic measurements [*Milhous et al.*, 1984a; *Maddock*, 1999; *Bloesch et al.*, 2005]. In the three projects considered in this work, surveys were made on the river reaches impacted by reduced flow with PHABSIM (Physical Habitat Simulation) [*Milhous et al.*, 1984b]. Fishing being the main ecosystem of interest in our case, Weighted Usable Areas (WUA) curves were computed for one dominant fish species, the *brown trout*, discriminating between *juveniles* and *adults* [*EcoControl*, 2013, 2011, 2012]. This method was chosen according to the available data, mainly the hydrograph. Figure A.4b shows a qualitative example of the preference curve resulting from PHABSIM method. A common practice to define static threshold, like Q_{mfr}, is to define a breaking point, intended as significant changes of the WUA curve slope, and to consider it as the limit above which a further increase in environmental flow is marginally low. As this method represents a static concept, we improve and extend its use for evaluating dynamic flow releases. We assume that fish stress due to inadequate combination of substrate, water depth and speed, is more relevant when prolonged in time [*Payne*, 2003]. We use the original WUA curves reproducing empirical data and the breaking points recommended in the official project reports in order to identify the threshold (blue line in Figure A.4b). Eventually, we quantify the number of consecutive days the environmental release is below the threshold and use this as a proxy for fish habitat conditions.

Appendix A. Improving the ecohydrological and economic efficiency of Small Hydropower Plants with water diversion

$Hab1_{sim}$ and $Hab2_{sim}$ thus represent the maximal number of consecutive days, computed over the whole simulation time, characterized by flows under the critical thresholds identified by breakpoints, for juveniles and adults, respectively. Such thresholds were fixed equal to 1.2 $[m^3/s]$ for young fish and 0.73 $[m^3/s]$ for adults in Buseno, 0.50 $[m^3/s]$ for both categories in Cauco, and 0.55 $[m^3/s]$ for young fish in Ponte Brolla, where impacts on adults were considered as negligible [*EcoControl*, 2013, 2011, 2012].

We then aggregate $Hyd1_{sim}$ and $Hyd2_{sim}$ into two hydrological sub-indicators, E_1 and E_2, bounded between 0 and 1 as

$$E_1 = 1 - \frac{Hyd1_{sim} - Hyd1_{min}}{Hyd1_{max} - Hyd1_{min}}; E_2 = 1 - \frac{Hyd2_{sim} - Hyd2_{min}}{Hyd2_{max} - Hyd2_{min}}. \tag{A.6}$$

The indicators with subscript min and max correspond to the scenarios having the minimal and maximal impact on the river, respectively; in this work they correspond to the natural flow regime (no-impact) and to the minimal flow requirement policy.

Similarly, we aggregate $Hab1_{sim}$ and $Hab2_{sim}$ into two fish habitat availability sub-indicators, E_3 and E_4,

$$E_3 = 1 - \frac{Hab1_{sim} - Hab1_{min}}{Hab1_{max} - Hab1_{min}}; E_4 = 1 - \frac{Hab2_{sim} - Hab2_{min}}{Hab2_{max} - Hab2_{min}}. \tag{A.7}$$

The hydrological indicator Hyd is calculated by doing the weighted geometric average of the sub-indicators E_1 and E_2,

$$Hyd = e^{w_1 \cdot \ln E_1 + w_2 \cdot \ln E_2}, \tag{A.8}$$

where w_1 and $w_2 = 1 - w_1$ are the weighting factors of E_1 and E_2. The exponential form is used here as a convenient way of representing the weighted geometrical mean.

The fish habitat indicator Hab is calculated by doing the weighted geometric average of the sub-indicators E_3 and E_4,

$$Hab = e^{w_3 \cdot \ln E_3 + w_4 \cdot \ln E_4}, \tag{A.9}$$

where w_3 and $w_4 = 1 - w_3$ are the weighting factors of E_3 and E_4.

The indicators Hyd and Hab are finally aggregated to calculate the dimensionless synthetic ecohydrological indicator Eco,

$$Eco = e^{w_5 \cdot \ln Hyd + w_6 \cdot lnHab}, \tag{A.10}$$

where w_5 and $w_6 = 1 - w_5$ are the weighting factors of Hyd and Hab.

Weights should be defined case-by-case, on the basis of expert's opinion and considering the status of the specific riparian ecosystem. In this work we chose not to express preferences and weighted all the indicators as equally important in all numerical simulations [*Richter et al.*, 1996b, 1997]. However, in order to explore how weighting impact the results, we performed a sensitivity analysis for the weighting factor w_5.

Table A.1 – List and parameters of the three case studies considered in this work.

Location	Catchment	Head	Turbine type	Q_N	Q_{mfr_1}	Q_{mfr_2}	Power	Energy Production
	$[km^2]$	$[m]$		$[m^3/s]$	$[m^3/s]$	$[m^3/s]$	$[kW]$	$[GWh]$
Buseno	120	66.5	Cross-flow	4.5	0.38	0.60	2340	8.8
Cauco	89	49.9	Cross-flow	3.5	0.315	0.60	1390	5.0
Ponte Brolla	592	39.5	2 x Francis	12	0.55	0.86	1900	13.9

A.2.3 Case studies

We chose three small hydropower case studies (henceforth denominated Buseno, Cauco, and Ponte Brolla) located in Southern Switzerland, whose details are reported in Tab.A.1. For the three case studies we compared the effects of the following sub-classes of water allocation policies: (i) scenarios MFR_1 and MFR_2, representing traditional minimal flow requirement policies with one or two thresholds (the second one is introduced to increase the minimal flow value from April 1st to September 30th), respectively Q_{mfr_1} and Q_{mfr_2} defined in Table A.1; (ii) dynamic flow releases, proportional to I(t) (fixed percentages going from 10% to 50% with a step of 5%); (iii) dynamic flow releases, non-proportional to I(t) (flow-dependent, variable percentages as previously described). In particular, the non-proportional water allocation policies were obtained by varying i and j from 0.02 to 0.70 with 0.01 increment, a from 2 to 8 with step equal to 2, b from 0 to 1 with step 1/8, and considering c constant and equal to 1, for a total of 168912 considered alternatives. The minimal flow requirement Q_{mfr_1} was enforced by law and was therefore always guaranteed for each simulated scenarios.

We used 29 years of streamflow data measured by the Swiss Federal Office for the Environment as natural inflows $I(t)$ to evaluate scenarios in the period $1983 - 2011$. For Cauco and Ponte Brolla, power plant locations along the river are not the same as the locations from which the historic flow series have been obtained. We therefore transposed streamflows measured at Buseno and Bignasco gauging stations using a surface ratio by rescaling them to the respective catchment areas [*Dingman and Dingman*, 1994; *Brutsaert*, 2005]. The dependence of hydropower production B_1 on river discharge Q_1 was approximated by a 2nd degree polynomial equation $B_1 = m \cdot Q_1^2 + p \cdot Q_1 + q$, with m, p, and q depending on each plant turbine and associated to a fitting law showing a fitting correlation coefficient R^2 larger than 0.9 (see *Gorla* [2014] for details).

A.2.4   Climate change impact on streamflow

The effect of climatic changes on water availability for the the periods 2020-49 and 2070-99 has been obtained by considering the emission RCP 6.0 scenario [*Flato et al.*, 2013], which has been extensively applied to project future climate in several alpine regions of Switzerland. In brief, this scenario foresees by the end of the century a mean global increase of Earth surface temperature of about 2.8°C during summer, with a possible range of +1.7 to +4.5°C in Alpine Swiss Cantons. The expected winter temperature variations are approximately 2°C smaller. The projected precipitation regime is even more uncertain given the present inherent stochasticity of the phenomenon [*Brönnimann et al.*, 2014]. Overall, streamflows are expected to increase in magnitude in the period $2020 - 2049$ due to the melting and shrinking of alpine glaciers. This scenario will progressively move to a nivo-pluvial flow regime in the period $2070 - 2099$ characterized by higher flows during late winter, early spring time. Those changes are shown in Figure A.5. A recent report [*Job et al.*, 2011] describes the evolution of the Gornera basin (located in Southern Switzerland near the considered catchments) in response to such changes and to stored ice and snow in the basin. We considered this scenario as representative for the three basins chosen and based on that we generated time series of daily streamflow expected for the periods $2020 - 2049$ and $2070 - 2099$ for each each basin (e.g. see *Gorla* [2014]).
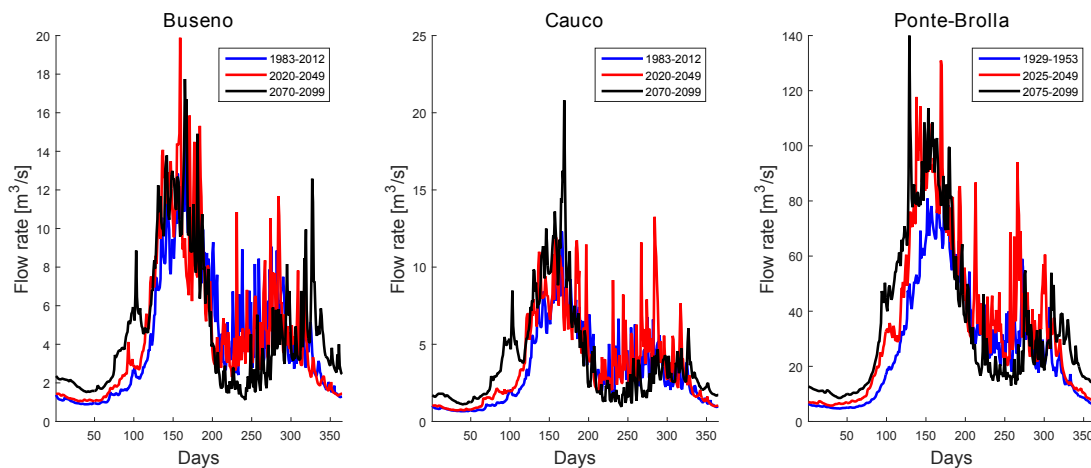
Figure A.5 – Changes in the mean annual hydrograph for medium and long term under the considered climate scenario RCP 6.0 [*Flato et al.*, 2013] for the three different case studies: Buseno, Cauco and Ponte Brolla.

A.2.5   Development of a Graphical User Interface and Numerical Simulations

A Graphical User Interface (GUI) (Figure A.2) has been developed using the software Matlab to facilitate the data treatment and the selection of the optimal water allocation functions among the different scenarios (non-proportional, proportional and MFRs repartition rules). For each scenario, the energy production and the ecohydrological indicators were computed based on the generated flows As a result, the efficiency graph, showing the mean annual energy

produced during the analyzed period versus the ecohydrological indicator, was plotted. The Pareto front, representing the ensemble of optimal water allocation scenarios, was identified and enhanced with a red line in the efficiency plot. More details are provided in Appendix.

A.3 Results

A.3.1 Efficiency plot and selection of optimal scenarios

Figure A.6 shows the performances of Buseno hydropower plant in terms of efficiency plot for all the 168912 water repartition rules obtained from Equation A.2. Each gray and pink point of the efficiency plot corresponds to a non-proportional repartition policy, and can thus be compared to more classic scenarios, e.g. based on minimal flow requirement and proportional water allocation policies.

As expected, scenario MFR_1 has the highest hydropower production and the lowest environmental performance. The scenario MFR_2 in Buseno, in which the minimal release is increased from April 1st to September 30th to a second fixed threshold, shows a reduction of hydropower production by 3.4% and an increase of ecohydrological indicators by 2.5% with respect to the performances of MFR_1. This scenario may be improved by applying proportional repartition rules. Among these, the one that leaves 10% of the incoming flow to the environment preserves the energy production of scenario MFR_2, while increasing the ecohydrological benefits by 4.7%.

However, the benefits obtained with the 10% proportional rule, can still be improved by moving vertically or horizontally toward the Pareto frontier, enhancing the ecohydrological indicators and the energy produced, respectively. A notable result is that the Pareto frontier is entirely composed by non-proportional repartition rules (henceforth referred to as "efficient"). It is worth recalling here that, at the Pareto frontier, it is not possible to improve a scenario by making an indicator better without making another one worse. For this power plant, changing a proportional repartition rule with an efficient one (i.e., that lies on the Pareto frontier) causes a 5% hydropower production average improvement and a 3% improvement for the ecohydrological indicators. These percentages were obtained, with reference to Figure A.6, by moving vertically and horizontally from proportional alternatives towards points located on the Pareto frontier.

Similar results are obtained for Cauco power plant, but not for the one in Ponte Brolla, as shown in the left-hand side panels of Figure A.7. For the latter case, proportional repartition rules perform already well and the ecohydrological indicator resulting from the simulated alternatives is already high, thus making the improvement almost negligible, (the potential improvement of using efficient non-proportional distribution to replace proportional distribution is between 0.0% and 0.1%). This is mainly due to the fact that, in Ponte Brolla, habitat thresholds (the blue line shown in Figure A.4b) turned out to be lower than Q_{mfr} because of the particular canyoning morphology of the regulated reach, where a minimal flow release

Appendix A. Improving the ecohydrological and economic efficiency of Small Hydropower Plants with water diversion

Table A.2 – Quantification of the averaged improvements for the alternatives shown in Figure A.7. They were obtained by replacing proportional repartition rules with efficient non-proportional ones, improving one indicator at a time.

Foreseen amelioration of non-proportional policies						
Case study	1983-2012		2020-2049		2070-2099	
	Eco	HP	Eco	HP	Eco	HP
Buseno	3.1%	2.4%	4.6%	2.2%	1.8%	1.9%
Cauco	8.6%	1.0%	19.8%	1.0%	22.8%	0.8%
Ponte Brolla	0.1%	2.3%	0.1%	2.6%	0.0%	0.3%

also guarantees fish survival. Consequently, among the indicators, mainly the hydrologic one (i.e., Hyd) concurred to the definition of the global ecohydrological indicator Eco. This result is consistent with that shown by the sensitivity analysis performed while changing the weights used to build the ecohydrological indicator (shown ahead). That is, results similar to Ponte Brolla power plant can be obtained for both Cauco and Buseno in the limit of non considering the fish habitat availability. A backwards control on sub-indicators and Fermi's functions (see e.g. subplots in Figure 6) should also be done case-by-case on the basis of experts opinions in order to check the soundness of interesting alternatives.

A.3.2 Climate change scenarios

Our study shows that a general increase in hydropower production is foreseen for the periods $2020 - 2049$ and $2070 - 2099$ for all the three basins (Figure A.7). This right shift toward higher energy production of the efficiency plot can be explained by an increase of streamflow from 2020 to 2049 and a seasonal temporal shift of water availability in the period $2070 - 2099$, as predicted by climate models (Figure A.5). While the aftermath of glacier melting in $2020 - 2049$ is obvious as far as energy production is concerned, the effects of higher winter and spring precipitation expected in the second three decades requires an explanation. The latter regime sees a flattening of the current river hydrograph with a strong reduction of the summer maximum. As a consequence of such redistribution of water availability during the year, the number of days when turbines can be activated will increase, as the flow necessary for the turbine to operate, Q_{mec}, will be reached more often. The impact of climate change on the number of possible operation hours at Q_N per year is more uncertain, especially if no storage is available.

The ecological effects of regulation under climate change are complex and must be analyzed case-by-case. While an exception can be made for Ponte Brolla, where river morphology always guarantees good habitat availability (even under low-flow MFR scenario), both Buseno and Cauco will see a worsening of both the proportional and constant flow release policies with respect to non-proportional ones. Table A.2 presents the average improvements obtained by moving from proportional to efficient non-proportional repartitions located on the Pareto frontier, for the three case studies and the three time periods. The results show that gains can

be obtained through the use of optimal allocation rules for the three case studies. For Buseno, the potential gain in ecohydrological indicator goes from 1.8% for the period 1983-2012 to 4.6% for the period 2020-2049. The foreseen amelioration of the energy production is around 2% for the three considered periods. The most important results concerning the ecohydrological indicator are those obtained for Cauco. Indeed, the foreseen amelioration of the ecohydrological indicator goes from 8.6% for the period 1983-2012 to 22.8% for the period 2070-2099. However, the potential gain in energy production is around 1%, which is lower than the two other case studies on average. Ponte Brolla shows the lowest gain in ecohydrological indicator, less than 1%, but the improvement of the energy production for the periods 1983-2012 and 2020-2049 are close to Buseno. These scenarios are valid assuming that even though the morphology of single river banks is dynamic, average fish habitat conditions in a river reach will not change over the considered time horizon.

A.4 Discussion

A.4.1 Role of ecohydrological indicator and sensitivity analysis

Figure A.8 shows the results of the sensitivity analysis performed for the three case studies: (a) Buseno, (b) Cauco and (c) Ponte Brolla. For each of the three plots, the two weighting factors w_1 and w_3 were set to 0.5 while the third factor w_5 was progressively increased from 0 to 1 with a step of 0.001. Thus the only parameter that was changed is the weighting of the hydrological indicator Hyd and the fish habitat indicator Hab to compute the final ecohydrological indicator Eco. For each combination of factors, a new efficiency plot is computed. The corresponding average amelioration in both ecohydrological indicator and energy production when replacing proportional rules by non-proportional ones were thus calculated and shown on the Y-axis of the plot.

Notably, the sensitivity analysis shows some different results depending on the case study. As far as Buseno (Figure A.8 (a)) is concerned, the average improvement of the ecohydrological indicator (red curve) with respect to proportional policies is decreasing when the weighting of the hydrological indicator is bigger than the habitat one, i.e. more weight is given to the hydrological indicator. The gain of energy production (blue curve) starts decreasing when w_5 is above 0.6. This shows that giving a superior weight to the hydrological indicator leads to a reduction in the power production gain. For Cauco (Figure A.8 (b)), the same tendency is observed for the environmental gain. However, the variation of the power production as a function of the weighting factor w_5 shows some fluctuations. In contrast to Buseno, no clear tendency is observed. The results for Ponte Brolla (Figure A.8 (c)) are different and the improvements of the power production and the ecohydrological indicator are constant, independently of the value of w_5. This is explained by the fact that for this specific case, the minimal flow release MFR is always greater than the value of the threshold defined to calculate the fish habitat indicator. Thus, the indicator Hab is always set to the constant maximum value. The order of magnitude of the power production gain is comparable to the

other stations but the environmental gain is lower.

The absolute value of the ecohydrological indicator has to be interpreted carefully since there is no other previous study applying the same methodology to combine the hydrological and fish habitat suitability indicators. The indicator has been built to evaluate how far from the natural series each scenario is, a value of 1 corresponding to the natural condition. Thus, we are more interested in the comparison of the different allocation scenarios and the results we are showing are more focused on the relative gain that may be obtained by using non-proportional policies. We show a method to choose the optimal distribution functions by comparing all the possible distribution methods. The sub-indicators have been chosen according to the available data, being mainly the natural hydrograph and the characteristics of the power plant, but may be improved if more data are available. The allocation rules we are presenting in the paper (non-proportional) have not been implemented yet so there are no empirical data available that allows a comparison between the pre-impact and post-impact systems.

A.4.2   General considerations and recommendations

Managing water resources to their maximal extent in Alpine countries will necessarily force people to be aware that each unit of energy is generated at some expense of the ecology of the riverine ecosystem. As a consequence, all the feasible measures to improve in efficiency should be taken into consideration together with implementation costs. Some costs are very much country dependent and this aspect is not addressed in this work, being beyond the scope of the work. However, the implementation costs for generating dynamic flow releases are worth a few comments.

This work showed that gains in hydropower production and ecohydrological indicator could be made on average by replacing proportional water allocation policies (today's best practice though not yet widespread) with non-proportional ones located on the Pareto frontier (TableA.2). Improving both criteria, such increments must be considered as actual win-win solutions. These results are based on testing non-proportional redistribution rules on only three homogeneous SHP case studies limited to the Swiss environment and its socio-economic context. We showed that the potential improvement lies in the wider range of non-proportional repartition rules, with respect to traditional policies. Moreover, Figure A.6 demonstrates how classic minimal flow requirement approaches (MFR_1 and MFR_2) can be improved, mainly in term of ecohydrological benefit, by applying non-proportional policies even more than by applying proportional ones (both dynamic). Considering the environment as an independent water user [*Perona et al.*, 2013], with specific needs and features, is thus the key to obtaining efficient environmental flow releases. Such rules will generally result in being non-proportional and flow-dependent. In fact, while the efficiency curve of a turbine does not change throughout the year, the environmental use of water follows seasonal trends. This could easily be added in the model and weighted case-by-case when specific ecological information is available. Increasing the number of case studies would statistically strengthen the results and suggest

more general rules to understand which power plants can actually be improved in global performances. This can be challenging to show, particularly because data are often not easily available.

In this work, we decided to express the economical indicator as the Energy Production in GWh. This study focuses on Small hydropower plants without storage, hence, this suggests that the optimal strategy would be to always turbine the water diverted according to the chosen allocation rule. However, a further improvement would consist in considering the variability of the electricity market price. This could be made by changing the dimensionless variable x of the Fermi function (Eq. 2) so it does not depend only on the flow rate but also on the market price. Thereby, the value of the produced hydropower production would be optimised [*Pereira-Cardenal et al.*, 2016].

Energy provision from renewable sources is a sign of human being responsibility, which however requires a strong harmonisation among social, economic and political parts. The question of how to implement non-proportional flow release rules has not been addressed in this work. However, our present research started to address this problem, particularly looking at suitable hydraulic infrastructures that may generate Fermi function redistribution rules at zero energy costs [*Bernhard and Perona*, 2017]. This is highly desirable in order to pursue innovation not only from an intelligent technological infrastructure point of view, but also from a sustainable one.

A.5   Conclusions

This work shows a simple and innovative numerical approach for defining sustainable and efficient environmental flow releases in river reaches of SHP without storage. The method has been tested on real data and constraints, and could be adopted as a prompt answer to the actual need to conciliate environmental protection and growth of hydropower production. A convenient class of functions, developed by *Gorla* [2014] and *Razurel et al.* [2016], was here comprehensively tested as a practical tool for exploring a representative sample of dynamic flow releases. Such functions provide a direct link between the practice of comparing different environmental flow policies, in particular those using fixed percentages of the incoming flows (proportional) and those with variable splits between diverted and released flows (non-proportional). The Pareto frontier is obtained from the simulated alternatives for each case study and it shows that non-proportional rules are generally more efficient than traditional ones, both proportional and static. It was shown that when applying efficient non-proportional repartition rules for regulating the run of the river hydropower plants, ameliorations in hydropower and ecohydrological performances can be attained, with respect to proportional policies. Although the three case studies are located in Switzerland the results vary from one case to another, leading to the conclusion that they depend on the river morphology. Indeed, the canyoning morphology in the case of Ponte Brolla implies that the MFR value is always higher than the threshold given by the WUA curve, which results in a

maximum value for the fish habitat suitability indicator. For Cauco, the foreseen amelioration for the ecohydrological indicator is the most important, it goes from 8.6% for the period 1983-2012 to 22.8% for the period 2070-2099 but the gain in energy production is the lowest (around 1%) in comparison to the two other case studies. Buseno and Ponte Brolla show some similar potential gains in energy production (around 2%) but for the latter the ecohydrological improvement is almost irrelevant (between 0.0% and 0.1%).

Appendix

Graphical User Interface (GUI) (Figure A.2) has been developed using the software Matlab to facilitate the data treatment and the selection of the optimal water allocation functions among the different scenarios (non-proportional, proportional and MFRs repartition rules). This tool takes the natural river hydrograph and the hydropower plant features (efficiency function, design flow, etc) as inputs. The desired water allocation policies as well as the ecological threshold can also be set. The user-friendly architecture of the GUI (freely available to any user that wants to reservedly test the performances of his own cases[2]) makes the model particularly suitable for stakeholder planning, for water managers operations or for academic purposes.

Numerical simulations were performed in order to model the different allocation functions. The natural daily flow, $I(t)$, was redistributed between the hydropower plant and the river by simulating Eqs(A.1-A.3) according to the selected Fermi function and for the entire time series of $I(t)$. For each scenario, the energy production and the ecohydrological indicators were computed based on the generated flows Q_1 and Q_2, respectively. The same procedure was repeated for the whole set of selected Fermi function parameters as well as for the proportional and MFRs repartition rules. As a result, the efficiency graph, showing the mean annual energy produced during the analyzed period versus the ecohydrological indicator, was plotted. The Pareto front, representing the ensemble of optimal water allocation scenarios, was identified and enhanced with a red line in the efficiency plot.

The simulations to asses the impact of the climate change have been performed in the same way for the three case studies (i.e., Buseno, Cauco and Ponte Brolla). The time series of daily streamflow for the three different time periods (i.e., 2000, 2050 and 2100) have been generated from the current natural data series by applying the trend of the RCP 6.0 scenario described in the previous section 2.4.

---

[2]free download from http://www.sccer-soe.ch/research/hydropower/task2.4/ or by simply contacting the authors (PR, PP)
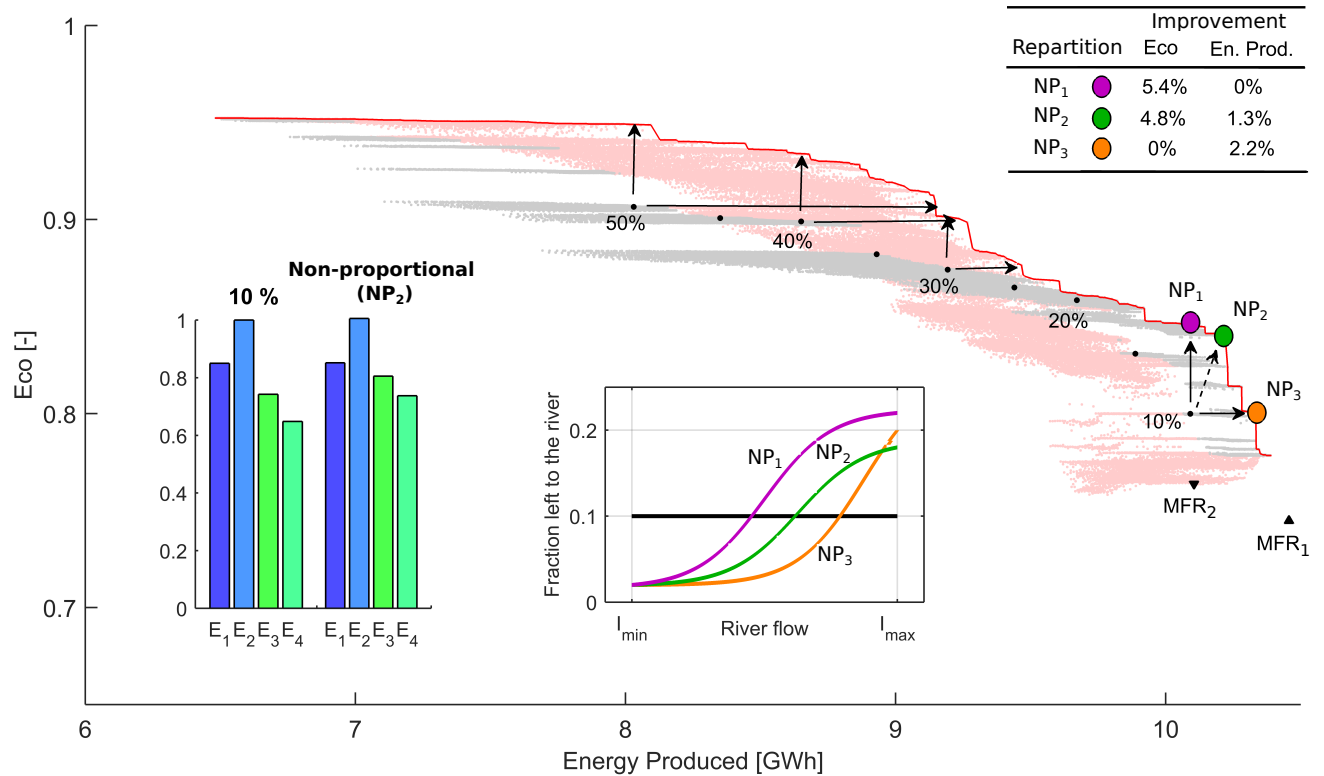
Figure A.6 – Pareto frontier (red line) and alternatives repartition rules simulated from the 29-years hydrograph (1983-2011) for the Buseno case study. In black are MFR and proportional allocation policies; grey and pink points correspond to non-proportional policies (a subset of these is shown in Figure A.3). The black arrows indicate the improvement in term of ecohydrological indicator (vertical ones) and energy produced (horizontal ones) by switching from proportional to non proportional alternatives. The histograms show an example of sub-indicators performances of a proportional (10%) and a non-proportional alternative (green point on the Pareto frontier). The colored curves in the central panel represent the Fermi functions obtained for the three effcient non proportional alternatives to the 10% policy. In the table, the percentages of improvement in ecohydrological indicator and energy production of the non-proportional alternatives NP_1, NP_2 and NP_3 with respect to the 10% proportional rule are shown.
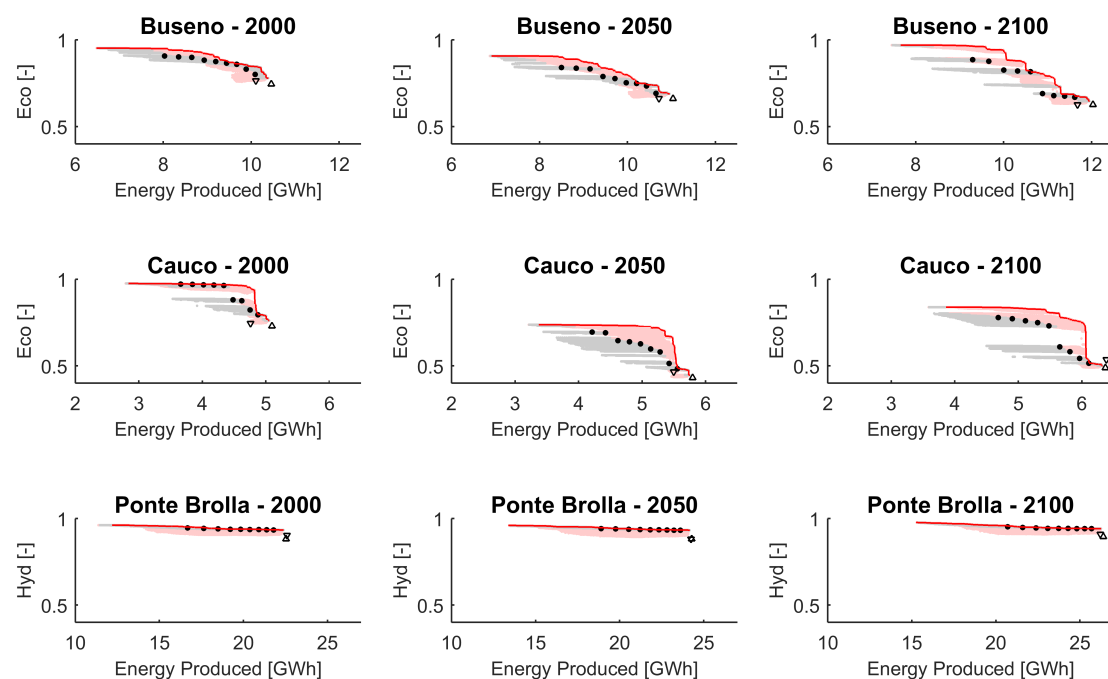
Figure A.7 – Overview of the alternatives simulated, and the relative Pareto frontiers, for the three case studies under the three considered climatic scenarios (RCP 6.0). Equal weights were assigned for ecohydrological indicators. Colours and symbols are the same of Figure A.6.
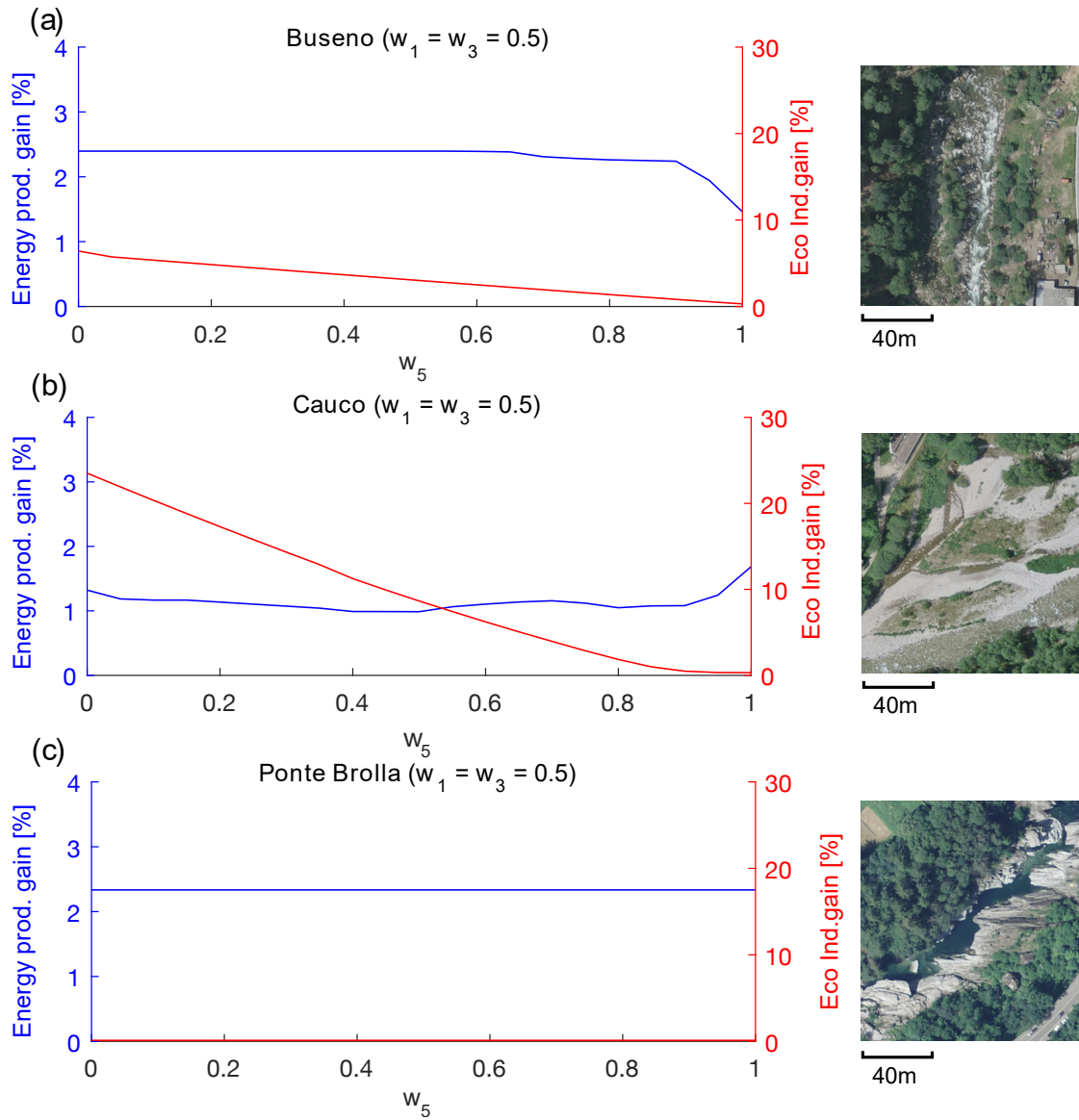
Figure A.8 – Sensitivity analysis showing the gain in power production (blue curve) and ecohydrological indicator (red curve) with respect to proportional policies and obtained by changing the sub-indicator weighting factors w_1, w_3 and w_5 as described in Section 2.2. Pictures of the river reach morphologies corresponding to the three case studies are also shown.

B Distinct air-water gas exchange regimes in low- and high-energy streams[1]

Gas exchange across the air-water interface drives the flux of climate-relevant gases and is critical for biogeochemical processes in aquatic ecosystems. Despite that mountain streams are found worldwide, we lack basic understanding of gas exchange through their turbulent surfaces, making global estimates of outgassing from streams and rivers difficult to constrain. Here we combined new estimates of gas transfer velocities from tracer gas additions in mountain streams with published data to cover streams differing in geomorphology and hydraulics. We found two different scaling relationships between turbulence-induced energy dissipation rate and gas transfer velocity for low- and high-slope streams, indicating that gas exchange in streams exists in two states. We suggest that turbulent diffusion drove the gas transfer velocity in low-energy streams. Whereas, in high-energy streams, turbulence entrained air bubbles in the water and the resulting bubble-mediated gas exchange accelerated with energy dissipation rate. Gas transfer velocities in these streams were among the highest yet reported. Our findings offer a framework to include mountain streams in future estimates of gas fluxes from streams and rivers at the global scale.

Aquatic ecosystems interact with the atmosphere through the exchange of matter and energy, which are critical to ecosystem processes and biogeochemical fluxes. For instance, aquatic metabolism relies on the flux of oxygen from the atmosphere to the water and, at the same time, is a source of climate-relevant gases (e.g., CO_2, CH_4, N_2O) to the atmosphere. Therefore, the gas flux through the air-water interface is needed to calculate biogeochemical fluxes in aquatic ecosystems. The gas flux is a function of the gas transfer velocity at the water-air interface, the gas solubility coefficient, and the difference in gas concentration between the air and water. Of these components, the gas transfer velocity is often rate-limiting for gas fluxes and, at the same time, the most problematic and associated with highest uncertainties

---

[1]The contents of this chapter are published in: Ulseth, A.J., Hall, R.O., Canadell, M.B., Madinger, H.L., Niayifar, A. and Battin, T.J., 2019. Distinct air–water gas exchange regimes in low-and high-energy streams. Nature Geoscience, p.1. I contributed to interpretation of the data and writing the manuscript.

Appendix B. Distinct air-water gas exchange regimes in low- and high-energy streams

Zappa et al. [2007]. For these reasons, the quantification of gas transfer velocity has been a mainstay in physical oceanography and lake limnology *Wanninkhof et al.* [2009]; *Jähne and Haußecker* [1998], whereas it has received less attention in stream research. The recognition, however, of streams and rivers as relevant sources of CO_2 and CH_4 to the atmosphere *Cole et al.* [2007]; *Battin et al.* [2009]; *Raymond et al.* [2013] has renewed interest in gas exchange in these ecosystems *Raymond et al.* [2012]; *Hall Jr and Madinger* [2018].

Gas exchange in the ocean and lakes is a function of physical (e.g., wind-induced turbulence) *Wanninkhof et al.* [2009]; *Jähne and Haußecker* [1998], chemical (e.g., pH) *Liss* [1973], and biological (e.g., surface microlayer) *Pereira et al.* [2018] factors. In streams and most rivers, turbulence generated by water flow and bed roughness is the dominant driver of gas exchange *Wanninkhof et al.* [1990]; *Raymond et al.* [2012]. Proxies for turbulence, such as the energy dissipation rate (eD), are often used to scale and predict gas exchange in the ocean *McNeil and D'Asaro* [2007], lakes *Vachon et al.* [2010], and streams and rivers *Raymond et al.* [2012]. However, these scaling relationships with near-surface turbulence do not work in lakes and oceans when breaking waves result in bubble-mediated gas exchange *Zappa et al.* [2007], a phenomena recognized in experimental stream flumes and channels *Chanson et al.* [2000]; *Chanson and Toombes* [2003], but rarely in streams and rivers (except see refs *Hall Jr et al.* [2012]; *Hall Jr and Madinger* [2018]) despite the potential for high turbulence in these ecosystems.

The gas transfer velocity is often quantified in streams, rivers, lakes, and the ocean by injecting tracer gases, such as sulfur hexafluoride (SF_6), propane, or argon *Wanninkhof et al.* [1990]; *Marzolf et al.* [1994]; *Cole and Caraco* [1998]; *Wanninkhof et al.* [2009]; *Hall Jr and Madinger* [2018]. The gas transfer velocity in streams has also been estimated via empirical equations based on channel geomorphology and hydraulics *O'Conner and Dobbins* [1958] or via ecosystem metabolism models *Holtgrieve et al.* [2010]; *Appling et al.* [2018].

Scaling relationships between k_{600} (that is, gas transfer velocity standardized to a common Schmidt number of 600, *Supplementary information*) and geomorphology and hydraulics are attractive for establishing gas fluxes and carbon budgets for streams and rivers at regional and global scales *Raymond et al.* [2013]; *Butman and Raymond* [2011]. However, such relationships are not general to all streams because they do not include data from steep-slope streams with high hydrological energy, which are typical of streams from mountainous catchments. In fact, most research on gas exchange in streams and rivers is based on ecosystems with low channel slope (< 4%, *Supplementary information* Table S1) *Raymond et al.* [2012]. This point contrasts with the fact that ~20% of the Earth's continental terrain has slopes greater than 4% *Larsen et al.* [2014] with mountainous regions constituting 25 to 39% of the continental surface *Viviroli et al.* [2007]. While streams draining mountainous landscapes disproportionately contribute to the worldwide runoff *Viviroli et al.* [2007], they have rarely been included in global scaling of physical and chemical processes *Larsen et al.* [2014]. This exclusion of mountainous regions is particularly evident for the role these streams play in large-scale biogeochemical fluxes through their water-air interface. Concentrations of CO_2, CH_4, and even N_2O in these streams can be supersaturated relative to atmospheric conditions *Qu et al.* [2017]; *Kuhn et al.* [2017]

and these streams can therefore be potentially important sources of greenhouse gases *Qu et al.* [2017].

High gas exchange velocities in mountain streams

We injected argon as a tracer gas *Hall Jr and Madinger* [2018] in 12 mountain streams (n=56) in the Swiss Alps and derived k_{600} (*Methods, Supplementary information*). Channel slope of these streams averaged 8.5% (standard deviation, SD: 3.8), which is significantly higher than average channel slope of the streams hitherto used for scaling gas exchange (Figure B.1, *Supplementary information* Table S1). k_{600} values in Alpine streams were unexpectedly high with an average of 464 ± 780 m d^{-1} and with a maximum of 4,018 m d^{-1}. Strikingly, these gas exchange velocities are among the highest measured for any aquatic ecosystem. In fact, average k_{600} values were 96 times higher than the average reported from low-energy *Raymond et al.* [2012], 15 times higher than from subalpine streams *Peter et al.* [2014]; *Schelker et al.* [2016], and still 8 times higher than average k_{600} reported from other steep-slope streams *Hall Jr and Madinger* [2018]; *Maurice et al.* [2017]; *McDowell and Johnson* [2018] (*Supplementary information* Table S1). Furthermore, our average k_{600} was up to 364 times higher than k_{600} reported from the ocean *Wanninkhof et al.* [2009] and 230 to 1213 times higher than k_{600} reported for ponds and lakes *Raymond et al.* [2013]; *Holgerson and Raymond* [2016].

The average error of our argon-derived k_{600} (32%, *Methods*) was within range of the error reported for k_{600} values derived from other tracer gases *Melching and Flores* [1999]; *Hall Jr and Madinger* [2018]. Furthermore, argon was recently shown to be an appropriate tracer gas to estimate k_{600} in turbulent streams *Hall Jr and Madinger* [2018]. Our k_{600} values overlap with these numbers but also with others measured from SF$_6$ *Maurice et al.* [2017] (Figure B.1, *Supplementary information* Table S1) and CO$_2$ releases in high-gradient streams *McDowell and Johnson* [2018]. Therefore, we are confident in the high k_{600} estimates from the Swiss streams and stress the necessity to properly factor steep-slope mountainous streams into global estimates of gas fluxes.

Differing scaling relationships with energy dissipation rate

We explored scaling relationships between k_{600} and stream hydraulics and geomorphology across a broad range of streams by combining our data from Swiss streams with published data (n=662) *Raymond et al.* [2012]; *Schelker et al.* [2016]; *Maurice et al.* [2017]; *Hall Jr and Madinger* [2018] (Figure B.1, *Supplementary information* Table S1). We found that empirical models based on channel slope, flow velocity and streamwater depth, as established for low-slope streams (*Supplementary information* Table S2) *Raymond et al.* [2012], underestimated k_{600} in high-slope streams (Figure B.1, *Supplementary information* Table S3, *Methods*). Elevated values of k_{600} (>30 m d^{-1}) were underestimated by 492% (median, min-max: 106-8636%) for all models that were initially developed from low-slope streams (Table S3; observed versus

Appendix B. Distinct air-water gas exchange regimes in low- and high-energy streams
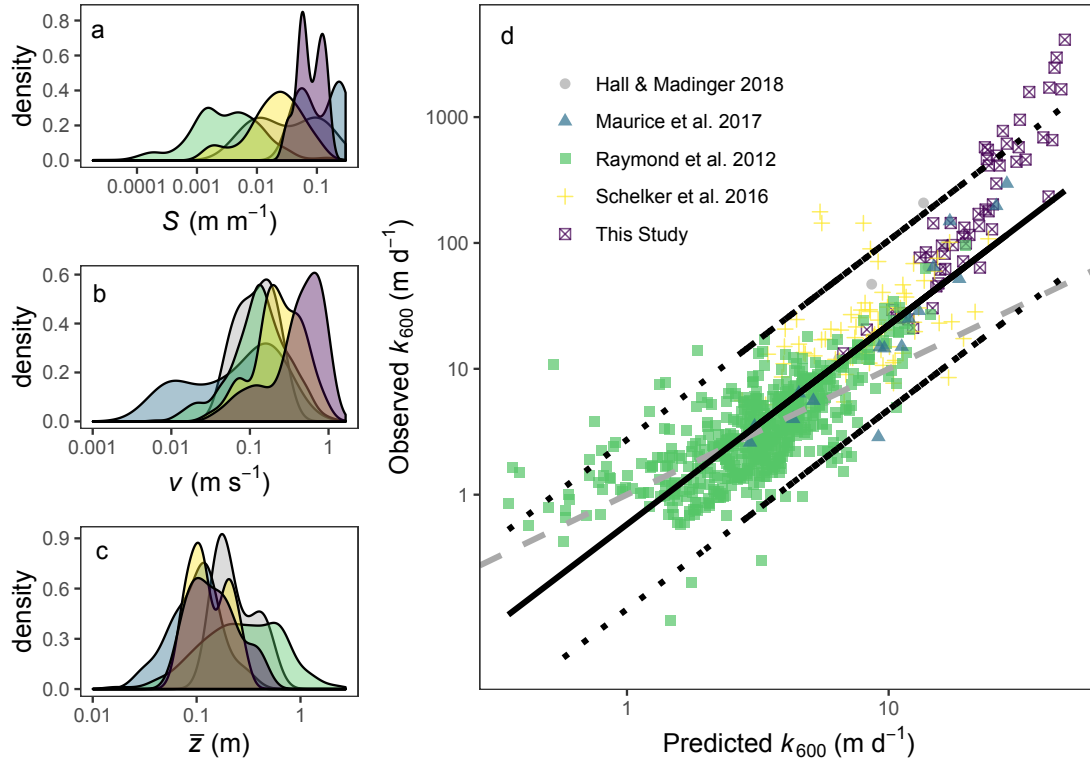
Figure B.1 – **Range of common gas exchange predictors and model fit based on low-sloped streams.** Density distributions for slope (S) (a), velocity (v) (b), and stream depth ($\bar{z}$) (c) grouped by data source *Hall Jr and Madinger* [2018]; *Maurice et al.* [2017]; *Schelker et al.* [2016]; *Raymond et al.* [2012]. High gas exchange (k_{600}) was under predicted using models based on low-slope streams (d) (equation 1 in *Supplementary information* Table S2) as the observed versus predicted k_{600} fall above (slope=1.58, solid black line, *Supplementary information* Table S3) the 1:1 line (dashed gray line). The 95% prediction confidence interval is designated by the dotted black lines.

predicted $\log(k_{600})$: average $R^2 = 0.73$, average slope = 1.58, *Supplementary information* Table S3). This finding shows that mechanisms that explain variation in k_{600} in low-slope streams failed to properly predict k_{600} in high-slope streams.

It is well established that turbulence drives gas exchange at the water-air interface, and models used to estimate k_{600} in streams therefore often are based on turbulence-related geomorphic and hydraulic variables *Zappa et al.* [2007]; *Raymond et al.* [2012]; *Tsivoglou and Neal* [1976]; *Melching and Flores* [1999]. We assumed that k_{600} would scale as a power law with the energy dissipation rate (eD) as a measure of surface turbulence *Raymond et al.* [2012]; *Tsivoglou and Neal* [1976]; *Melching and Flores* [1999] (*Methods*), and predicted therefore a simple linear relationship in the log-log space across hundreds of streams covering various geomorphological and hydraulic characteristics. Instead, we found a non-linear relationship between $\log(k_{600})$ with $\log(eD)$ (Figure B.2).

Therefore, we fitted a breakpoint regression to these data; piece-wise linear regression estimates breakpoints within the data via maximum likelihood and fits separate intercepts and slopes between breakpoints *Muggeo* [2003]; *Muggeo et al.* [2008]. Using this approach, *eD* explained 78% of the variability in k_{600} across all streams (Figure B.2). The breakpoint estimated by the model equated to *eD* = 0.020 (95% CI 0.016, 0.026) m^2 s^{-3} and intersected closely with the upper limit of the prediction estimate at k_{600} = 35 m d^{-1}. The difference in the slopes of the regression on either side of this breakpoint was 3-fold (0.35 below and 1.18 above *eD* = 0.02 m^2 s^{-3}). Furthermore, the slope of 0.35 for streams falling below the breakpoint is within close range of the scaling prediction of 0.25 between gas exchange and *eD* based on the surface renewal theory*Zappa et al.* [2007]. This log-log scaling slope <1, indicates an attenuating relationship between k_{600} and *eD*, whereas the slope >1 indicates an accelerating relationship between k_{600} and *eD*. This model fit provided evidence for a regime shift of gas exchange velocities along the stream *eD* continuum where we consider streams falling below the breakpoint to be low-energy as k_{600} attenuates with *eD* and those above as high-energy, as k_{600} accelerates with *eD*.

Stream hydraulics and bubble-mediated gas exchange

Here we propose a conceptual framework based on geomorphology and hydraulics to mechanistically underpin the disproportionately high increase of k_{600} with *eD* in high-energy streams. First, we argue that channel slope rather than flow velocity accelerated the observed increase in *eD* in the high-energy streams compared to the low-energy streams. Within a stream reach, velocity, and ultimately stream discharge, will likely drive the temporal variability of *eD* and correspondingly k_{600}, as found within our Swiss stream reaches (*Supplementary information*) and steep-slope streams in the UK*Maurice et al.* [2017] and Canada*McDowell and Johnson* [2018]. This notion of slope driving the observed change in k_{600} with *eD* across the *eD* continuum is based on the 11-fold increase in average channel slope versus a 2-fold increase with considerable overlap in average flow velocity between high- and low-energy streams (Figure B.3); average water depth was 2 times higher in low- than in high-energy streams, but also overlapped considerably between both stream types (Figure B.3).

Next, owing to the balance between sediment erosion, transport, and accumulation, steep-slope streams draining mountainous terrain typically have elevated bed roughness, even including macro-roughness as induced by cascades or step-pools *Montgomery and Buffington* [1997]; *Schneider et al.* [2015]; *Knighton* [2014]. As expected, channel slope positively co-varied with reach-scale streambed roughness as estimated from imaging and semivariance analysis (*Methods*) (R^2 = 0.32, $p < 0.001$). It is well established that the energy dissipation rate results from turbulence that is caused by the flow friction over rough beds in low-submergence streams (that is, streams with a high ratio of roughness to water depth) *Knighton* [2014]; *Moog and Jirka* [1999b]. We found a positive relationship (R^2 = 0.36, $p < 0.001$) between reach-scale roughness and log(k_{600}) across eight of our study streams (Figure B.4). In combination with the relationship between *eD* and k_{600}, this relationship is empirical evidence of the

geomorphological and hydraulic controls on gas exchange. This finding on natural streams agrees with theory from engineered flumes predicting gas exchange to increase with streambed roughness *Moog and Jirka* [1999b]; *Chanson and Toombes* [2003].

Where surface turbulence in the ocean and in lakes originates from wind, surface turbulence in streams originates from both bed friction and water column turbulence. If the momentum generated by bed friction is transported upwards to the free water surface, this turbulence induces the energy dissipation rate (*eS*, *Methods*), which enhances the gas exchange at the air-water interface. We found that *eS* for streams above the *eD* breakpoint (> 0.02 m^2 s^{-3}) was on average 26-fold higher than for streams below the *eD* breakpoint (Figure B.3). This high turbulence driven by streambed roughness likely entrained air, forming bubbles, and greatly increased rates of gas exchange. This finding is further corroborated by 3-fold higher average Froude numbers in a high-energy than in the low-energy streams (Figure B.3). In fact, high Froude numbers translate into instabilities of the free water surface, which facilitates the entrainment of air, generates bubbles in the water leading to 'whitewater'. Bubbles increase the water-air interface area per unit volume of water (and air) and therefore greatly enhances gas exchange *Chanson et al.* [2000]; *Chanson and Toombes* [2003]

Depending of turbulence, gas exchange can exist in two states in aquatic ecosystems, switching from turbulent diffusive to bubble-mediated exchange. Our findings suggest that this switch may occur at $k_{600} > 35$ m d^{-1} in streams, as evidenced by the intersection of the breakpoint between low- and high-energy streams and the upper confidence interval of the predicted gas exchange velocities at ~35 m d^{-1} (Figure B.2). Several additional lines of evidence support the notion that bubbles govern gas exchange beyond a threshold of 35 m d^{-1}. It was shown that maximum diffusive gas exchange at the scale of single bubbles approximates 35 m d^{-1} *Wüest et al.* [1992]. Furthermore, experiments with laboratory flumes indicated that the maximum k_{600} without bubble entrainment was 35 m d^{-1} *Moog and Jirka* [1999b]. Finally, a similar state shift from diffusive to bubble-mediated gas exchange in the ocean during a hurricane occurred at a k_{600} value of 36 m d^{-1} *D'Asaro and McNeil* [2007]; *McNeil and D'Asaro* [2007]. Collectively, these observations suggest that such turbulence-induced state shifts may be universal across various types of aquatic ecosystems, ranging from streams to the ocean.

This regime shift from turbulent diffusion to bubble-mediated gas exchange can confound scaling the gas transfer velocity from one gas to another. Bubble-mediated gas exchange can be complicated as the bubbles or entrained air may fall under three different scenarios: dissolved completely and therefore independent of solubility and diffusivity (i.e., Schmidt scaling), equilibrated and dependent on solubility, or non-equilibrated with the surrounding water and reliant on both diffusivity and solubility*Asher and Wanninkhof* [1998a]. In aquatic ecosystems, it is likely that a mix of all three of these scenarios are occurring at any given time, thus complicating the scaling of the gas exchange velocity from one gas to another, especially if solubility and diffusivity differ*Asher and Wanninkhof* [1998b]. Therefore, both diffusivity and solubility may need to be considered when gas exchange is bubble-mediated, especially for scaling from a less soluble gas (e.g., common tracer gases such as argon, SF_6,
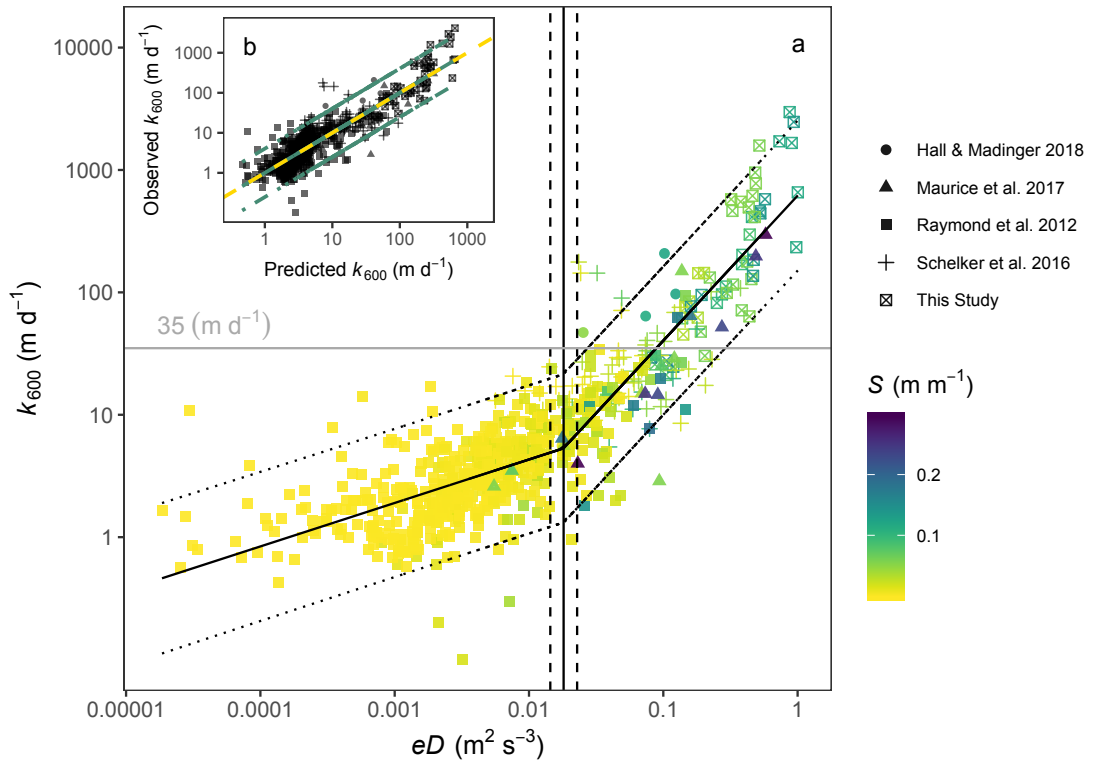
Figure B.2 – k_{600} **scaled with energy dissipation rate (***eD***).** Model fit (black line, 95% prediction confidence interval (CI), dashed lines) estimated via piecewise linear regression analysis (R^2 = 0.78), where (natural log) $\log(k_{600})$=3.10+0.35(95%CI: 0.31, 0.41)×$\log(eD)$ for $eD < 0.02$ (vertical line, dashed vertical lines are 95%CI (0.016, 0.026)) and $\log(k_{600})$=6.43+1.18(95%CI: 1.10, 1.30)×$\log(eD)$ for $eD > 0.02$. The gray line equates to theoretically the maximum gas exchange due to diffusivity alone (a). The inset figure is the observed versus predicted k_{600}, where the solid green line is the model fit (95% prediction CI, dashed-dot green lines), which falls along the 1:1 line (dashed yellow line) (b).

propane) to more soluble gas, such as CO_2 *Asher and Wanninkhof* [1998b]; *Woolf et al.* [2007]. This issue of scaling bubble-mediated gas exchange is better studied in the oceans *Asher and Wanninkhof* [1998b]; *Woolf* [1993], but less so in stream ecosystems *Hall Jr et al.* [2012]; *Hall Jr and Madinger* [2018] as the role of bubble-mediated gas exchange in these ecosystems has been overlooked.

Distinct gas exchange regimes

Our findings revealed yet unrecognized different regimes in gas exchange in streams as induced by channel geomorphology and related hydraulics. When $eD < 0.02$ m^2 s^{-3}, turbulent diffusion controlled k_{600} such that a 10-fold increase in eD increased gas exchange 2 times. Whereas for $eD > 0.02$ m^2 s^{-3}, air entrainment and bubble formation increase gas exchange more rapidly such that a tenfold increase in eD increases k_{600} 15 times. This accelerating
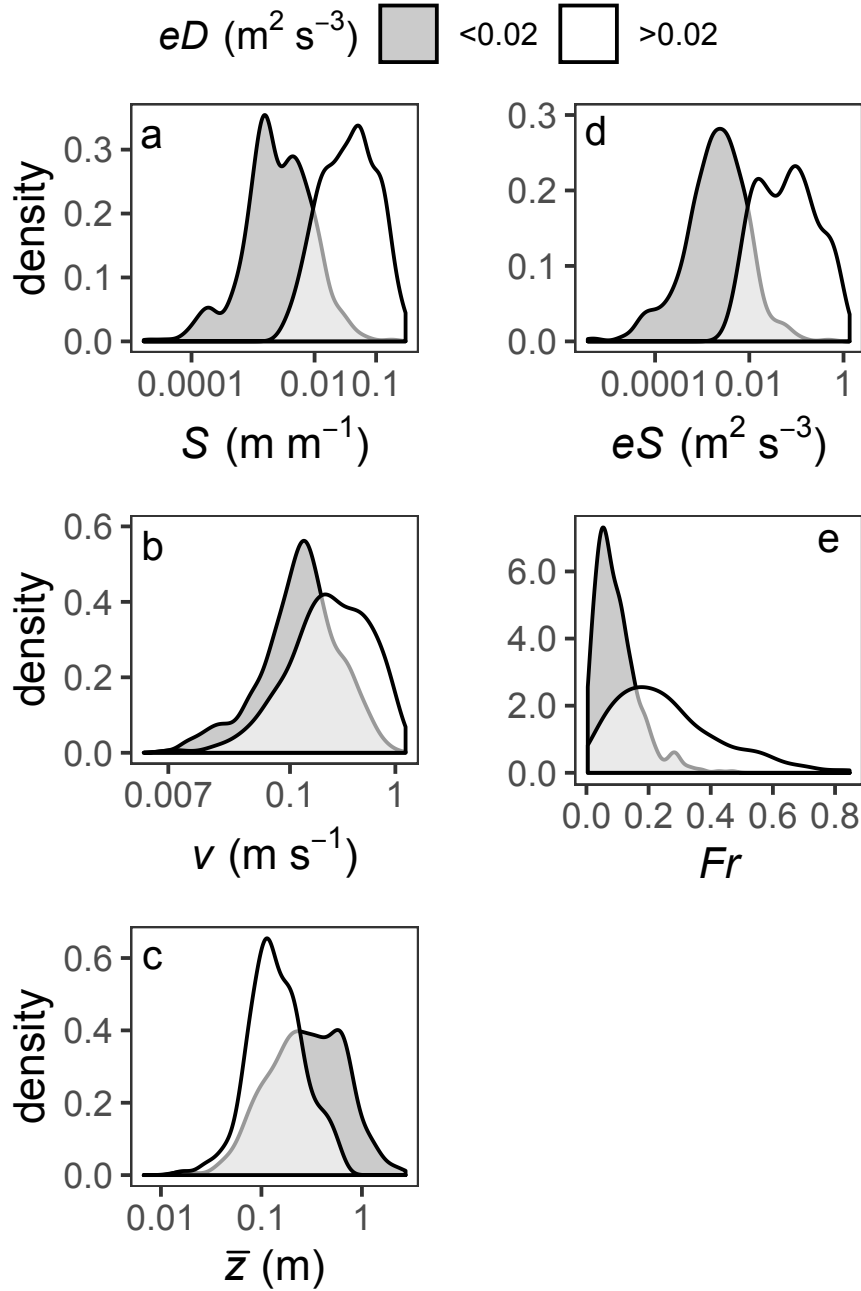
Figure B.3 – **Density distributions of stream characteristics of low- versus high-energy streams.** Streams with an energy dissipation rate (*eD*) higher than the breakpoint (*eD* > 0.02 m^2 s^{-1}) in Figure B.2 had steeper slopes (*S*) (a), higher energy dissipation rate owing to bed friction (*eS*) (d), and higher Froude number (*Fr*) (e) than those below the breakpoint, as illustrated by the density distributions. While there was greater overlap above and below the breakpoint for stream velocity (*v*) (b) and depth ($\bar{z}$) (c).
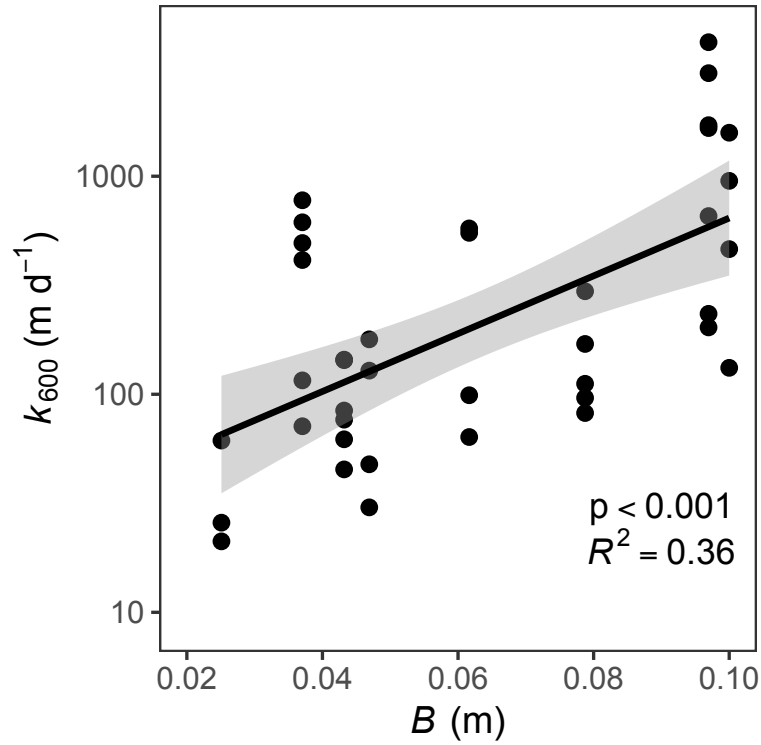
Figure B.4 – **Gas exchange increased with streambed roughness**. k_{600} increased with median stream bed roughness (B) across 8 of the Swiss Alpine stream reaches. The black line is the fit from semi-natural log (log) linear regression, $\log(k_{600}) = 3.41 + 30.52 \times B$), and the gray band represents the 95% confidence interval of the predicted k_{600}.

relationship of gas exchange with eD in steep streams as they drain mountainous terrain worldwide means that scaling exercises for regional and global fluxes of climate-relevant gases from these streams may have been underestimated.

Methods

Deriving k_{600} from argon releases in high-sloped streams

We measured gas exchange using argon (Ar) tracer additions following ref*Hall Jr and Madinger* [2018]. Ar is a suitable tracer gas to estimate gas exchange in high gradient and turbulent streams*Hall Jr and Madinger* [2018]. We conducted 56 Ar releases in 12 Alpine streams (Switzerland, Vaud and Valais cantons, *Supplementary information*) with an average slope of 8.5± (standard deviation (SD)) 3.8% and average discharge of 0.64±0.84 m^3 s^{-1}. At a constant rate (see *Supplementary information* for details), we continuously injected Ar into the streamwater. After Ar reached temporal equilibrium at the downstream site (4× travel time *Workshop* [1990]), we sampled streamwater for gas analysis at multiple points along the reach

downstream of the injection site. As we used a membrane inlet mass spectrometer (MIMS) (Bay Instruments Inc., Easton, MD)*Kana et al.* [1994] to analyze the Ar gas samples as described in ref *Hall Jr and Madinger* [2018], measuring ratios is more precise rather than absolute concentrations*Kana et al.* [1994]. We therefore used the decline in Ar:N_2 ratios to estimate gas exchange*Hall Jr and Madinger* [2018]. And because as we enriched the Ar concentration in the stream by no more than 5%, we were confident that the N_2 gas concentrations in the water were minimally affected. We modeled the exponential decline of Ar:N_2 (A) (corrected for ambient Ar:N_2 and normalized to the most-upstream Ar:N_2, i.e., the first station downstream of the point of gas injection) to estimate the decay rate of gas m^{-1} using

$$A_x = A_0 \times e^{-K_A x} + \varepsilon_A \tag{B.1}$$

where A_0 is the y-intercept, K_A is the decay rate of Ar at streamwater temperature, and x is the distance along the reach (m). ε_A is a random normal variable distributed as $\varepsilon_A \sim N(0, \sigma_A)$. We chose to fit a non-linear model because the absolute error was constant as Ar:N_2 declined downstream. We fitted equation B.1 to the Ar data with A_0, K_A, and σ_A as free parameters using a Bayesian approach with the *rstan* package in program R *Team et al.* [2016, 2013]; *Hall Jr and Madinger* [2018]. A_0 and K_A had normal prior probabilities ($A_0 \sim N(1, 0.05)$, $K_A \sim N(0, 0.10)$) and ε_A had a half normal prior probability ($\varepsilon_A \sim |N(0, 0.2)|$). The error around the estimate of K_A was calculated as the difference between the 97.5% and 2.5% credible interval of the estimated K_A divided by the mean K_A and ranged from 6.5 - 69.1% across the 56 gas releases. To convert K_A (m^{-1}) to the gas exchange velocity (k_A, m d^{-1}), $k_A = K_A \times v \times \bar{z} \times 86400$ where v is stream flow velocity (m s^{-1}), $\bar{z}$ is the average depth (m) of the reach and 86400 to convert s to d. We standardized k_A to a common Schmidt number of 600 (k_{600}, m d^{-1}) *Wanninkhof* [1992]; *Jähne et al.* [1987] (*Supplementary information*). From slug additions of sodium chloride, we estimated discharge (Q, m^3 s^{-1}) and v (see below). We measured stream widths (w, m) and estimated mean depth ($\bar{z}$) assuming hydraulic continuity, i.e, $\bar{z} = Q/(wv)$.

Stream slope, discharge, travel time, and velocity

We measured the stream slope for all 12 Swiss study reaches to coincide with the Ar releases. Stream slope was measured via either a digital GPS (DGPS, Trimble R10 GNSS receiver) or, due to poor satellite reception at 2 of our 12 sites, a theodolite (Leica). Slope was calculated for each stream reach based on the change in elevation (m) divided by the change in distance (m) along the reach.

We used slug releases of sodium chloride to estimate Q and travel time, and to calculate v. We added dissolved sodium chloride to the top of the reach, and continuously monitored the change in specific conductivity at the bottom of the reach (conductivity loggers (WTW, Xylem, Inc.), similar to ref *Peter et al.* [2014]) until conductivity returned to background conditions. For each slug addition, we dissolved enough sodium chloride for each release to increase the background conductivity by 50-100% (0.5 to 5 kg, depending on stream size and background

conductivity). Travel time was the amount of time the slug addition took to reach peak conductivity. To calculate v (m s^{-1}), stream length (m) was divided by travel time (s). And to estimate stream Q (m^3 s^{-1}), we integrated under the specific conductivity curve

$$Q = \frac{SC_{add}}{\Sigma_{i=1}^{n}(SC_{meas} \times \triangle t)} \tag{B.2}$$

where SC_{add} was the specific conductivity of the salt slug we added at the top of the reach. We calculated SC_{add} via the relationship we empirically measured in the laboratory of salt mass in solution versus specific conductivity. SC_{meas} was the specific conductivity measured at the bottom of the reach and $\triangle t$ was the time step of the specific conductivity measurements (1 s).

Stream Bed Roughness

Across 8 of the 12 Alpine stream reaches in Switzerland, we were able to estimate stream bed roughness. Stream bed roughness was estimated using high-resolution orthoimaginery and digital elevation models (DEMs) produced from structure-from-motion (SfM) photogrammetry *Fonstad et al.* [2013]. Low altitude aerial photographs for each reach (similar in length to the argon releases) were taken during periods of low-flow stream discharge (September and October 2017) with an unmanned aircraft system (UAV) from SZ DJI Technology Co. Ltd. equipped with a 12.4 megapixel camera. Image overlap was approximately 80% along the flight path. Prior to each flight, we marked ground control points (GCPs) spaced throughout the reach for posterior image georeferencing and we determined their position to within a few centimeters using a Trimble real-time kinematic (RTK) Global Position System (GPS) unit. All the images were processed with Pix4D software (Pix4D SA, Switzerland). The resulting orthomosaics and DEMs had spatial resolutions between 1.08 and 1.76 cm/pixel and were georeferenced to the Swiss grid system (x, y) and mean annual sea level. Before the generated DEMs could be used for roughness analysis, we delimited and corrected wetted areas of DEMs for refractive effects following ref*Dietrich* [2017]. Streambed roughness was characterized using semivariance analysis of the elevation data from the active channel of the DEM. From each semivariance calculated, we estimated the sill (c), which is the value of the semivariance where the variance is stable. Using the median sill for each site, we approximated streambed roughness (B) as $B = \sqrt{2c}$, which was found to be comparable to other metrics of roughness *Schneider et al.* [2015].

Energy dissipation metrics and the Froude number

Turbulence at the air-water interface in streams originates from the water column turbulence and from the streambed. We calculated the energy dissipation rate from the water column turbulence, that is form drag, (eD, m^2 s^{-3}) as $eD = gSv$ *Moog and Jirka* [1999b]; *Raymond et al.* [2012], where g is gravitational acceleration (m s^{-2}) and stream reach slope (S, m m^{-1}). However, the energy dissipation rate can also originate from the channel bed or bed friction

(eS, m^2 s^{-3}). eS can be approximated as $eS = u^{*3}/\bar{z}$, where u^* is the friction velocity and calculated as $u^* = \sqrt{gR_h S}$, R_h is the hydraulic radius *Moog and Jirka* [1999a, b]; *Raymond et al.* [2012]. We also calculated the Froude number (Fr), which describes the stability of the water surface, as $Fr = v/\sqrt{g\bar{z}}$.

Predicting k_{600} in high-slope streams from low-slope streams

To evaluate the predictability of k_{600} in high-slope streams from low-slope streams, we revisited published gas exchange models. We estimated the coefficients for six models using ref *Raymond et al.* [2012] subset of data (*Supplementary information* Table S2-S3), which comprised mainly low-sloped streams (97.5% quantile = 3.6%). We used natural log-transformed data in the linear models because assuming a multiplicative error structure provided better model fit than the additive structure of power models *Xiao et al.* [2011]. The statistical models we used were the log-transformed variants of the models from ref *Raymond et al.* [2012]. After estimating coefficients based on data presented in ref *Raymond et al.* [2012] (*Supplementary information* Table S2), we predicted log(k_{600}) for the entire data set of gas exchange velocities and compared observed and predicted log(k_{600}) (*Supplementary information* Table S3) using log-linear regression for each model. We conducted all data analyses in R *Team et al.* [2013].

C Analytical modeling of wind farms: A new approach for power prediction[1]

Abstract

Wind farm power production is known to be strongly affected by turbine wake effects. The purpose of this study is to develop and test a new analytical model for the prediction of wind turbine wakes and the associated power losses in wind farms. The new model is an extension of the one recently proposed by Bastankhah and Porté-Agel for the wake of stand-alone wind turbines. It satisfies the conservation of mass and momentum and assumes a self-similar Gaussian shape of the velocity deficit. The local wake growth rate is estimated based on the local streamwise turbulence intensity. Superposition of velocity deficits is used to model the interaction of the multiple wakes. Furthermore, the power production from the wind turbines is calculated using the power curve. The performance of the new analytical wind farm model is validated against power measurements and large-eddy simulation (LES) data from the Horns Rev wind farm for a wide range of wind directions, corresponding to a variety of full-wake and partial-wake conditions. A reasonable agreement is found between the proposed analytical model, LES data, and power measurements. Compared with a commonly used wind farm wake model, the new model shows a significant improvement in the prediction of wind farm power.

C.1   Introduction

Renewable energies play an increasingly important role in the global energy market as sources of sustainable and clean energy. Specifically, wind energy is witnessing continuous growth at an average annual rate of approximately 25% and currently contributes to more than 2.6% of electricity generation worldwide. This contribution is expected to increase to 18% of the world's electricity generation by 2050 [*Council*, 2012].

Power production from wind farms is significantly affected by wind turbine wakes. This power loss can be up to 25% of the total power output [*Barthelmie et al.*, 2010]. For this reason, the accurate prediction of turbine wakes is imperative to minimize power losses

---

[1] The contents of this chapter are published in: Niayifar, A. and Porté-Agel, F., 2016. Analytical modeling of wind farms: A new approach for power prediction. Energies, 9(9), p.741.

and, thus, increase the overall efficiency of wind farms. Turbine wake effects have been investigated in numerous experimental, numerical, and analytical studies. Recent advances in turbulence-resolving computational fluid dynamics methods, such as large-eddy simulation (LES) and cutting-edge experimental techniques, have allowed detailed characterization of wind turbine wake flows. Although both experimental and numerical approaches have the potential of providing accurate results, the simplicity and low computational cost associated with analytical models make them appealing for wind farm optimization purposes [*Crespo et al.*, 1999; *Chowdhury et al.*, 2013]. For that reason, analytical modeling of wind farms has been and continues to be an important topic of research in the field of wind energy. Analytical wind farm models can be divided into two main types: Kinematic models [e.g., *S. Lissaman*, 1979; *Katic et al.*, 1987] and distributed roughness models [e.g., *Frandsen*, 1992; *Calaf et al.*, 2010; *Abkar and Porté-Agel*, 2013]. Kinematic models consider each turbine wake individually and apply superposition principles to address the interaction of neighboring wakes. In distributed roughness models, turbines act as distributed roughness elements in which the ambient atmospheric flow is modified. Furthermore, there are some models that combine kinematic models with distributed roughness models [e.g., *Stevens et al.*, 2015, 2016]. In the present study, we propose a new wind farm analytical model, which is a type of kinematic model, to predict the performance of wind farms of arbitrary size and layout. Although several analytical wind farm models have been developed to estimate the power generated from wind turbines, there are still some critical issues related to the modeling of the velocity deficit and the velocity deficit superposition (due to the interaction of multiple wakes) that need to be addressed to increase the accuracy and robustness of these models.

Several analytical wake models have been developed to estimate the wake flow inside wind farms [*S. Lissaman*, 1979; *Jensen*, 1983; *Voutsinas et al.*, 1990; *Frandsen et al.*, 2006; *Bastankhah and Porté-Agel*, 2014]. One of the most commonly used wake models is the one proposed by Jensen [*Katic et al.*, 1987; *Jensen*, 1983]. This model, which has been extensively used in the literature [e.g., *González et al.*, 2010] and in commercial software [e.g., *Barthelmie et al.*, 2006; *Crasto et al.*, 2012; *Hassan*, 2003; *Truepower*, 2010; *Thogersen et al.*, 2006], considers a top-hat shape for the normalized velocity deficit and is defined as:

$$\frac{\Delta U}{U_\infty} = \frac{U_\infty - U_w}{U_\infty} = \frac{1 - \sqrt{1 - C_T}}{(1 + (2k_{wake}x)/d_0)^2} \tag{C.1}$$

where U_∞ is the undisturbed velocity, U_w is the wake velocity, C_T is the thrust coefficient of the turbine, k_{wake} is the wake spreading parameter, d_0 is the wind turbine diameter, and x is the distance behind the turbine. It should be noted that this model was derived using only mass conservation [*Bastankhah and Porté-Agel*, 2014].

In a later study, *Frandsen et al.* [2006] also assumed a top-hat shape for the velocity deficit and applied conservation of mass and momentum to a control volume around the turbine to derive the following model:

$$\frac{\Delta U}{U_\infty} = \frac{1}{2}(1 - \sqrt{1 - 2\frac{A_0}{A_w}C_T}), \tag{C.2}$$

where A_0 denotes the circular area swept by the wind turbine blades and A_w represents the cross-sectional area of the wake. Despite the wide use of these turbine wake models in the literature and commercial software, the unrealistic assumption of a top-hat velocity deficit results in a tendency for these models to overestimate power prediction in the full-wake condition and underestimate power prediction in the partial-wake condition.

The normalized velocity deficit in the turbine wakes has been observed to follow a self-similar Gaussian profile in several experimental and numerical research studies [e.g., *Chamorro and Porté-Agel*, 2009; *Wu and Porté-Agel*, 2012; *Xie and Archer*, 2015; *Abkar and Porté-Agel*, 2015a]. In agreement with this observation, a recently developed Gaussian wake model by Bastankhah and Porté-Agel was found to provide substantially better results in both full-wake and partial-wake conditions when compared to top-hat wake models [*Bastankhah and Porté-Agel*, 2014]. In their analytical wake model, mass and momentum conservation is applied to a control volume around one turbine where a self-similar Gaussian profile is assumed for the velocity deficit to derive the following equation for the normalized velocity deficit:

$$\frac{\Delta U}{U_\infty} = (1 - \sqrt{1 - 2\frac{C_T}{8(k^* x/d_0)^2}})exp(-\frac{1}{2(k^* x/d_0)^2}((\frac{z - z_h}{d_0})^2 + (\frac{y}{d_0})^2)), \tag{C.3}$$

where $x, y, and z$ are streamwise, spanwise, and vertical coordinates, respectively, and z_h is the hub height level. k^* denotes the wake growth rate which is a function of thrust coefficient and local streamwise turbulence intensity [*Bastankhah and Porté-Agel*, 2014]. They also proposed the following expression for ϵ:

$$\epsilon = 0.2\sqrt{\beta}, \tag{C.4}$$

where β is a function of C_T and can be expressed as:

$$\beta = \frac{1}{2}\frac{1 + \sqrt{1 - C_T}}{\sqrt{1 - C_T}}, C_T < 0.9, \tag{C.5}$$

Depending on the wind direction, wind turbines inside wind farms are often exposed to multiple wakes from several upstream wind turbines. Therefore, analytical wind farm wake models need to account for the cumulative wake flows that are formed by the interaction of multiple wakes. To achieve that, wind farm models predict cumulative wake effects by applying stand-alone wake models to each individual turbine, together with superposition principles to represent the combined effects of multiple overlapping wakes. Lissaman [*S. Lissaman*, 1979] proposed a model for the cumulative velocity deficit based on the linear superposition of velocity deficits. This model considers an analogy between the point-source pollutant dispersion (e.g., from smoke stacks) and the wind turbine wake expansion in the atmospheric boundary layer and is defined as:

$$U_i = U_\infty - \sum_k (U_\infty - U_{ki}), \tag{C.6}$$

where U_i is the velocity at the turbine i and U_{ki} is the wake velocity of the turbine k at turbine i considering only those turbines whose wakes interact with turbine i. *Katic et al.* [1987] later on used the superposition of energy deficits, instead of velocity deficits, to model the interaction of multiple wakes as follows:

$$U_i = U_\infty - \sqrt{\sum_k (U_\infty - U_{ki})^2}, \tag{C.7}$$

where for each individual wake inside the wind farm, the kinetic energy deficit of multiple wakes is assumed to be equal to the sum of the energy deficits from the relevant upwind turbines. *Voutsinas et al.* [1990] followed the same approach as *Katic et al.* [1987], but to estimate the energy deficit of each wake, they considered the difference between the inflow velocity at the turbine and the wake velocity as follows:

$$U_i = U_\infty - \sqrt{\sum_k (U_k - U_{ki})^2}, \tag{C.8}$$

In wind farms, turbine wake flows lead to a substantial increase in the level of turbulence intensity with respect to the turbulence level of the incoming atmospheric boundary layer flow. This effect has been observed in several numerical and experimental studies [e.g., *Porté-Agel et al.*, 2013; *Abkar and Porté-Agel*, 2014; *Abkar et al.*, 2016; *Porté-Agel et al.*, 2011]. Furthermore, some recent research studies have shown that the wake growth rate increases as the turbulence intensity level increases [e.g., *Bastankhah and Porté-Agel*, 2014], yet most of the common analytical wind farm models assume a constant wake growth rate inside a wind farm. Since the constant wake growth rate assumption is likely unrealistic, we propose an empirical equation for the local wake growth rate that is based on the local streamwise turbulence intensity to consider the turbulence effect in wind farms. Several research studies have attempted to model the added streamwise turbulence intensity inside wind farms [*Quarton and Ainslie*, 1990; *Hassan*, 1993; *Crespo et al.*, 1996]. In general, these models use the thrust coefficient of the turbines and the ambient turbulence intensity to estimate the added streamwise turbulence intensity at the wind turbine hub height as follows:

$$I_+ = \sqrt{I_{wake}^2 - I_0^2}, \tag{C.9}$$

where I_{wake} is the streamwise turbulence intensity in the wake and I_0 is the ambient turbulence intensity. *Quarton and Ainslie* [1990] proposed the following empirical expression to predict the added streamwise turbulence intensity generated by a wind turbine:

$$I_+ = 4.8 C_T^{0.7} I_0^{0.68} (x/x_n)^{-0.57}, \tag{C.10}$$

where x_n is the length of the near-wake region, which is defined as [*Vermeulen*, 1980]:

$$x_n = \frac{\sqrt{0.214 + 0.144m}(1 - \sqrt{0.134 + 0.124m})}{(1 - \sqrt{0.214 + 0.144m})\sqrt{0.134 + 0.124m}} \frac{r_0}{dr/dx},$$ (C.11)

where $m = \frac{1}{\sqrt{1-C_T}}$, $r_0 = d_0/2\sqrt{\frac{m+1}{2}}$ and dr/dx is defined by the following expression:

$$dr/dx = \sqrt{(\frac{dr}{dx})_a^2 + (\frac{dr}{dx})_m^2 + (\frac{dr}{dx})_\lambda^2},$$ (C.12)

where $\frac{dr}{dx})_a = 2.5I_0 + 0.005$, $(\frac{dr}{dx})_a = \frac{1 - m(\sqrt{1.49+m})}{9.76(1+m)}$, and $\frac{dr}{dx})_\lambda = 0.012B\lambda$. B is the number of blades and λ is the tip speed ratio. Later, *Hassan* [1993] suggested the following expression for the added streamwise turbulence intensity:

$$I_+ = 5.7C_T^{0.7}I_0^{0.68}(x/x_n)^{-0.96},$$ (C.13)

Based on a numerical study, *Crespo et al.* [1996] suggested the following empirical equation for the parameter ranges $5 < x/d_0 < 15$, $0.07 < I_u < 0.14$, and $0.1 < a < 0.4$, where a is the induction factor:

$$I_+ = 0.73a^{0.8325}I_0^{0.0325}(x/d)^{-0.32}.$$ (C.14)

This paper is structured as follows: The proposed analytical wind farm wake model is presented in Section C.2. A description of the case study (the Horns Rev wind farm) is then given in Section C.3. In Section C.4, the results obtained with the new analytical wind farm model are discussed and compared with power measurements and with results from LES and a commonly-used analytical wind farm model. Finally, a summary and conclusion are provided in Section C.5.

C.2 Description of the New Analytical Wind Farm Model

The proposed analytical wind farm model uses the self-similar Gaussian model, recently developed by *Bastankhah and Porté-Agel* [2014], together with the assumption of superposition of the velocity deficit for the cumulative wake effects. Next, details of the formulation and implementation of the new wind farm model are given.

C.2.1 Analytical Model for the Velocity Deficit

The Gaussian wake model of *Bastankhah and Porté-Agel* [2014] is applied individually to each of the turbines in the wind farm. For single wakes, this model considers a self-similar Gaussian

distribution for the normalized velocity deficit, in which mass and momentum are conserved. In this study, the operating conditions of the wind turbines are within a range for which the thrust coefficient is approximately constant (Figure C.4). For this reason, wake growth rate is assumed to be only a function of local streamwise turbulence intensity. Figure C.2 shows the wake growth rate behind a V-80 turbine obtained from LES for a wide range of streamwise turbulence intensities of the incoming boundary layer wind at hub height level. Based on the aforementioned numerical data, the following empirical expression is proposed to calculate the growth rate of the wake behind each turbine for the range of conditions considered herein $(0.065 < I < 0.15)$:

$$k^* = 0.3837 I + 0.003678, \tag{C.15}$$

where I is the local streamwise turbulence intensity immediately upwind of the rotor center, which is estimated while neglecting any potential effect of that turbine on the upwind turbulence level . The generalization of Equation C.15 to include a wider range of turbine operation conditions and inflow characteristics will be the focus of our future research.
The interaction among multiple wakes is modeled by applying a new approach, which is based on the velocity deficit superposition principle. Previously, *S. Lissaman* [1979] applied velocity deficit superposition that explicitly considers the difference between the undisturbed velocity and the wake velocity. It should be noted that this method of wake superposition results in an overestimation of the velocity deficit, specifically where there are several rows of wind turbines [*Crespo et al.*, 1996]. Here, instead, to estimate the velocity deficit, we propose to calculate the difference between the inflow velocity at the turbine and the wake velocity as follows:

$$U_i = U_\infty - \sum_k (U_k - U_{ki})^2, \tag{C.16}$$

Similar to the single-wake model, it is vital that the wake superposition procedure conserves mass and momentum. *S. Lissaman* [1979] justified the linear superposition of the wakes. He argued that there is an analogy between turbine wakes and pollution plumes, whose Gaussian concentration distribution can be superimposed as a result of the linearity of the process. In the same way that pollutant superposition conserves mass, the linearized momentum deficit is conserved by applying superposition of velocity deficit.

C.2.2 Turbulence Intensity Model

For the local streamwise turbulence intensity, we propose to use a top-hat distribution with a wake diameter of 4σ, which has been derived empirically based on LES data [*Porté-Agel et al.*, 2013], where σ denotes the standard deviation of the Gaussian-like velocity deficit. It is defined [*Bastankhah and Porté-Agel*, 2014] as:

$$\sigma / d_0 = (k^* x) / d_0 + \epsilon. \tag{C.17}$$

The enhancement of streamwise turbulence intensity for individual turbines is calculated from Equation (C.14). Then, the local streamwise turbulence intensity is found using Equation (C.9).

Several numerical and experimental studies have shown that the level of turbulence intensity increases inside a wind farm. Furthermore, the level of turbulence intensity has been observed to quickly reach an equilibrium after 2–3 rows of wind turbines [*Porté-Agel et al.*, 2013; *Abkar and Porté-Agel*, 2015b]. A previous study by [*Frandsen and Thøgersen*, 1999] has also shown that to predict the turbulence intensity in the wake of a given turbine, the only important effect is that of neighboring upstream turbines. In this respect, for every turbine, we consider solely the added streamwise turbulence intensity caused by the nearest upstream turbine whose wake has the most significant impact. It is defined as:

$$I_{+_j} = max(\frac{A_w 4}{\pi d_0^2} I_{+_{kj}}),$$ (C.18)

where I_{+_j} is the added streamwise turbulence intensity at the turbine j, A_w is the intersection between the wake (using Equation C.17) and the rotor area, and $I_{+_{kj}}$ is the added streamwise turbulence intensity induced by the turbine k at the turbine j.
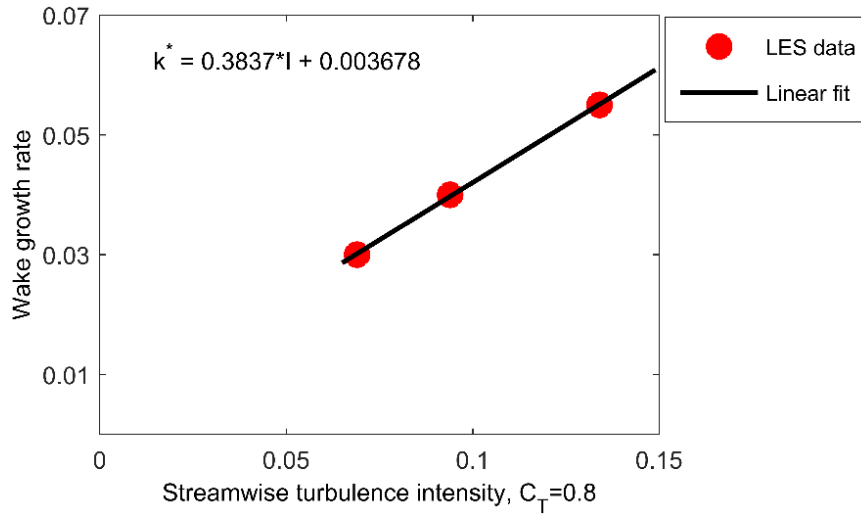
Figure C.1 – Wake growth rate for the V-80 turbine in boundary layer flow with different streamwise turbulence intensities at hub height.

C.2.3   Power Prediction

The power curve, which gives the power production as a function of incoming wind speed, is used to predict the power generated by each turbine. Here, the data available for Vestas V-80 wind turbines is used where a fifth degree polynomial is fitted to the data, as shown in Figure C.2.
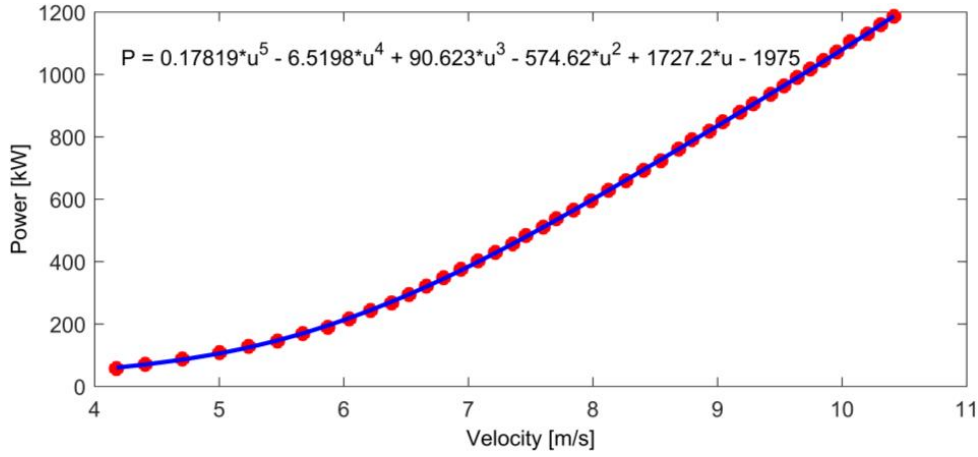
Figure C.2 – Power curve of the V-80 wind turbine. Red circles correspond to the manufacturer's data and the blue line represents a polynomial fit.

C.3   Case Description

We selected the Horns Rev offshore wind farm as a case study because LES flow and power predictions [*Porté-Agel et al.*, 2013; *Wu and Porté-Agel*, 2015] and power measurements [*Barthelmie et al.*, 2006, 2009] are available to evaluate the performance of the proposed analytical wind farm model. The wind farm has a total rated power capacity of 160 MW and consists of eighty Vestas V-80 wind turbines within an area of approximately 20 km2. It is located in the North Sea, approximately 15 km off the westernmost point of Denmark. Each turbine has a rotor diameter of d=80 m and a hub height of H_{hub}=70 m (above sea level). Figure C.3 shows a schematic of the Horns Rev wind farm layout. The wind farm has a rhomboid shape with wind turbines arranged in 8 columns (aligned with the East-West direction) and 10 rows (turned approximately 7° counterclockwise from the North-South direction). The turbines are regularly spaced, with a minimum spacing between two consecutive turbines of 7 rotor diameters.

The wind turbine power curve and thrust coefficient curve, both of which are inputs required by the new analytical wind farm model, are typically available from the manufacturer. The curves for the Vestas V-80 turbine are shown in Figure 4. The same curves were also used by *Wu and Porté-Agel* [2015] in their LES study of wake flows in the Horns Rev wind farm. To specify the incoming flow conditions, the aerodynamic surface roughness of the sea surface was set to z_0=0.0002 m. The inflow wind condition is characterized by a turbulence intensity of 7.7% at the hub height and an average velocity of 8 ms$^{(-1)}$ at the same height. These conditions are the same as those for the available power measurements [*Barthelmie et al.*, 2006], LES flow, and power results [*Wu and Porté-Agel*, 2015].
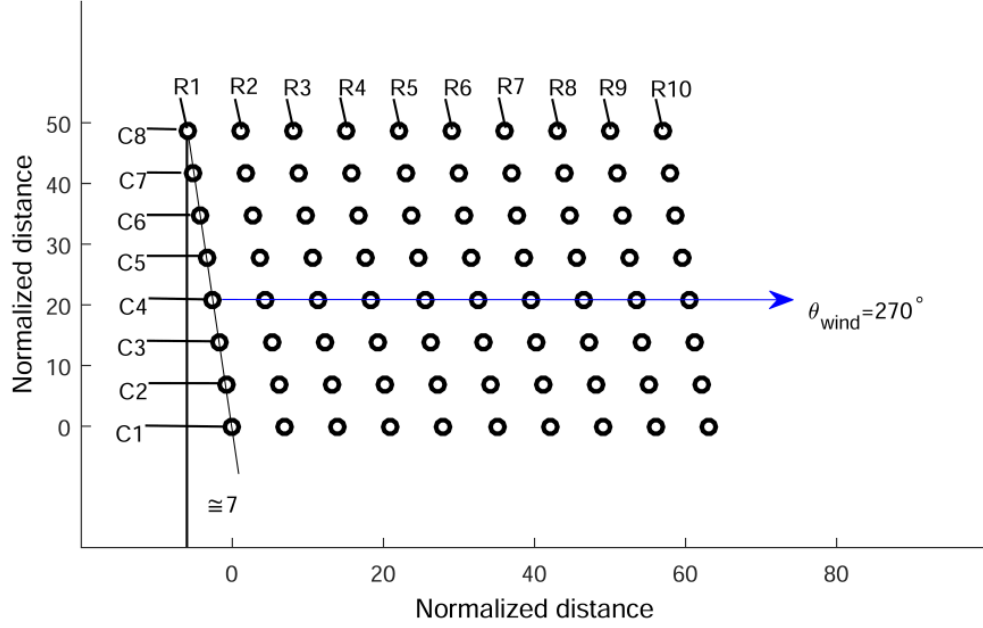
Figure C.3 – Layout of the Horns Rev wind farm. Distances are normalized by the rotor diameter d=80.

C.4 Results and Discussion

In this section, predictions obtained with the new analytical model for the turbine wakes and associated power losses in the Horns Rev wind farm are presented. The results are also compared with available power measurements [*Barthelmie et al.*, 2006, 2009] and LES data [*Porté-Agel et al.*, 2013; *Wu and Porté-Agel*, 2015], as well as with predictions from an existing analytical top-hat wake model. The top-hat wake model is based on the one proposed by *Katic et al.* [1987] and is commonly used in a variety of software (e.g., the Wind Atlas Analysis and Application Program (WAsP) and the PARK model). In this top-hat wake model, the wake growth rate is set to a constant (and spatially uniform) value of 0.04, which is based on the formula proposed by *Frandsen et al.* [2006].

The simulated total normalized power output from the Horns Rev wind farm calculated with the new model, LES [*Porté-Agel et al.*, 2013], and the top-hat model [*Katic et al.*, 1987] is shown in Figure C.5 for a wide range of wind directions (from 173° to 353°). This enables an extensive model evaluation over a variety of both full-wake and partial-wake operating conditions. Furthermore, we normalize the simulated power output by the power of an equivalent number of stand-alone wind turbines operating in the same incoming wind condition. As shown in Figure C.1, a good agreement is found between the proposed analytical model and LES, while the top-hat model significantly under predicts the normalized power. Furthermore, wind farm power production substantially decreases (approximately 30%) as the wind farm is exposed to wind direction angles (173°, 270°, and 353°), corresponding to full-wake conditions with short streamwise distances between consecutive wind turbines. Additionally, when the wind farm is
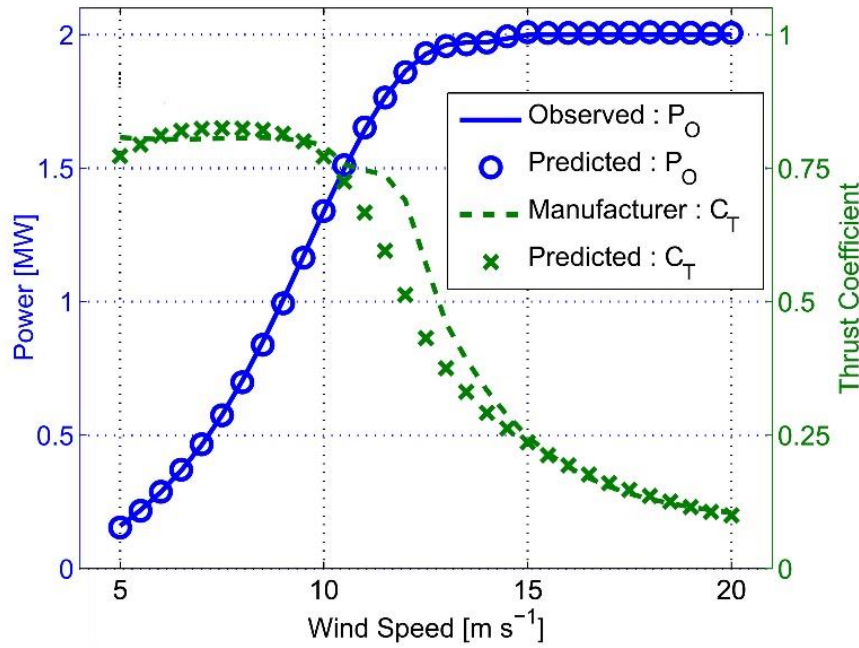
Figure C.4 – Measured and simulated power curve and thrust coefficient curve of the Vestas V-80 2 MW wind turbine, for a range of wind speeds (Source: Wu and Porté-Agel, 2014).

exposed to the wind directions in which there is a large streamwise distance between turbines (e.g., 185° and 340°), several local maxima can be distinguished.

Next, the performance of different multiple wake superposition approaches is evaluated. For
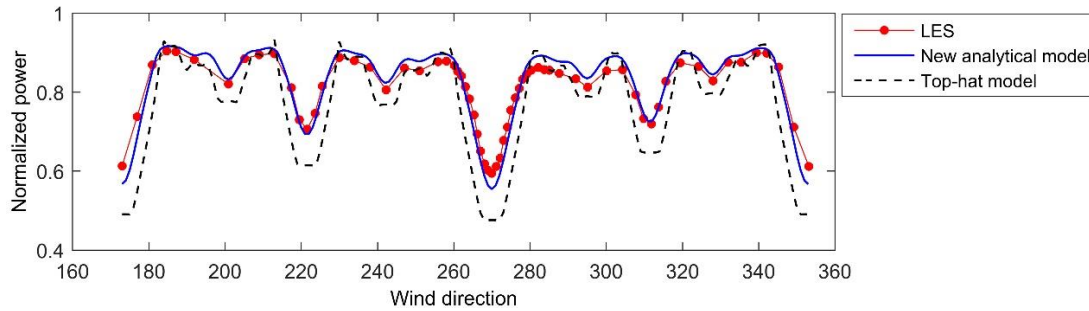
Figure C.5 – Distribution of the normalized Horns Rev wind farm power output obtained with the new analytical model and LES for different wind directions.

this purpose, we compare the normalized power output simulated with the new analytical model using both velocity deficit superpositionand energy deficit superposition with the one obtained with LES. The normalized power output as a function of turbine row (averaged over columns 2, 3, and 4) in the wind farm is shown in Figure C.2. The difference between the inflow velocity at the turbine and the wake velocity is used for calculation of the velocity and energy deficits. It is important to mention that if the difference between the incoming velocity to the turbine and the wake velocity is used, unrealistic negative velocities can occur as a result of a

large number of turbine rows. As shown in Figure C.6, although energy deficit superposition substantially overestimates the normalized power output, velocity deficit superposition shows good agreement with LES.

To show the impact of the local wake growth rate on wind farm power prediction, the simulated
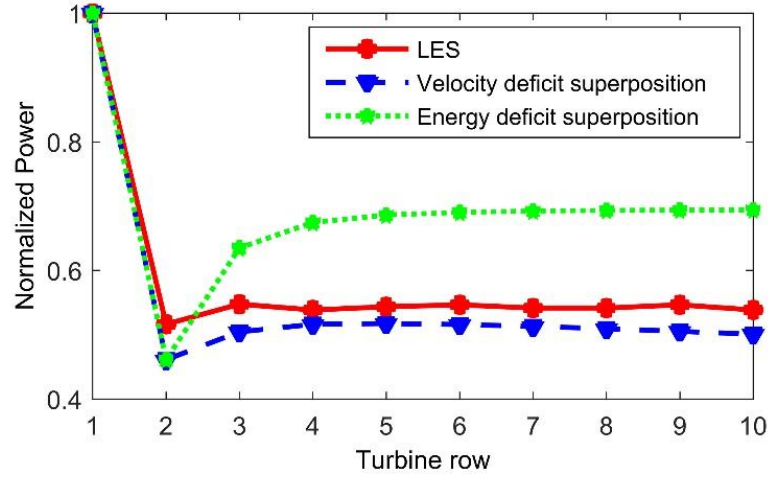
Figure C.6 – Comparison of the wind-farm power output for $\theta_{wind} = 270°$ obtained using LES as well as the new analytical model with both energy and velocity deficit superpositions.

normalized power output obtained using constant and variable wake growth rates (the latter calculated based on the local streamwise turbulence intensity, Equation C.15) is compared with LES. As shown in Figure C.7, reasonable agreement between the analytical model and LES can be achieved using a variable wake growth rate. In contrast, assuming a constant wake growth rate leads to a clear underestimation of the normalized power output. This is because, inside the wind farm, the wakes recover faster (and thus have a larger growth rate) due to the increased flow entrainment induced by the relatively higher turbulence levels in the wakes, compared with the incoming flow. Our results show the importance of taking into account the increased level of turbulence intensity and the associated increased growth rate for the prediction of wakes and power inside wind farms.

Figure C.8 shows the normalized power output for three wind sectors (i.e., ±5°, ±10°, and ±15°) centered on three mean wind directions ($\theta_{wind} = 270°$, 222°, and 312°) simulated by the new analytical model and WAsP, as well as the measurements [*Barthelmie et al.*, 2009]. As shown in this figure, WAsP clearly tends to under predict the power output, while a very good agreement between the measurements and the proposed model is found. This result reveals the fact that considering a top-hat shape for normalized velocity deficit can lead to substantial error in both full-wake and partial-wake conditions. One of the main features of the new analytical wind farm model is the capability of computing the mean velocity field inside a wind farm and the associated power output in a computationally efficient way while keeping the accuracy acceptable. Figure 9 shows a two-dimensional contour plot of the streamwise velocity on a horizontal plane at hub level simulated by LES [*Porté-Agel et al.*, 2013; *Wu and Porté-Agel*, 2015], the new analytical model, and the classical top-hat analytical model [*Katic et al.*, 1987].
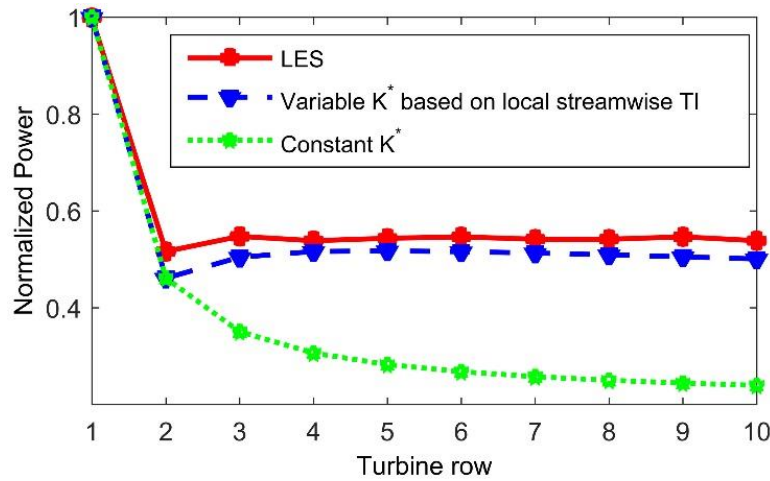
Figure C.7 – Comparison of the power output for $\theta_{wind} = 270°$ obtained with the new analytical model using a constant wake growth rate and a variable wake growth rate based on the local streamwise turbulence intensity.

It should be mentioned that the analytical wake models can only predict the velocity deficit in the far-wake region (after a downwind distance of approximately two rotor diameters from each turbine) where the wake flows have a self-similar Gaussian behavior and can be described by global parameters such as the thrust coefficient. To this effect, a white rectangle is placed in the near wake region in Figure C.9. Reasonable agreement between the proposed analytical model and LES is found, while the top-hat model gives a less realistic prediction of the velocity flow field due to the top-hat assumption for the velocity deficit, which results in a uniform wake velocity distribution in the spanwise direction. Furthermore, it is obvious that wake flows are responsible for a significant reduction of the velocity immediately upstream of the wind turbines inside the wind farm.

As discussed previously, the wake growth rate is dependent on the local streamwise turbulence intensity. Therefore, the local streamwise turbulence intensity in the wind farm should be predicted in the analytical wind farm model. Furthermore, it is imperative to estimate the level of turbulence intensity at the turbine locations to investigate the impact of fatigue loading due to turbulence on the turbines. Figure C.10 presents the level of streamwise turbulence intensity at hub height in the wind farm obtained from the models of *Quarton and Ainslie* [1990], *Hassan* [2003], and *Crespo et al.* [1996], as well as the LES predictions. It clearly shows that both the models of Quarton and Ainslie and of Hassan and Hassan over predict the level of streamwise turbulence intensity when compared with LES. In contrast, the model of Crespo and Hernandez, which is used in the new proposed model, predicts turbulence intensity levels that are very similar to those simulated by LES.
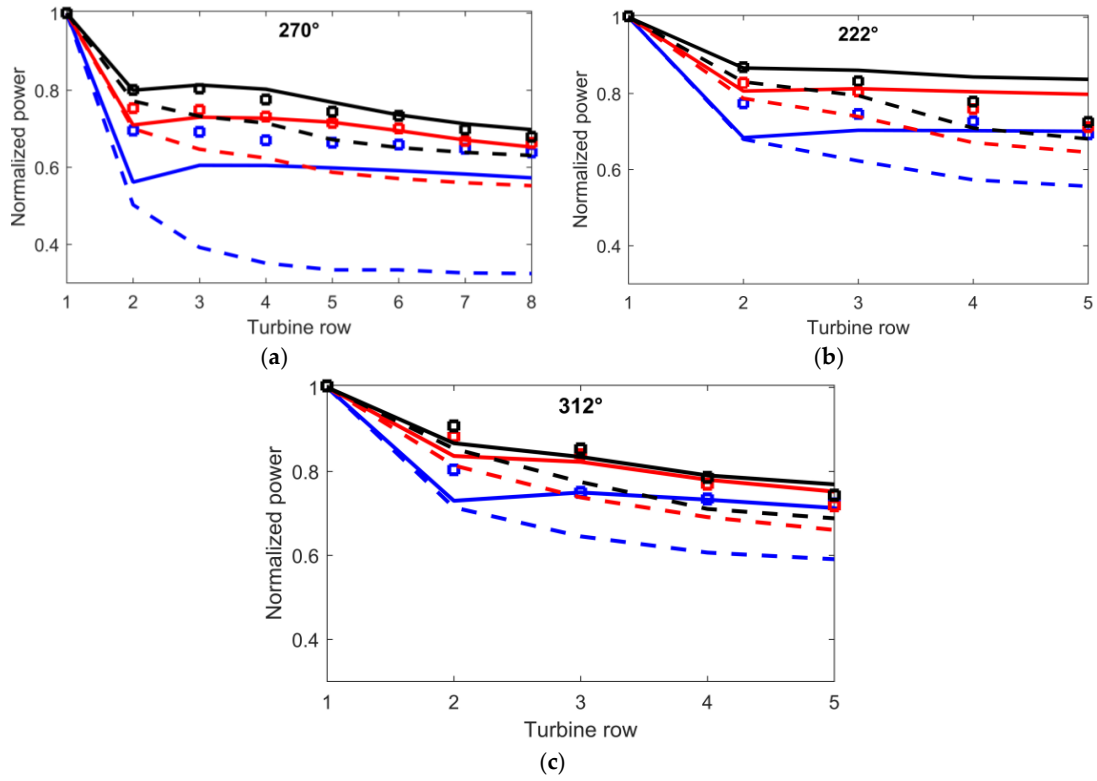
Figure C.8 – Comparisons of the simulated and observed power output centered on three mean wind directions $\theta_{wind} = 270°$ (a); $\theta_{wind} = 222°$ (b) and $\theta_{wind} = 312°$ (c) . Symbols, lines, and dashed lines denote the observed, new analytical model, and WAsP data, respectively. Blue, red, and black colors represent ±5°, ±10°, and ±15° wind sectors, respectively.

C.5   Conclusion

A new analytical wind-farm wake model is proposed to predict wake flows and associated power losses inside wind farms. The model combines the self-similar Gaussian model recently developed by *Bastankhah and Porté-Agel* [2014] for stand-alone wind turbine wakes with a new wake superposition procedure that is based on the superposition of velocity deficits. This combination guarantees that mass and momentum are conserved by the model. The growth rate of each individual wake needs to be specified and is computed using an empirical expression based on the local streamwise turbulence intensity, which is predicted inside the wind farm using the model proposed by *Crespo et al.* [1996]. Finally, the power curve of the wind turbines is used to estimate the power production. The Horns Rev wind farm was selected as a validation case study because power measurements and previous LES predictions of the wake flows and turbine power are available for a wide range of inflow conditions. Comparison between the measurements and LES results reveal that the new analytical wind-farm model yields reasonably accurate predictions of the power output from the Horns Rev wind farm for all of the wind directions considered in this study. Additionally, we show that the power prediction of the new analytical wind farm model is significantly better than the one estimated
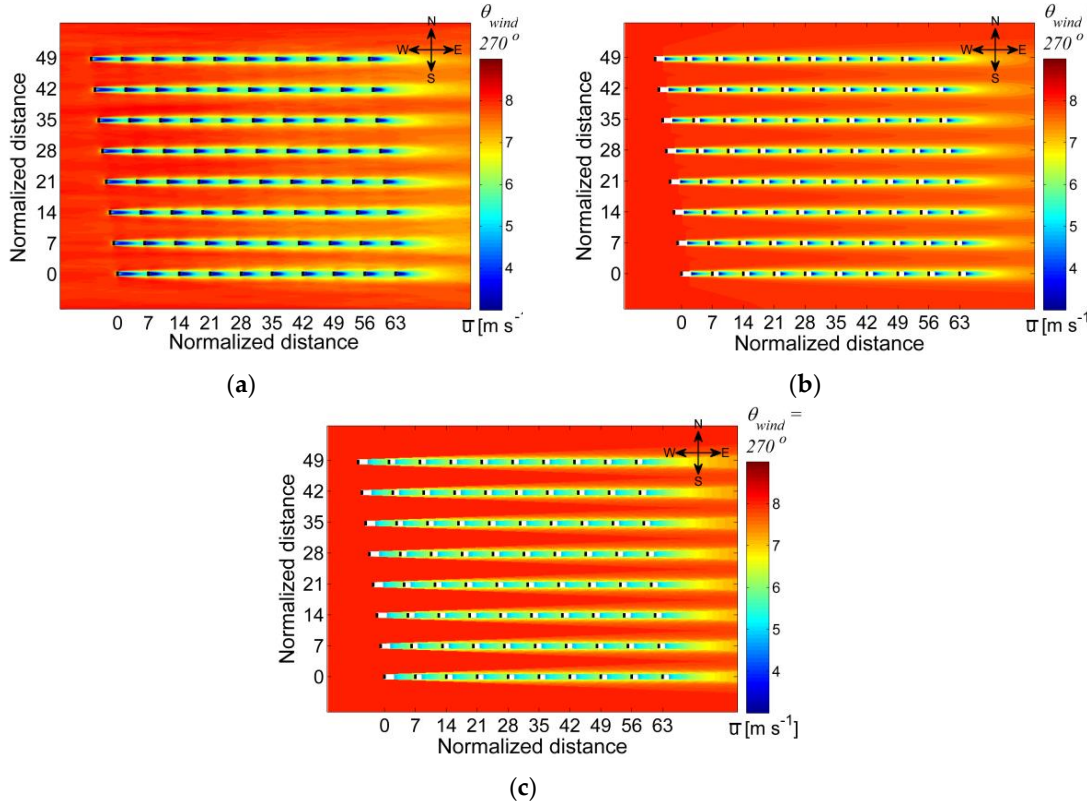
Figure C.9 – Comparison of the time-averaged streamwise velocity at a horizontal plane at hub height: (a) LES; (b) new analytical model and (c) top-hat model.

by WAsP. Future research will consider the development of more general parametrization of the local turbulence intensity and the wake growth rate, which can then be used by the new model for a wider range of inflow characteristics (e.g., including thermal stability) and turbine operation conditions (e.g., turbine down-regulation or yawing). Furthermore, because of its low computational cost, the newly proposed model can be used for the optimization of wind farm layouts to maximize power output and minimize the fatigue load on the wind turbines.
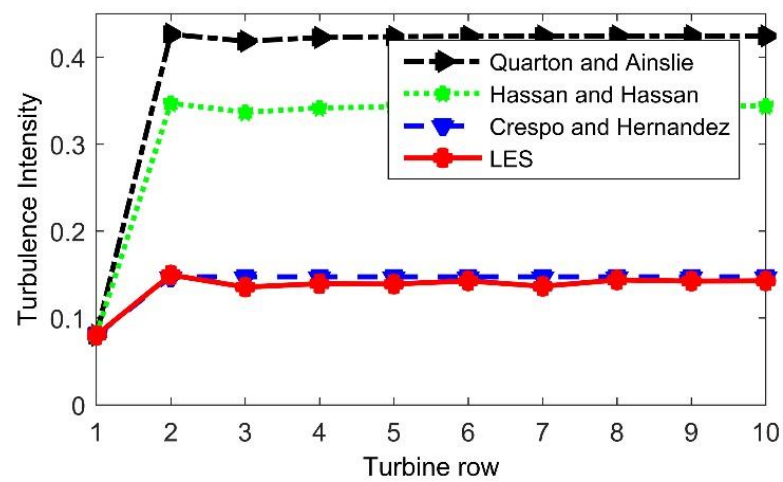
Figure C.10 – Comparison of the streamwise turbulence intensity at hub height immediately upstream of each turbine row, obtained with LES and three simple models.

Bibliography

Abkar, M., and F. Porté-Agel, The effect of free-atmosphere stratification on boundary-layer flow and power output from very large wind farms, *Energies*, *6*(5), 2338–2361, 2013.

Abkar, M., and F. Porté-Agel, Mean and turbulent kinetic energy budgets inside and above very large wind farms under conventionally-neutral condition, *Renewable Energy*, *70*, 142–152, 2014.

Abkar, M., and F. Porté-Agel, Influence of atmospheric stability on wind-turbine wakes: A large-eddy simulation study, *Physics of fluids*, *27*(3), 035,104, 2015a.

Abkar, M., and F. Porté-Agel, A new wind-farm parameterization for large-scale atmospheric models, *Journal of Renewable and Sustainable Energy*, *7*(1), 013,121, 2015b.

Abkar, M., A. Sharifi, and F. Porté-Agel, Wake flow in a wind farm during a diurnal cycle, *Journal of Turbulence*, *17*(4), 420–441, 2016.

Annear, T. C., and A. L. Conder, Relative bias of several fisheries instream flow methods, *North American Journal of Fisheries Management*, *4*(4B), 531–539, 1984.

Appling, A. P., R. O. Hall, C. B. Yackulic, and M. Arroita, Overcoming equifinality: Leveraging long time series for stream metabolism estimation, *Journal of Geophysical Research: Biogeosciences*, *123*(2), 624–645, 2018.

Arthington, A. H., S. E. Bunn, N. L. Poff, and R. J. Naiman, The challenge of providing environmental flow rules to sustain river ecosystems, *Ecological Applications*, *16*(4), 1311–1318, 2006.

Asher, W., and R. Wanninkhof, Transient tracers and air-sea gas transfer, *Journal of Geophysical Research: Oceans*, *103*(C8), 15,939–15,958, 1998a.

Asher, W. E., and R. Wanninkhof, The effect of bubble-mediated gas transfer on purposeful dual-gaseous tracer experiments, *Journal of Geophysical Research: Oceans*, *103*(C5), 10,555–10,560, 1998b.

Assani, A. A., J.-F. Quessy, M. Mesfioui, and M. Matteau, An example of application: The ecological "natural flow regime" paradigm in hydroclimatology, *Advances in Water Resources*, *33*(5), 537–545, 2010.

111

Bibliography

Barthelmie, R. J., G. Larsen, S. Frandsen, L. Folkerts, K. Rados, S. Pryor, B. Lange, and G. Schepers, Comparison of wake model simulations with offshore wind turbine wake profiles measured by sodar, *Journal of atmospheric and oceanic technology*, *23*(7), 888–901, 2006.

Barthelmie, R. J., et al., Modelling and measuring flow and wind turbine wakes in large wind farms offshore, *Wind Energy: An International Journal for Progress and Applications in Wind Power Conversion Technology*, *12*(5), 431–444, 2009.

Barthelmie, R. J., et al., Quantifying the impact of wind turbine wakes on power output at offshore wind farms, *Journal of Atmospheric and Oceanic Technology*, *27*(8), 1302–1317, 2010.

Bartholow, J. M., Constructing an interdisciplinary flow regime recommendation 1, *JAWRA Journal of the American Water Resources Association*, *46*(5), 892–906, 2010a.

Bartholow, J. M., Constructing an interdisciplinary flow regime recommendation, *JAWRA Journal of the American Water Resources Association*, *46*(5), 892–906, doi:10.1111/j.1752-1688.2010.00461.x, 2010b.

Basso, S., and G. Botter, Streamflow variability and optimal capacity of run-of-river hydropower plants, *Water Resources Research*, *48*(10), 2012.

Bastankhah, M., and F. Porté-Agel, A new analytical model for wind-turbine wakes, *Renewable Energy*, *70*, 116–123, 2014.

Battin, T. J., S. Luyssaert, L. A. Kaplan, A. K. Aufdenkampe, A. Richter, and L. J. Tranvik, The boundless carbon cycle, *Nature Geoscience*, *2*(9), 598, 2009.

Bellman, R., Dynamic programming, *Science*, *153*(3731), 34–37, 1966.

Bernhard, F. A., and P. Perona, Dynamical behavior and stability analysis of hydromechanical gates, *Journal of Irrigation and Drainage Engineering*, *143*(9), 04017,039, 2017.

Biggs, B. J., M. J. Duncan, S. N. Francoeur, and W. D. Meyer, Physical characterisation of microform bed cluster refugia in 12 headwater streams, New Zealand, *New Zealand Journal of Marine and Freshwater Research*, *31*(4), 413–422, 1997.

Birsan, M.-V., P. Molnar, P. Burlando, and M. Pfaundler, Streamflow trends in Switzerland, *Journal of Hydrology*, *314*(1), 312–329, 2005.

Bizzi, S., F. Pianosi, and R. Soncini-Sessa, Valuing hydrological alteration in multi-objective water resources management, *Journal of hydrology*, *472*, 277–286, 2012.

Bloesch, J., M. Schneide, and J. Ortlepp, An application of physical habitat modelling to quantify ecological flow for the Rheinau hydropower plant, River Rhine, *Archiv für Hydrobiologie. Supplementband. Large rivers*, *16*(1-2), 305–328, 2005.

Brönnimann, S., et al., Climate change in switzerland: a review of physical, institutional, and political aspects, *Wiley Interdisciplinary Reviews: Climate Change*, *5*(4), 461–481, 2014.

Brutsaert, W., *Hydrology: an introduction*, Cambridge University Press, 2005.

Buffington, J. M., D. R. Montgomery, and H. M. Greenberg, Basin-scale availability of salmonid spawning gravel as influenced by channel type and hydraulic roughness in mountain catchments, *Canadian Journal of Fisheries and Aquatic Sciences*, *61*(11), 2085–2096, 2004.

Butman, D., and P. A. Raymond, Significant efflux of carbon dioxide from streams and rivers in the united states, *Nature Geoscience*, *4*(12), 839, 2011.

Calaf, M., C. Meneveau, and J. Meyers, Large eddy simulation study of fully developed wind-turbine array boundary layers, *Physics of fluids*, *22*(1), 015,110, 2010.

Capra, H., P. Breil, and Y. Souchon, A new tool to interpret magnitude and duration of fish habitat variations, *Regulated Rivers: Research & Management*, *10*(2-4), 281–289, 1995.

Carolli, M., D. Geneletti, and G. Zolezzi, Assessing the impacts of water abstractions on river ecosystem services: an eco-hydraulic modelling approach, *Environmental Impact Assessment Review*, *63*(Supplement C), 136 – 146, doi:https://doi.org/10.1016/j.eiar.2016.12.005, 2017.

Castelletti, A., D. de Rigo, A. E. Rizzoli, R. Soncini-Sessa, and E. Weber, Neuro-dynamic programming for designing water reservoir network management policies, *Control Engineering Practice*, *15*(8), 1031–1038, 2007.

Castelletti, A., F. Pianosi, and R. Soncini-Sessa, Water reservoir control under economic, social and environmental constraints, *Automatica*, *44*(6), 1595–1607, 2008.

Chamorro, L. P., and F. Porté-Agel, A wind-tunnel investigation of wind-turbine wakes: boundary-layer turbulence effects, *Boundary-layer meteorology*, *132*(1), 129–149, 2009.

Chanson, H., Air bubble entrainment in open channels: flow structure and bubble size distributions, *International Journal of Multiphase Flow*, *23*(1), 193–203, 1997.

Chanson, H., and L. Toombes, Strong interactions between free-surface aeration and turbulence in an open channel flow, *Experimental Thermal and Fluid Science*, *27*(5), 525–535, 2003.

Chanson, H., L. Toombes, D. B. Moog, and G. H. Jirka, Stream reaeration in nonuniform flow: macroroughness enhancement, *Journal of Hydraulic Engineering*, *126*(3), 222–224, 2000.

Chen, D., and G. H. Jirka, Experimental study of plane turbulent wakes in a shallow water layer, *Fluid dynamics research*, *16*(1), 11, 1995.

Chowdhury, S., J. Zhang, A. Messac, and L. Castillo, Optimizing the arrangement and the selection of turbines for wind farms subject to varying wind conditions, *Renewable Energy*, *52*, 273–282, 2013.

Bibliography

Cole, J. J., and N. F. Caraco, Atmospheric exchange of carbon dioxide in a low-wind oligotrophic lake measured by the addition of sf6, *Limnology and Oceanography*, *43*(4), 647–656, 1998.

Cole, J. J., et al., Plumbing the global carbon cycle: integrating inland waters into the terrestrial carbon budget, *Ecosystems*, *10*(1), 172–185, 2007.

Council, G. W. E., Global wind report annual market update 2013, *Brussels: GWEC*, 2012.

Coutanceau, M., and R. Bouard, Experimental determination of the main features of the viscous flow in the wake of a circular cylinder in uniform translation. Part 1. Steady flow, *Journal of Fluid Mechanics*, *79*(02), 231–256, 1977.

Crasto, G., A. Gravdahl, F. Castellani, and E. Piccioni, Wake modeling with the actuator disc concept, *Energy Procedia*, *24*, 385–392, 2012.

Crespo, A., J. Herna, et al., Turbulence characteristics in wind-turbine wakes, *Journal of wind engineering and industrial aerodynamics*, *61*(1), 71–85, 1996.

Crespo, A., J. Hernandez, and S. Frandsen, Survey of modelling methods for wind turbine wakes and wind farms, *Wind Energy: An International Journal for Progress and Applications in Wind Power Conversion Technology*, *2*(1), 1–24, 1999.

Cui, L., and G. Kuczera, Optimizing water supply headworks operating rules under stochastic inputs: Assessment of genetic algorithm performance, *Water Resources Research*, *41*(5), 2005.

Dariane, A. B., and S. Momtahen, Optimization of multireservoir systems operation using modified direct search genetic algorithm, *Journal of Water Resources Planning and Management*, *135*(3), 141–148, 2009.

D'Asaro, E., and C. McNeil, Air–sea gas exchange at extreme wind speeds measured by autonomous oceanographic floats, *Journal of Marine Systems*, *66*(1-4), 92–109, 2007.

Dietrich, J. T., Bathymetric structure-from-motion: extracting shallow stream bathymetry from multi-view stereo photogrammetry, *Earth Surface Processes and Landforms*, *42*(2), 355–364, 2017.

Dingman, S. L., and S. L. Dingman, *Physical hydrology*, vol. 575, Prentice Hall Englewood Cliffs, NJ, 1994.

Džubáková, K., P. Molnar, K. Schindler, and M. Trizna, Monitoring of riparian vegetation response to flood disturbances using terrestrial photography, *Hydrology and Earth System Sciences*, *19*(1), 195–208, 2015.

EcoControl, *Centralina idroelettrica di Cauco. Effetti della captazione sull'ecosistema acquatico della Calancasca (in Italian)*, 2011.

EcoControl, *Valutazione dell'ecosistema fluviale e ricadute del progetto sulla fauna ittica (in Italian)*, 2012.

EcoControl, *Effetti della captazione sull'ecosistema della Calancasca (in Italian)*, 2013.

Enders, E., and D. Boisclair, Effects of environmental fluctuations on fish metabolism: Atlantic salmon salmo salar as a case study, *Journal of fish biology*, *88*(1), 344–358, 2016.

Enders, E. C., D. Boisclair, and A. G. Roy, A model of total swimming costs in turbulent flow for juvenile atlantic salmon (salmo salar), *Canadian Journal of Fisheries and Aquatic Sciences*, *62*(5), 1079–1089, 2005.

Ernst, J., B. J. Dewals, S. Detrembleur, P. Archambeau, S. Erpicum, and M. Pirotton, Micro-scale flood risk analysis based on detailed 2d hydraulic modelling and high resolution geographic data, *Natural Hazards*, *55*(2), 181–209, 2010.

Fan, J., and G. L. Morris, Reservoir sedimentation. i: Delta and density current deposits, *Journal of Hydraulic Engineering*, *118*(3), 354–369, 1992.

Flato, G., et al., Climate change 2013: The physical science basis, contribution of working group 1 to the fifth assessment report of the intergovernmental panel on climate change, *Climate Change 2013*, 2013.

Fonstad, M. A., J. T. Dietrich, B. C. Courville, J. L. Jensen, and P. E. Carbonneau, Topographic structure from motion: a new development in photogrammetric measurement, *Earth Surface Processes and Landforms*, *38*(4), 421–430, 2013.

Franchini, M., E. Ventaglio, and A. Bonoli, A procedure for evaluating the compatibility of surface water resources with environmental and human requirements, *Water resources management*, *25*(14), 3613, 2011.

Frandsen, S., On the wind speed reduction in the center of large clusters of wind turbines, *Journal of Wind Engineering and Industrial Aerodynamics*, *39*(1-3), 251–265, 1992.

Frandsen, S., and M. L. Thøgersen, Integrated fatigue loading for wind turbines in wind farms by combining ambient turbulence and wakes, *Wind Engineering*, pp. 327–339, 1999.

Frandsen, S., R. Barthelmie, S. Pryor, O. Rathmann, S. Larsen, J. Højstrup, and M. Thøgersen, Analytical modelling of wind speed deficit in large offshore wind farms, *Wind Energy: An International Journal for Progress and Applications in Wind Power Conversion Technology*, *9*(1-2), 39–53, 2006.

Gao, Y., R. M. Vogel, C. N. Kroll, N. L. Poff, and J. D. Olden, Development of representative indicators of hydrologic alteration, *Journal of Hydrology*, *374*(1-2), 136–147, 2009.

Gippel, C. J., and M. J. Stewardson, Use of wetted perimeter in defining minimum environmental flows, *Regulated rivers: research & management*, *14*(1), 53–67, 1998.

Bibliography

Giuliani, M., A. Castelletti, F. Pianosi, E. Mason, and P. M. Reed, Curses, tradeoffs, and scalable management: Advancing evolutionary multiobjective direct policy search to improve water reservoir operations, *Journal of Water Resources Planning and Management*, *142*(2), 04015,050, 2015.

González, J. S., A. G. G. Rodriguez, J. C. Mora, J. R. Santos, and M. B. Payan, Optimization of wind farm turbines layout using an evolutive algorithm, *Renewable energy*, *35*(8), 1671–1681, 2010.

Gorla, L., The riparian environment as a non-traditional water user, *Tech. rep.*, EPFL, 2014.

Gorla, L., and P. Perona, On quantifying ecologically sustainable flow releases in a diverted river reach, *Journal of Hydrology*, *489*, 98–107, 2013.

Gostner, W., M. Alp, A. J. Schleiss, and C. T. Robinson, The hydro-morphological index of diversity: a tool for describing habitat heterogeneity in river engineering projects, *Hydrobiologia*, *712*(1), 43–60, 2013a.

Gostner, W., P. Parasiewicz, and A. Schleiss, A case study on spatial and temporal hydraulic variability in an alpine gravel-bed stream based on the hydromorphological index of diversity, *Ecohydrology*, *6*(4), 652–667, 2013b.

Hadka, D., and P. Reed, Borg: An auto-adaptive many-objective evolutionary computing framework, *Evolutionary computation*, *21*(2), 231–259, 2013.

Hall Jr, R. O., and H. L. Madinger, Use of argon to measure gas exchange in turbulent mountain streams, *Biogeosciences*, *15*(10), 3085–3092, 2018.

Hall Jr, R. O., T. A. Kennedy, and E. J. Rosi-Marshall, Air–water oxygen exchange in a large whitewater river, *Limnology and Oceanography: Fluids and Environments*, *2*(1), 1–11, 2012.

Hassan, G., Gh windfarmer: Theory manual, *Garrad Hassan and Partners Limited*, 2003.

Hassan, U., *A wind tunnel investigation of the wake structure within small wind turbine farms*, Harwell Laboratory, Energy Technology Support Unit, 1993.

Hayes, J., and I. Jowett, Microhabitat models of large drift-feeding brown trout in three New Zealand rivers, *North American journal of fisheries management*, *14*(4), 710–725, 1994.

Heidrich-Meisner, V., and C. Igel, Variable metric reinforcement learning methods applied to the noisy mountain car problem, pp. 136–150, 2008.

Heinemarm, H., A new sediment trap efficiency curve for small reservoirs, *JAWRA Journal of the American Water Resources Association*, *17*(5), 825–830, 1981.

Holgerson, M. A., and P. A. Raymond, Large contribution to inland water co 2 and ch 4 emissions from very small ponds, *Nature Geoscience*, *9*(3), 222, 2016.

Holtgrieve, G. W., D. E. Schindler, T. A. Branch, and Z. T. A'mar, Simultaneous quantification of aquatic ecosystem metabolism and reaeration using a bayesian statistical model of oxygen dynamics, *Limnology and Oceanography*, *55*(3), 1047–1063, 2010.

IEA, Energy and climate change, 2015.

Jähne, B., and H. Haußecker, Air-water gas exchange, *Annual Review of Fluid Mechanics*, *30*(1), 443–468, 1998.

Jähne, B., G. Heinz, and W. Dietrich, Measurement of the diffusion coefficients of sparingly soluble gases in water, *Journal of Geophysical Research: Oceans*, *92*(C10), 10,767–10,776, 1987.

Jensen, N. O., *A note on wind generator interaction*, 1983.

Job, D., et al., *Auswirkungen der Klimaänderung auf die Wasserkraftnutzung: Synthesebericht*, *Beiträge zur Hydrologie der Schweiz*, vol. 38, Schweizerische Gesellschaft für Hydrologie und Limnologie SGHL, Bern, 2011.

Kalyanmoy, D., A. Pratap, S. Agarwal, and T. Meyarivan, A fast and elitist multiobjective genetic algorithm: Nsga-ii, *IEEE Transactions on evolutionary computation*, *6*(2), 182–197, 2002.

Kana, T. M., C. Darkangelo, M. D. Hunt, J. B. Oldham, G. E. Bennett, and J. C. Cornwell, Membrane inlet mass spectrometer for rapid high-precision determination of n2, o2, and ar in environmental water samples, *Analytical Chemistry*, *66*(23), 4166–4170, 1994.

Katic, I., J. Højstrup, and N. O. Jensen, A simple model for cluster efficiency, in *European wind energy association conference and exhibition*, A. Raguzzi, 1987.

Kennard, M. J., B. J. Pusey, J. D. Olden, S. J. Mackay, J. L. Stein, and N. Marsh, Classification of natural flow regimes in australia to support environmental flow management, *Freshwater biology*, *55*(1), 171–193, 2010.

Kern, J. D., G. W. Characklis, M. W. Doyle, S. Blumsack, and R. B. Whisnant, Influence of deregulated electricity markets on hydropower generation and downstream flow regime, *Journal of Water Resources Planning and Management*, *138*(4), 342–355, 2011.

Knighton, D., *Fluvial forms and processes: a new perspective*, Routledge, 2014.

Konar, M., M. J. Todd, R. Muneepeerakul, A. Rinaldo, and I. Rodriguez-Iturbe, Hydrology as a driver of biodiversity: Controls on carrying capacity, niche formation, and dispersal, *Advances in Water Resources*, *51*, 317–325, 2013.

Kramer, D. L., Dissolved oxygen and fish behavior, *Environmental biology of fishes*, *18*(2), 81–92, 1987.

Kucukali, S., and S. Cokgor, Boulder-flow interaction associated with self-aeration process, *Journal of Hydraulic Research*, *46*(3), 415–419, 2008.

Bibliography

Kuhn, C., C. Bettigole, H. Glick, L. Seegmiller, C. Oliver, and P. Raymond, Patterns in stream greenhouse gas dynamics from mountains to plains in northcentral wyoming, *Journal of Geophysical Research: Biogeosciences*, *122*(9), 2173–2190, 2017.

Lacey, R. J., V. S. Neary, J. C. Liao, E. C. Enders, and H. M. Tritico, The ipos framework: linking fish swimming performance in altered flows from laboratory experiments to rivers, *River Research and Applications*, *28*(4), 429–443, 2012.

Lane, S., D. Mould, P. Carbonneau, R. Hardy, and N. Bergeron, Fuzzy modelling of habitat suitability using 2d and 3d hydrodynamic models: biological challenges., *Taylor & Francis*, 2006.

Larsen, I. J., D. R. Montgomery, and H. M. Greenberg, The contribution of mountains to global denudation, *Geology*, *42*(6), 527–530, 2014.

Lazzaro, G., S. Basso, M. Schirmer, and G. Botter, Water management strategies for run-of-river power plants: Profitability and hydrologic impact between the intake and the outflow, *Water Resources Research*, *49*(12), 8285–8298, 2013.

Lifshitz, E., and L. Landau, Statistical physics (course of theoretical physics, volume 5), 1984.

Liss, P., Processes of gas exchange across an air-water interface, *20*(3), 221–238, 1973.

Maddock, I., The importance of physical habitat assessment for evaluating river health, *Freshwater biology*, *41*(2), 373–391, 1999.

Mao, L., A. Dell'Agnese, and F. Comiti, Sediment motion and velocity in a glacier-fed stream, *Geomorphology*, *291*, 69–79, 2017.

Marchese, E., V. Scorpio, I. Fuller, S. McColl, and F. Comiti, Morphological changes in Alpine rivers following the end of the Little Ice Age, *Geomorphology*, *295*(Supplement C), 811 – 826, doi:https://doi.org/10.1016/j.geomorph.2017.07.018, 2017.

Marzolf, E. R., P. J. Mulholland, and A. D. Steinman, Improvements to the diurnal upstream–downstream dissolved oxygen change technique for determining whole-stream metabolism in small streams, *Canadian Journal of Fisheries and Aquatic Sciences*, *51*(7), 1591–1599, 1994.

Maurice, L., B. Rawlins, G. Farr, R. Bell, and D. Gooddy, The influence of flow and bed slope on gas transfer in steep streams and their implications for evasion of co2, *Journal of Geophysical Research: Biogeosciences*, *122*(11), 2862–2875, 2017.

McDowell, M. J., and M. S. Johnson, Gas transfer velocities evaluated using carbon dioxide as a tracer show high streamflow to be a major driver of total co2 evasion flux for a headwater stream, *Journal of Geophysical Research: Biogeosciences*, *123*(7), 2183–2197, 2018.

McNeil, C., and E. D'Asaro, Parameterization of air–sea gas fluxes at extreme wind speeds, *Journal of Marine Systems*, *66*(1-4), 110–121, 2007.

Meijer, K., W. Van der Krogt, and E. van Beek, A new approach to incorporating environmental flow requirements in water allocation modeling, *Water resources management*, *26*(5), 1271–1286, 2012.

Melching, C. S., and H. E. Flores, Reaeration equations derived from us geological survey database, *Journal of Environmental Engineering*, *125*(5), 407–414, 1999.

Milhous, R., et al., *User's guide to the physical habitat simulation system (PHABSIM)*, Department of the Interior, US Fish and Wildlife Service, 1984a.

Milhous, R. T., D. L. Wegner, and T. Waddle, User's guide to the physical habitat simulation system (phabism), *Tech. rep.*, US Fish and Wildlife Service, 1984b.

Milhous, R. T., M. A. Updike, and D. M. Schneider, Physical habitat simulation system reference manual: version ii, *Tech. rep.*, US Fish and Wildlife Service, 1989.

Moghadam, M. K., and A. Keshavarzi, Flow separation behind habitat structure in gravel bed rivers, *Journal of Fisheries and Aquatic Science*, *2*(4), 294–301, 2007.

Montgomery, D. R., and J. M. Buffington, Channel-reach morphology in mountain drainage basins, *Geological Society of America Bulletin*, *109*(5), 596–611, 1997.

Moog, D. B., and G. H. Jirka, Air-water gas transfer in uniform channel flow, *Journal of hydraulic engineering*, *125*(1), 3–10, 1999a.

Moog, D. B., and G. H. Jirka, Stream reaeration in nonuniform flow: Macroroughness enhancement, *Journal of Hydraulic Engineering*, *125*(1), 11–16, 1999b.

Moyle, P. B., and J. F. Mount, Homogenous rivers, homogenous faunas, *Proceedings of the National Academy of Sciences*, *104*(14), 5711–5712, 2007.

Muggeo, V. M., Estimating regression models with unknown break-points, *Statistics in medicine*, *22*(19), 3055–3071, 2003.

Muggeo, V. M., et al., Segmented: an r package to fit regression models with broken-line relationships, *R news*, *8*(1), 20–25, 2008.

Negretti, M., G. Vignoli, M. Tubino, and M. Brocchini, On shallow-water wakes: an analytical study, *Journal of Fluid Mechanics*, *567*, 457–475, 2006.

Niayifar, A., and P. Perona, Dynamic water allocation policies improve the global efficiency of storage systems, *Advances in Water Resources*, *104*, 55–64, 2017.

Niayifar, A., H. J. Oldroyd, S. N. Lane, and P. Perona, Modeling macroroughness contribution to fish habitat suitability curves, *Water Resources Research*, *54*(11), 9306–9320, 2018.

Nitsche, M., D. Rickenmann, J. M. Turowski, A. Badoux, and J. W. Kirchner, Evaluation of bedload transport predictions using flow resistance equations to account for macro-roughness in steep mountain streams, *Water Resources Research*, *47*(8), 2011.

Bibliography

O'Conner, D., and W. Dobbins, Mechanism of reaeration in natural streams: American society of civil engineer transaction paper no. 2934, 1958.

O'Connor, J. E., J. J. Duda, and G. E. Grant, 1000 dams down and counting, *Science*, *348*(6234), 496–497, 2015.

Oliveira, R., and D. P. Loucks, Operating rules for multireservoir systems, *Water resources research*, *33*(4), 839–852, 1997.

Parasiewicz, P., Developing a reference habitat template and ecological management scenarios using the mesohabsim model, *River Research and Application*, *23*(8), 924–932, 2007.

Pasternack, G. B., M. K. Bounrisavong, and K. K. Parikh, Backwater control on riffle–pool hydraulics, fish habitat quality, and sediment transport regime in gravel-bed rivers, *Journal of Hydrology*, *357*(1-2), 125–139, 2008.

Payne, T. R., The concept of weigthed usable area as relative suitability index, pp. 1–5, 2003.

Pereira, R., I. Ashton, B. Sabbaghzadeh, J. D. Shutler, and R. C. Upstill-Goddard, Reduced air–sea co 2 exchange in the atlantic ocean due to biological surfactants, *Nature Geoscience*, p. 1, 2018.

Pereira-Cardenal, S. J., B. Mo, A. Gjelsvik, N. D. Riegels, K. Arnbjerg-Nielsen, and P. Bauer-Gottwein, Joint optimization of regional water-power systems, *Advances in Water Resources*, *92*, 200–207, 2016.

Perona, P., D. J. Dürrenmatt, and G. W. Characklis, Obtaining natural-like flow releases in diverted river reaches from simple riparian benefit economic models, *Journal of environmental management*, *118*, 161–169, 2013.

Peter, H., G. A. Singer, C. Preiler, P. Chifflard, G. Steniczka, and T. J. Battin, Scales and drivers of temporal pCO_2 dynamics in an Alpine stream, *Journal of Geophysical Research: Biogeosciences*, *119*(6), 1078–1091, 2014.

Petts, G. E., Instream flow science for sustainable river management, *JAWRA Journal of the American Water Resources Association*, *45*(5), 1071–1086, doi:10.1111/j.1752-1688.2009.00360.x, 2009.

Poff, N. L., J. D. Allan, M. B. Bain, J. R. Karr, K. L. Prestegaard, B. D. Richter, R. E. Sparks, and J. C. Stromberg, The natural flow regime, *BioScience*, *47*(11), 769–784, 1997.

Poff, N. L., J. D. Olden, D. M. Merritt, and D. M. Pepin, Homogenization of regional river dynamics by dams and global biodiversity implications, *Proceedings of the National Academy of Sciences*, *104*(14), 5732–5737, doi:10.1073/pnas.0609812104, 2007.

Poff, N. L., et al., The ecological limits of hydrologic alteration (ELOHA): a new framework for developing regional environmental flow standards, *Freshwater Biology*, *55*(1), 147–170, doi:10.1111/j.1365-2427.2009.02204.x, 2010.

Porté-Agel, F., Y.-T. Wu, H. Lu, and R. J. Conzemius, Large-eddy simulation of atmospheric boundary layer flow through wind turbines and wind farms, *Journal of Wind Engineering and Industrial Aerodynamics*, *99*(4), 154–168, 2011.

Porté-Agel, F., Y.-T. Wu, and C.-H. Chen, A numerical study of the effects of wind direction on turbine wakes and power losses in a large wind farm, *Energies*, *6*(10), 5297–5313, 2013.

Powell, W. B., *Approximate Dynamic Programming: Solving the curses of dimensionality*, vol. 703, John Wiley & Sons, 2007.

Qu, B., K. S. Aho, C. Li, S. Kang, M. Sillanpää, F. Yan, and P. A. Raymond, Greenhouse gases emissions in rivers of the tibetan plateau, *Scientific reports*, *7*(1), 16,573, 2017.

Quarton, D., and J. Ainslie, Turbulence in wind turbine wakes, *Wind Engineering*, pp. 15–23, 1990.

Raymond, P. A., C. J. Zappa, D. Butman, T. L. Bott, J. Potter, P. Mulholland, A. E. Laursen, W. H. McDowell, and D. Newbold, Scaling the gas transfer velocity and hydraulic geometry in streams and small rivers, *Limnology and Oceanography: Fluids and Environments*, *2*(1), 41–53, 2012.

Raymond, P. A., et al., Global carbon dioxide emissions from inland waters, *Nature*, *503*(7476), 355, 2013.

Razurel, P., L. Gorla, B. Crouzy, and P. Perona, Non-proportional repartition rules optimize environmental flows and energy production, *Water Resources Management*, *30*(1), 207–223, 2016.

Razurel, P., L. Gorla, S. Tron, A. Niayifar, B. Crouzy, and P. Perona, Improving the ecohydrological and economic efficiency of small hydropower plants with water diversion, *Advances in Water Resources*, 2018.

Richter, B., J. Baumgartner, R. Wigington, and D. Braun, How much water does a river need?, *Freshwater Biology*, *37*(1), 231–249, doi:10.1046/j.1365-2427.1997.00153.x, 1997.

Richter, B. D., J. V. Baumgartner, J. Powell, and D. P. Braun, A method for assessing hydrologic alteration within ecosystems, *Conservation biology*, *10*(4), 1163–1174, 1996a.

Richter, B. D., J. V. Baumgartner, J. Powell, and D. P. Braun, A method for assessing hydrologic alteration within ecosystems, *Conservation Biology*, *10*(4), 1163–1174, 1996b.

Richter, B. D., S. Postel, C. Revenga, T. Scudder, B. Lehner, A. Churchill, and M. Chow, Lost in development's shadow: the downstream human consequences of dams., *Water Alternatives*, *3*(2), 2010.

Roulund, A., B. M. Sumer, J. Fredsøe, and J. Michelsen, Numerical and experimental investigation of flow and scour around a circular pile, *Journal of Fluid Mechanics*, *534*, 351–401, 2005.

Bibliography

S. Lissaman, P., Energy effectiveness of arbitrary arrays of wind turbines, *Journal of Energy*, *3*(6), 323–328, 1979.

Salazar, J. Z., P. M. Reed, J. D. Herman, M. Giuliani, and A. Castelletti, A diagnostic assessment of evolutionary algorithms for multi-objective surface water reservoir control, *Advances in Water Resources*, *92*, 172–185, 2016.

Scheffer, M., *Critical transitions in nature and society*, Princeton University Press, Princeton and Oxford, 2009.

Scheffer, M., S. Carpenter, T. M. Lenton, and et al., Anticipating critical transitions, *Science*, *338*, 344–348, 2012.

Schelker, J., G. A. Singer, A. J. Ulseth, S. Hengsberger, and T. J. Battin, Co2 evasion from a steep, high gradient stream network: importance of seasonal and diurnal variation in aquatic pco2 and gas transfer, *Limnology and Oceanography*, *61*(5), 1826–1838, 2016.

Schmutz, S., C. Giefing, and C. Wiesner, The efficiency of a nature-like bypass channel for pike-perch (stizostedion lucioperca) in the marchfeldkanalsystem, *Hydrobiologia*, *371*, 355, 1998.

Schneider, J. M., D. Rickenmann, J. M. Turowski, and J. W. Kirchner, Self-adjustment of stream bed roughness and flow velocity in a steep mountain channel, *Water Resources Research*, *51*(10), 7838–7859, 2015.

Schneider, M., *Habitat-und Abflussmodellierung für Fließgewässer mit unscharfen Berechnungsansätzen*, Inst. für Wasserbau, 2001.

Schweizer, S., M. Borsuk, and P. Reichert, Predicting the morphological and hydraulic consequences of river rehabilitation, *River research and Applications*, *23*(3), 303–322, 2007.

Shen, Y., and P. Diplas, Application of two-and three-dimensional computational fluid dynamics models to complex ecological stream flows, *Journal of Hydrology*, *348*(1), 195–214, 2008.

Soncini-Sessa, R., L. Villa, E. Weber, and A. E. Rizzoli, Twole: a software tool for planning and management of water reservoir networks, *Hydrological sciences journal*, *44*(4), 619–631, 1999.

Stalnaker, C., and J. Arnette, Methodologies for determining instream flows for fish and other aquatic life, *Methodologies for the determination of stream resource flow requirements. Report FWS/OBS-76-03. US Fish and Wildlife Service, Washington, DC*, pp. 89–138, 1976.

Stevens, R. J., D. F. Gayme, and C. Meneveau, Coupled wake boundary layer model of wind-farms, *Journal of renewable and sustainable energy*, *7*(2), 023,115, 2015.

Stevens, R. J., D. F. Gayme, and C. Meneveau, Generalized coupled wake boundary layer model: applications and comparisons with field and les data for two wind farms, *Wind Energy*, *19*(11), 2023–2040, 2016.

Ta, J., T. R. Kelsey, J. K. Howard, J. R. Lund, S. Sandoval-Solis, and J. H. Viers, Simulation modeling to secure environmental flows in a diversion modified flow regime, *Journal of Water Resources Planning and Management*, *142*(11), 05016,010, 2016.

Taguchi, M., and J. C. Liao, Rainbow trout consume less oxygen in turbulence: the energetics of swimming behaviors at different speeds, *Journal of Experimental Biology*, *214*(9), 1428–1436, 2011.

Team, R. C., et al., R: A language and environment for statistical computing, 2013.

Team, S. D., et al., Stan modeling language users guide and reference manual, *Technical report*, 2016.

Tennekes, H., and J. L. Lumley, *A first course in turbulence*, MIT press, 1972.

Thogersen, M. L., T. Sorensen, P. Nielsen, A. Grotzner, and S. Chun, Introduction to wind turbine wake modelling and wake generated turbulence, *Risø National Laboratory, EMD International A/S: Aalborg, Denmark*, 2006.

Tritico, H. M., and A. J. Cotel, The effects of turbulent eddies on the stability and critical swimming speed of creek chub (semotilus atromaculatus), *Journal of Experimental Biology*, *213*(13), 2284–2293, 2010.

Truepower, A., openwind theoretical basis and validation, *Albany, NY, Technical Report*, (1.3), 2010.

Tsitsiklis, J. N., and B. Van Roy, Feature-based methods for large scale dynamic programming, *Machine Learning*, *22*(1-3), 59–94, 1996.

Tsivoglou, E., and L. Neal, Tracer measurement of reaeration: Iii. predicting the reaeration capacity of inland streams, *Journal (Water Pollution Control Federation)*, pp. 2669–2689, 1976.

Ulseth, A. J., R. O. Hall, M. Boix Canadell, H. L. Madinger, A. Niayifar, and T. J. Battin, Distinct air-water gas exchange regimes in low- and high-energy streams, *Nature Geoscience*, 2019.

UNIDO, World small hydropower report 2016, *Tech. rep.*, Department of Energy at the United Nations Industrial Development Organization, 2016.

Vachon, D., Y. T. Prairie, and J. J. Cole, The relationship between near-surface turbulence and gas transfer velocity in freshwater systems and its implications for floating chamber measurements of gas exchange, *Limnology and Oceanography*, *55*(4), 1723–1732, 2010.

Bibliography

Verhulst, P., La loi d'accroissement de la population, *Nouv. Mem. Acad. Roy. Soc. Belle-lettr. Bruxelles*, *18*(1), 1845.

Vermeulen, P., An experimental analysis of wind turbine wakes, in *3rd international symposium on wind energy systems*, pp. 431–450, 1980.

Vezza, P., P. Parasiewicz, M. Spairani, and C. Comoglio, Habitat modeling in high-gradient streams: the mesoscale approach and application, *Ecological Applications*, *24*(4), 844–861, 2014.

Viviroli, D., H. H. Dürr, B. Messerli, M. Meybeck, and R. Weingartner, Mountains of the world, water towers for humanity: Typology, mapping, and global significance, *Water resources research*, *43*(7), 2007.

Voutsinas, S., K. Rados, and A. Zervos, On the analysis of wake effects in wind parks, *Wind Engineering*, pp. 204–219, 1990.

Wanninkhof, R., Relationship between wind speed and gas exchange over the ocean, *Journal of Geophysical Research: Oceans*, *97*(C5), 7373–7382, 1992.

Wanninkhof, R., P. Mulholland, and J. Elwood, Gas exchange rates for a first-order stream determined with deliberate and natural tracers, *Water Resources Research*, *26*(7), 1621–1630, 1990.

Wanninkhof, R., W. E. Asher, D. T. Ho, C. Sweeney, and W. R. McGillis, Advances in quantifying air-sea gas exchange and environmental forcing, 2009.

WCD, *Dams and development: A new framework for decision-making: The report of the world commission on dams*, Earthscan, 2000.

Wilkes, M. A., E. Enders, A. T. Silva, M. Acreman, and I. Maddock, Position choice and swimming costs of juvenile atlantic salmon salmo salar in turbulent flow, *Journal of Ecohydraulics*, *2*(1), 16–27, 2017.

Woolf, D., et al., Modelling of bubble-mediated gas transfer: Fundamental principles and a laboratory test, *Journal of Marine Systems*, *66*(1-4), 71–91, 2007.

Woolf, D. K., Bubbles and the air-sea transfer velocity of gases, *Atmosphere-Ocean*, *31*(4), 517–540, 1993.

Workshop, S. S., Concepts and methods for assessing solute dynamics in stream ecosystems, *Journal of the North American Benthological Society*, *9*(2), 95–119, 1990.

Wu, Y.-T., and F. Porté-Agel, Atmospheric turbulence effects on wind-turbine wakes: An les study, *energies*, *5*(12), 5340–5362, 2012.

Wu, Y.-T., and F. Porté-Agel, Modeling turbine wakes and power losses within a wind farm using les: An application to the horns rev offshore wind farm, *Renewable Energy*, *75*, 945–955, 2015.

Wüest, A., N. H. Brooks, and D. M. Imboden, Bubble plume modeling for lake restoration, *Water Resources Research*, *28*(12), 3235–3250, 1992.

Xiao, X., E. P. White, M. B. Hooten, and S. L. Durham, On the use of log-transformation vs. nonlinear regression for analyzing biological power laws, *Ecology*, *92*(10), 1887–1894, 2011.

Xie, S., and C. Archer, Self-similarity and turbulence characteristics of wind turbine wakes via large-eddy simulation, *Wind Energy*, *18*(10), 1815–1838, 2015.

Yang, Z.-S., H.-J. Wang, Y. Saito, J. Milliman, K. Xu, S. Qiao, and G. Shi, Dam impacts on the Changjiang (Yangtze) River sediment discharge to the sea: The past 55 years and after the Three Gorges Dam, *Water Resources Research*, *42*(4), 2006.

Yeh, W. W.-G., Reservoir management and operations models: A state-of-the-art review, *Water resources research*, *21*(12), 1797–1818, 1985.

Zappa, C. J., W. R. McGillis, P. A. Raymond, J. B. Edson, E. J. Hintsa, H. J. Zemmelink, J. W. Dacey, and D. T. Ho, Environmental turbulent mixing controls on air-water gas exchange in marine and aquatic systems, *Geophysical Research Letters*, *34*(10), 2007.

Amin Niayifar

📍 Chemin des Roches 8, 1003 Lausanne

📞 +41788892608   💬 amin.niayifar

✉ a.niayifar@gmail.com

*École Polytechnique Fédérale de Lausanne (EPFL)***, Lausanne (CH)**

Doctor of Science (PhD) in Civil and Environmental Engineering

2015- 2019

*École Polytechnique Fédérale de Lausanne (EPFL)***, Lausanne (CH)**

Master of Science (MSc) in Energy Management and sustainability

2012-2014

- Minor in Management of Technology

University of Tehran (UT), **Tehran (IR)**

Bachelor of Science (BSc) in Mechanical Engineering

2008-2012

Honor and awards

- Selected paper in *Water Resources Research* journal to be featured as a Research Spotlight
- Granted scholarship for perusing master studies, EPFL
- Being exempted from M.Sc. program entrance exam as an "Exceptionally Talented Student", UT

Languages

English	fluent	**French**	B2-C1 level
Arabic	A2 level	**German**	B1 level
Persian	Native language		

Publications

- Ulseth, A. J., Hall, R. O., Canadell, M. B., Madinger, H. L., **Niayifar, A.**, & Battin, T. J. (2019). Distinct air–water gas exchange regimes in low-and high-energy streams. ***Nature Geoscience***, 1.
- **Niayifar, A.**, Oldroyd, H. J., Lane, S. N., & Perona, P. (2018). Modeling Macroroughness Contribution to Fish Habitat Suitability Curves. ***Water Resources Research***, *54*(11), 9306-9320.
- Razurel, P., Gorla, L., Tron, S., **Niayifar, A.**, Crouzy, B., & Perona, P. (2018). Improving the ecohydrological and economic efficiency of Small Hydropower Plants with water diversion. ***Advances in Water Resources***, *113*, 249-259.
- **Niayifar, A.**, & Perona, P. (2017). Dynamic water allocation policies improve the global efficiency of storage systems. ***Advances in Water Resources***, *104*, 55-64.
- **Niayifar, A.**, & Porté-Agel, F. (2016). Analytical modeling of wind farms: A new approach for power prediction. ***Energies***, *9*(9), 741.
- **Niayifar, A.**, & Perona, P. (2016). Searching Pareto-efficient dynamic environmental flows by means of nondominated sorting genetic algorithms II. In ***River Flow 2016***.
- **Niayifar, A.**, & Porté-Agel, F. (2015). A new analytical model for wind farm power prediction. In ***Journal of physics: conference series*** (Vol. 625, No. 1, p. 012039). IOP Publishing.

In preparation

- **Niayifar, A.**, Ulseth, A. J., Lane, S. N., Perona, P. & Battin, T. J. (2019). Streambed macroroughness contributes significantly to gas exchange.
- Razurel, P., **Niayifar, A.**, & Perona, P. (2019). A stream-scale model to optimize the water allocation for Small Hydropower Plants and the application to traditional systems.

References:

Prof. Tom Ian Battin, EPFL, Lausanne (tom.battin@epfl.ch)

Prof. Paolo Perona, UoE, Edinburgh (paolo.perona@ed.ac.uk)